Charge Transport, Configuration Interaction and Rydberg States under Density Functional Theory

by

Chiao-Lun Cheng

B.S., Univ. of California, Berkeley (2003)
B.A., Univ. of California, Berkeley (2003)

Submitted to the Department of Chemistry
in partial fulfillment of the requirements for the degree of

Doctor of Philosophy

at the

MASSACHUSETTS INSTITUTE OF TECHNOLOGY

September 2008

© Massachusetts Institute of Technology 2008. All rights reserved.

Author .....
Department of Chemistry
Aug 15, 2008

Certified by .....
Troy Van Voorhis
Associate Professor of Chemistry
Thesis Supervisor

Accepted by .....
Robert W. Field
Chairman, Department Committee on Graduate Students

This doctoral thesis has been examined by a Committee of the Department of Chemistry as follows:

Professor Jianshu Cao .....

Chairman, Thesis Committee

Associate Professor of Chemistry

Professor Troy Van Voorhis .....

Thesis Supervisor

Associate Professor of Chemistry

Professor Robert W. Field .....

Member, Thesis Committee

Haslam and Dewey Professor of Chemistry

Charge Transport, Configuration Interaction and Rydberg States under Density Functional Theory

by

Chiao-Lun Cheng

Submitted to the Department of Chemistry
on Aug 15, 2008, in partial fulfillment of the
requirements for the degree of
Doctor of Philosophy

Abstract

Density functional theory (DFT) is a computationally efficient formalism for studying electronic structure and dynamics. In this work, we develop DFT-based excited-state methods to study electron transport, Rydberg excited states and to characterize diabatic electronic configurations and couplings. We simulate electron transport in a molecular wire using real-time time-dependent density functional theory in order to study the conduction of the wire. We also use constrained density functional theory to obtain diabatic states and diabatic couplings, and use these excited-state properties in a configuration-interaction method that treats both dynamic and static correlation. Lastly, we use eDFT, an excited-state self-consistent-field method, to determine the energies of excited Rydberg atomic states.

Thesis Supervisor: Troy Van Voorhis
Title: Associate Professor of Chemistry

Acknowledgments

I thank my advisor Prof. Troy Van Voorhis for his leadership and guidance. His door was always open when I had questions or ideas (however silly and impractical) I needed advice on, and his broad knowledge base and endless patience as a mentor has had a huge impact on my learning the past five years. I am especially thankful to Troy for giving me the independence to pursue my own ideas, even with their dismal success rate. This exploration space has helped me develop as a scientist and a thinker over my years of graduate study.

I would like to thank my thesis committee members Profs. Robert W. Field and Jianshu Cao for their advice. I thank my undergraduate physical chemistry lecturer Prof. Max Wolfsberg for starting me on this journey - without those early discussions I would not have chosen this path. I thank my undergraduate research advisors Profs. Paul A. Bartlett and Judith P. Klinman for introducing me to the world of research. I would especially like to thank my Klinman group mentor Matthew P. Meyer for showing me what an interesting place the world can be.

Fellow physical chemistry colleagues have helped make my five years very enjoyable. I thank Jim Witkoskie, Steve Presse, Qin Wu, Xiaogeng Song, Jeremy Evans, Seth Difley and Steve Coy for many interesting and stimulating discussions. I thank Ziad Ganim for his assistance in figuring out CHARMM. I would also like to thank Aiyan Lu, Yuan-Chung Cheng, Shilong Yang, Xiang Xia, Jianlan Wu, Serhan Altunata, Vassiliy Lubchenko, Leeping Wang, Tim Kowalczyk and Ben Kaduk for maintaining the spirit of camaraderie I've felt in the "zoo".

I thank friends in Salon Chaos, the MIT Aikido Club, MIT ROCSA and the MIT Singapore Students Society - they have been an invaluable source of warmth and sanity. Salon Chaos offered a truly unique forum for exchanging ideas, I would like to thank Mo-Han Hsieh and I-Fan Lin for organizing it. I thank my neighbors Emma Chung and her housemates for providing me with a second home during my last few years of graduate school. I thank Rebecca Somers for her perspective during stressful times, and Huiyi Chen for always being there.

I thank my sister Ting-Yen for her encouraging words throughout the years. Most of all, I thank my parents, a constant source of support throughout my life, for granting me the freedom to pursue my dreams. This dissertation is dedicated to them.

To my parents

鄭高州

黃鳳滿

Contents

List of Figures

List of Tables

Chapter 1

Introduction

In this chapter, we introduce some of the fundamental laws and approaches to electronic structure, which will set the background and notation for the work in this dissertation. We end by describing how the rest of this dissertation is structured.

1.1 The Many-Body Schroedinger Equation

Here we introduce the Schroedinger equation, assuming non-relativistic electrons, i.e. the kinetic energy is small compared to the rest mass of the electron, and also immobile nuclei, i.e. the Bohn-Oppenheimer approximation and no magnetic interactions.

The electronic Hamiltonian $\mathbf{H}$ is a Hermitian operator with units of energy, and can be expressed as the sum of several parts:

$$\begin{aligned} \mathbf{H} &= \mathbf{T} + \mathbf{v_{ext}} + \mathbf{v_{ee}} \\ \mathbf{T} &= \sum_i -\frac{1}{2}\nabla_i^2 \\ \mathbf{v_{ext}} &= \sum_i \mathrm{v_{ext}}(r_i) \\ \mathbf{v_{ee}} &= \sum_{i<j} \frac{1}{|r_i - r_j|} \end{aligned} \tag{1.1}$$

$\mathbf{T}$ is the kinetic energy operator, and is the sum of kinetic energy operators for each electron coordinate r_i. $\mathbf{v_{ext}}$ is the external potential, which is the single-particle external potential summed over all the electron coordinates. The single-particle ex-

ternal potential is a function which maps a single 3-d electron coordinate in length units to an energy, $\mathrm{v_{ext}(r)}$. It represents the electric potential experienced by electrons, which in molecular systems originates from the nuclei. $\mathbf{v_{ee}}$ is the Coulomb repulsion between electrons, and is a sum of the reciprocal distance between all pairs of electron positions.

A given electronic system is completely specified by the function $\mathrm{v_{ext}}$, and has a state specified by a wavefunction $\Psi(\mathrm{x_1}, \mathrm{x_2}, \cdots, \mathrm{x_N})$ where N is the number of electrons and $\mathrm{x_i}$ include both spin and spatial coordinates.

Assuming that Ψ is normalized, the energy of a system in the state Ψ is obtained by taking its expectation with respect to the Hamiltonian $\mathbf{H}$.

$$E = \int \Psi^\dagger(\vec{r})\mathbf{H}\Psi(\vec{r})d\vec{r}$$

We now extremize the energy of an electronic system while enforcing the constraint of normalizability using the Lagrange multiplier λ

$$W = \int \Psi^\dagger(\vec{r})\mathbf{H}\Psi(\vec{r})d\vec{r} - \lambda \cdot \left(\int \Psi^\dagger(\vec{r})\Psi(\vec{r})d\vec{r} - 1 \right)$$

By using the Lagrange multiplier λ, we have converted the optimization of E over normalizable Ψ to an optimization of W over all Ψ and λ. For a given value of λ, we extremize W over Ψ using the Euler-Lagrange equations

$$\frac{\partial W}{\partial \Psi(\vec{r})} = \mathbf{H}\Psi(\vec{r}) - \lambda \cdot \Psi(\vec{r}) = 0 \tag{1.2}$$

By taking the inner product of equation 1.2 against $\Psi^\dagger$, we find that $\lambda = E$. We thus derive the Schroedinger equation:

$$\mathbf{H}\Psi_i(\vec{r}) = E_i\Psi_i(\vec{r}) \tag{1.3}$$

Equation 1.3 is a linear differential equation, and its solutions Ψ_i are the eigen-

states of the Hamiltonian **H**. The eigenstate with the lowest E_i is the ground state. The Ψ_i form a complete orthonormal basis, and any state Φ can be expanded as a linear combination of the Ψ_i, $\Phi(\vec{r}) = \sum_i C_i \Psi_i(\vec{r})$, and the time-dependent Schroedinger equation

$$\mathbf{H}\Phi(\vec{r}, t) = i\frac{d\Phi(\vec{r}, t)}{dt}$$

then gives its time-evolution as

$$\Phi(\vec{r}, t) = \sum_i C_i \Psi_i(\vec{r}) e^{-E_i t}$$

1.1.1 Hartree-Fock

For electrons, the wavefunction Ψ has to be normalized and completely antisymmetric. Both requirements can be satisfied by the Slater determinant form [6] for the wavefunction. Hartree-Fock is based on this functional form, and is a mean-field theory, where each electron only feels the average effects of the other electrons on itself. This simplifies the interaction into an effective one-body potential, which in turn allows the wavefunction of $3N$ dimensions to be expressed in terms of N 3-dimensional spin-orbitals.

The Slater determinant takes the set of orthonormal spin-orbitals $\phi_i(\mathrm{x})$, where x includes both spatial r and spin coordinates s, and constructs Ψ by taking the determinant of matrix $\phi_i(\mathrm{x_j})$ where i and j are the row and column indices start from 1 and run up to the number of electrons N:

$$\Psi(\mathrm{x_1}, \mathrm{x_2}, \cdots, \mathrm{x_N}) = \frac{1}{\sqrt{\mathrm{N!}}} \begin{vmatrix} \phi_1(\mathrm{x_1}) & \phi_1(\mathrm{x_2}) & \cdots & \phi_1(\mathrm{x_N}) \\ \phi_2(\mathrm{x_1}) & \phi_2(\mathrm{x_2}) & \cdots & \phi_2(\mathrm{x_N}) \\ \vdots & \vdots & \ddots & \vdots \\ \phi_N(\mathrm{x_1}) & \phi_N(\mathrm{x_2}) & \cdots & \phi_N(\mathrm{x_N}) \end{vmatrix}$$

Since the orbitals are normalized, the factor of $\frac{1}{\sqrt{N!}}$ provides the right normalization for the many-body wavefunction.

Since all electron positions are equivalent, the expectation of a one-body operator in terms of the orbitals is then

$$\begin{aligned}
&\int \Psi^\dagger(\mathrm{x}_1, \mathrm{x}_2, \cdots, \mathrm{x}_\mathrm{N}) \sum_\mathrm{i} \mathbf{O}_\mathrm{i} \Psi(\mathrm{x}_1, \mathrm{x}_2, \cdots, \mathrm{x}_\mathrm{N}) \mathrm{dx}_1 \mathrm{dx}_2 \cdots \mathrm{dx}_\mathrm{N} \\
= \;& N \int \Psi^\dagger(\mathrm{x}_1, \mathrm{x}_2, \cdots, \mathrm{x}_\mathrm{N}) \mathbf{O}_1 \Psi(\mathrm{x}_1, \mathrm{x}_2, \cdots, \mathrm{x}_\mathrm{N}) \mathrm{dx}_1 \mathrm{dx}_2 \cdots \mathrm{dx}_\mathrm{N} \\
= \;& \sum_j \int \phi_j^\dagger(\mathrm{x}_1) \mathbf{O}_1 \phi_\mathrm{j}(\mathrm{x}_1) \mathrm{dx}_1
\end{aligned}$$

and the expectation of a two-body operator is

$$\begin{aligned}
&\int \Psi^\dagger(\mathrm{x}_1, \mathrm{x}_2, \cdots, \mathrm{x}_\mathrm{N}) \sum_{\mathrm{i<j}} \mathbf{O}_\mathrm{ij} \Psi(\mathrm{x}_1, \mathrm{x}_2, \cdots, \mathrm{x}_\mathrm{N}) \mathrm{dx}_1 \mathrm{dx}_2 \cdots \mathrm{dx}_\mathrm{N} \\
= \;& \frac{N(N-1)}{2} \int \Psi^\dagger(\mathrm{x}_1, \mathrm{x}_2, \cdots, \mathrm{x}_\mathrm{N}) \mathbf{O}_{12} \Psi(\mathrm{x}_1, \mathrm{x}_2, \cdots, \mathrm{x}_\mathrm{N}) \mathrm{dx}_1 \mathrm{dx}_2 \cdots \mathrm{dx}_\mathrm{N} \\
= \;& \frac{1}{2} \sum_{j,k} \int \phi_j^\dagger(\mathrm{x}_1) \phi_\mathrm{k}^\dagger(\mathrm{x}_2) \mathbf{O}_{12} \phi_\mathrm{j}(\mathrm{x}_1) \phi_\mathrm{k}(\mathrm{x}_2) \mathrm{dx}_1 \mathrm{dx}_2 \qquad (1.4) \\
- \;& \frac{1}{2} \sum_{j,k} \int \phi_j^\dagger(\mathrm{x}_1) \phi_\mathrm{k}^\dagger(\mathrm{x}_2) \mathbf{O}_{12} \phi_\mathrm{j}(\mathrm{x}_2) \phi_\mathrm{k}(\mathrm{x}_1) \mathrm{dx}_1 \mathrm{dx}_2 \qquad (1.5)
\end{aligned}$$

The detailed derivation of these rules can be found in reference [7]. For the inter-electron Coulomb operator $\mathbf{v_{ee}}$, the integral corresponding to line 1.4 is simply the classical Coulomb repulsion denoted E_J and is strictly positive, while line 1.5 corresponds to the energy savings that come from the anti-symmetry of the single-determinant wavefunction, has a strictly negative contribution, and is called the exchange term, denoted as E_K. The Hartree-Fock energy is then

$$
\begin{aligned}
E_{HF} &= E_T + E_{v_{ext}} + E_J - E_K \\
E_T &= \sum_i \int \phi_i^\dagger(r1)\mathbf{T_1}\phi_i(\mathrm{x}_1)\mathrm{dx}_1 \\
E_{v_{ext}} &= \sum_i \int \phi_i^\dagger(r1)\mathbf{v_{ext}}(\mathrm{x}_1)\phi_\mathrm{i}(\mathrm{x}_1)\mathrm{dx}_1 \\
E_J &= \frac{1}{2}\sum_{j,k} \int \phi_j^\dagger(\mathrm{x}_1)\phi_\mathrm{k}^\dagger(\mathrm{x}_2)\frac{1}{|\mathrm{r}_1 - \mathrm{r}_2|}\phi_\mathrm{j}(\mathrm{x}_1)\phi_\mathrm{k}(\mathrm{x}_2)\mathrm{dx}_1\mathrm{dx}_2 \qquad (1.6) \\
E_K &= \frac{1}{2}\sum_{j,k} \int \phi_j^\dagger(\mathrm{x}_1)\phi_\mathrm{k}^\dagger(\mathrm{x}_2)\frac{1}{|\mathrm{r}_1 - \mathrm{r}_2|}\phi_\mathrm{j}(\mathrm{x}_2)\phi_\mathrm{k}(\mathrm{x}_1)\mathrm{dx}_1\mathrm{dx}_2 \qquad (1.7)
\end{aligned}
$$

By minimizing E_{HF} with respect to the orbitals, and enforcing normality of the orbitals with Lagrange multipliers ϵ_i, one gets the Hartree-Fock equations

$$
\begin{aligned}
\mathbf{H}_{HF}\phi_i &= \epsilon_i\phi_i \qquad (1.8) \\
& \qquad (1.9)
\end{aligned}
$$

where the effective single-particle Hamiltonian, the Fock operator $\mathbf{H}_{HF}$, is given by

$$
\mathbf{H}_{HF} = \mathbf{T} + \mathbf{v_{ext}} + \mathbf{J} - \mathbf{K} \qquad (1.10)
$$

and the Coulomb $\mathbf{J}$ and exchange $\mathbf{K}$ operators have been defined as

$$
\begin{aligned}
\mathbf{J}f(\mathrm{x}_1) &= \sum_j \left(\int \frac{\phi_j^\dagger(\mathrm{x}_2)\phi_\mathrm{j}(\mathrm{x}_2)}{|\mathrm{r}_1 - \mathrm{r}_2|}\mathrm{dx}_2 \right) f(\mathrm{x}_1) \\
\mathbf{K}f(\mathrm{x}_1) &= \sum_j \left(\int \frac{\phi_j^\dagger(\mathrm{x}_2)\mathrm{f}(\mathrm{x}_2)}{|\mathrm{r}_1 - \mathrm{r}_2|}\mathrm{dx}_2 \right) \phi_j(\mathrm{x}_1)
\end{aligned}
$$

The eigenstates of the Fock operator are the Hartree-Fock orbitals. In this picture, the electrons interact with each other purely through the Coulomb term $\mathbf{J}$ and the

exchange term $\mathbf{K}$.

The Hamiltonian has no spin dependence, and hence commutes with the spin operator. This makes the spatial and spin dependence of each spin-orbital separable - each spin-orbital $\phi_i(\mathrm{x})$ can be expressed as $\phi_i(\mathrm{r})\sigma_\mathrm{i}(\mathrm{s})$ where σ has two possible values, α and β. Accounting for this explicitly, we get the unrestricted Hartree-Fock equations

$$\begin{aligned}
\mathbf{H}_{UHF}\phi_i &= \epsilon_i\phi_i \qquad (1.11)\\
\mathbf{H}_{UHF} &= \mathbf{T} + \mathbf{v_{ext}} + \mathbf{J} - \mathbf{K}\\
\mathbf{J}f(\mathrm{r}_1) &= \sum_j \left(\int \frac{\phi_j^\dagger(\mathrm{r}_2)\phi_\mathrm{j}(\mathrm{r}_2)}{|\mathrm{r}_1 - \mathrm{r}_2|}\mathrm{dr}_2 \right) f(\mathrm{r}_1)\\
\mathbf{K}f(\mathrm{r}_1) &= \sum_j \left(\int \frac{\phi_j^\dagger(\mathrm{r}_2)\mathrm{f}(\mathrm{r}_2)}{|\mathrm{r}_1 - \mathrm{r}_2|}\mathrm{dr}_2 \right) \phi_j(\mathrm{r}_1)\delta_{\sigma_\mathrm{j},\sigma_\mathrm{f}}
\end{aligned}$$

where all the operators are now spatial integrals. The orbitals are occupied as in figure 1-1.

So far, by assuming the single determinant form, we have reduced the search for the N-electron wavefunction $\Psi(\mathrm{x}_1, \mathrm{x}_2, \cdots, \mathrm{x}_\mathrm{N})$ to a search for N orbitals $\phi_i(\mathrm{r})$. Each orbital at this point could be any 3-d function. We introduce a further simplification of a basis set at this point. A basis set is a set of functions which is used to expand the orbital functions: ϕ_i is represented as a linear combination of basis functions: $\phi_i(r) = \sum_j C_{ij}\chi_j(r)$. Within a given basis set, the orbital coefficients C_{ij} then specify the orbital.

We now introduce a change in the representation of state. The one-body reduced density matrix $\rho_\sigma(\mathrm{r}, \mathrm{r}') = \sum_\mathrm{i} \delta(\sigma, \sigma_\mathrm{i})\phi_\mathrm{i}(\mathrm{r})\phi_\mathrm{i}^\dagger(\mathrm{r}')$ is a one-body projection operator onto the occupied orbital space, and can be built from the orbitals. The UHF orbitals can also be obtained from it (up to a unitary transformation) by diagonalization. This operator contains the same information as the orbitals, and is generally more convenient to work with.

Equation 1.11 is an integro-differential equation because of the $\mathbf{J}$ and $\mathbf{K}$ terms,

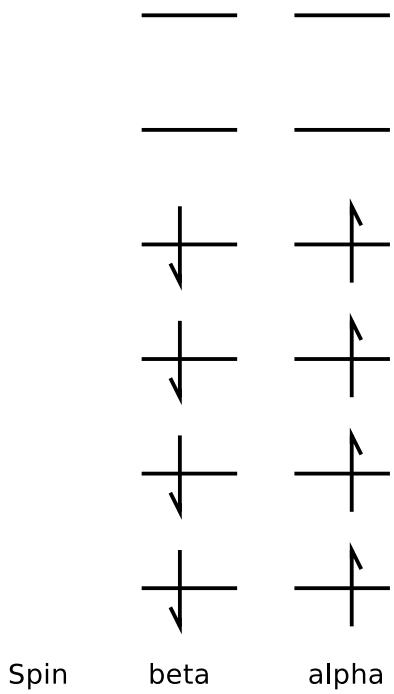

Figure 1-1: UHF orbital filling - $\uparrow$ are α-electrons, $\downarrow$ are β-electrons. Each horizontal line represents a different orbital, and the α and β electrons fill different orbitals in an Aufbau manner, from the bottom up. In this particular example, there are 4 α electrons, 4 β electrons and 6 basis functions forming 12 spin-orbitals

and is usually solved using iterative techniques (fig. 1-2) which compute $\mathbf{J}$ and $\mathbf{K}$ from $\{\phi_i\}$ and use numerical linear algebra to solve the eigenproblem in equation 1.11. For the solution to equation 1.11 to be a minimum, the self-consistency criterion must be satisfied, i.e. ϕ_i must be the eigensolution to the mean-field Fock matrix $\mathbf{H}_{UHF}$ computed from itself, which also means that the reduced density matrix $\rho_\sigma(\mathrm{r}, \mathrm{r}')$ commutes with the Fock matrix $\mathbf{H}_{UHF}$

$$\int \rho_\sigma(\mathrm{r}, \mathrm{r}')\mathbf{H}_{\mathrm{UHF}}(\mathrm{r}', \mathrm{r}'') - \mathbf{H}_{\mathrm{UHF}}(\mathrm{r}, \mathrm{r}')\rho_\sigma(\mathrm{r}', \mathrm{r}'')\mathrm{dr}' = 0$$

The Direct Inversion in Iterative Space (DIIS) step in figure 1-2 is an extrapolation method that uses past Fock matrices to produce a better guess for the next iteration [8, 9].

The Hartree-Fock energy is variational, i.e. it is always higher than the correct ground-state energy.

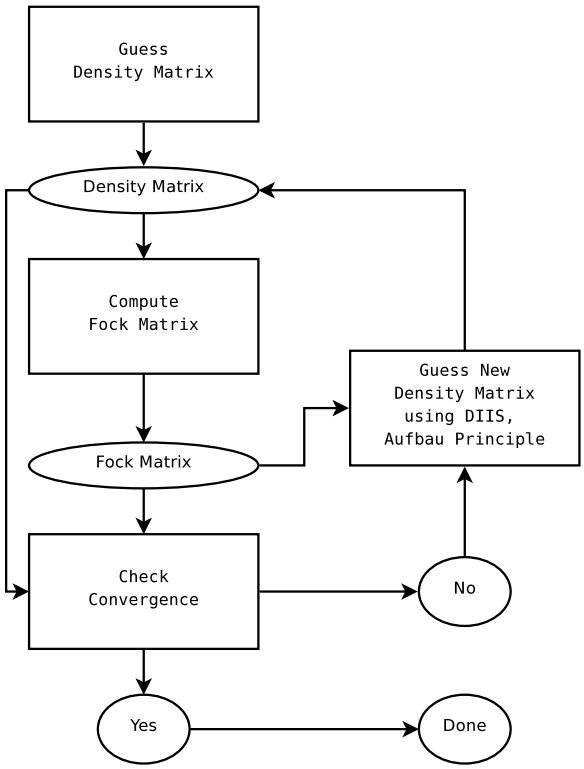

Figure 1-2: Typical Algorithm for Solving the HF equations

$$E_{HF} \geq E_{ground}$$

This is because the only approximation we have made is to restrict the search to the space of single-determinant wavefunctions made of orbitals in some finite basis, which is a subset of the space of all antisymmetric wavefunctions.

1.1.2 Electronic Correlation

Eigenstates of the full Hamiltonian (equation 1.1) are $3N$-dimensional antisymmetric, normalized functions. N-body eigenstates of non-interacting Hamiltonians are Slater determinants, which are a subset of these functions. Under Hartree-Fock, all the interactions come in the form of a effective one-body operator, the Fock operator, which means many many-body effects are being neglected. This is why we call Slater determinants non-interacting states.

The correlation energy is defined as the difference between the ground-state energy and the Hartree-Fock energy in the complete basis limit, and is negative because of

the variational nature of the Hartree-Fock energy. Even in the complete basis limit, the correlation energy is non-zero because the exact ground-state wavefunction is not a single determinant.

$$E_c = E_{ground} - E_{HF}$$

As described before, the Slater determinant takes N spin-orbitals and constructs an N-body wavefunction out of them. The non-interacting ground-state is the Slater determinant constructed from the N lowest eigenvalue spin-orbitals. Non-interacting excited-states are also Slater determinants, and are constructed from all the other sets of N spin-orbitals. Altogether, from a basis of M spin-orbitals, $\binom{M}{N}$ Slater determinants including the ground state can be formed. These are all the eigenstates of a Hermitian N-body operator, and thus form a complete basis for expressing any other N-body wavefunction, including the interacting ground-state Φ_0. Following chapter 4 from Ref. [7], we denote the non-interacting ground state with Ψ_0 and denote the excited states by listing the orbital substitutions. For example, the excited-state determinant that substitutes unoccupied orbitals r and s for occupied orbitals a and b would be denoted as Ψ_{ab}^{rs}.

$$\Phi_0 = c_0\Psi_0 + \sum_{ar} c_a^r \Psi_a^r + \sum_{\substack{a<b \\ r<s}} c_{ab}^{rs} \Psi_{ab}^{rs} + \sum_{\substack{a<b<c \\ r<s<t}} c_{abc}^{rst} \Psi_{abc}^{rst} + \sum_{\substack{a<b<c<d \\ r<s<t<u}} c_{abcd}^{rstu} \Psi_{abcd}^{rstu} + \cdots \quad (1.12)$$

This is the CI expansion for the exact wavefunction. Given a basis of reference spin-orbitals, usually from Hartree-Fock, the exact ground state is expressable in terms of the coefficients c in equation 1.12. There are, however, $\binom{M}{N}$ coefficients, a number which grows exponentially with the basis size - as of 2008, the biggest systems treatable with Full CI are only of 10-12 electrons.

All differences between the exact wavefunction Φ_0 and the Hartree-Fock wavefunction Ψ_0 are bundled under the title of correlation. Correlation is further qualitatively divided into two types, dynamical and static correlation.

Static correlation is the long-range correlation that results from there not being a good single-determinant representation for the ground state. For example, the exact electronic wavefunction in a dissociated singlet $H^{\cdot}$-$H^{\cdot}$ molecule is equal parts $H^{\uparrow}$-$H^{\downarrow}$ and $H^{\downarrow}$-$H^{\uparrow}$. However, in the large R limit, the best single-determinant wavefunction is

$$\begin{aligned}
\Psi(\mathrm{r}_1,\mathrm{r}_2) &= \frac{1}{\sqrt{2}}\begin{vmatrix} \frac{1}{\sqrt{2}}(\phi_{L\uparrow}(\mathrm{r}_1)+\phi_{\mathrm{R}\uparrow}(\mathrm{r}_1)) & \frac{1}{\sqrt{2}}(\phi_{L\uparrow}(\mathrm{r}_2)+\phi_{\mathrm{R}\uparrow}(\mathrm{r}_2)) \\ \frac{1}{\sqrt{2}}(\phi_{L\downarrow}(\mathrm{r}_1)+\phi_{\mathrm{R}\downarrow}(\mathrm{r}_1)) & \frac{1}{\sqrt{2}}(\phi_{L\downarrow}(\mathrm{r}_2)+\phi_{\mathrm{R}\downarrow}(\mathrm{r}_2)) \end{vmatrix} \\
&\propto \{(\phi_{L\uparrow}(\mathrm{r}_1)+\phi_{\mathrm{R}\uparrow}(\mathrm{r}_1))(\phi_{\mathrm{L}\downarrow}(\mathrm{r}_2)+\phi_{\mathrm{R}\downarrow}(\mathrm{r}_2))\} - \{\mathrm{r}_1 \leftrightarrow \mathrm{r}_2\} \\
&= \{\phi_{L\uparrow}(\mathrm{r}_1)\phi_{\mathrm{L}\downarrow}(\mathrm{r}_2)+\phi_{\mathrm{R}\uparrow}(\mathrm{r}_1)\phi_{\mathrm{R}\downarrow}(\mathrm{r}_2)+\phi_{\mathrm{L}\uparrow}(\mathrm{r}_1)\phi_{\mathrm{R}\downarrow}(\mathrm{r}_2)+\phi_{\mathrm{R}\uparrow}(\mathrm{r}_1)\phi_{\mathrm{L}\downarrow}(\mathrm{r}_2)\} \\
&- \{\mathrm{r}_1 \leftrightarrow \mathrm{r}_2\}
\end{aligned}$$

The first two terms are energetically unfavorable ionic $H^{-\uparrow\downarrow}$-H^{+} and H^{+}-$H^{-\uparrow\downarrow}$ terms which have energies that go as $-1/R$ [10]. This is a case we discuss further in chapter 3. Static correlation can be treated by explicitly using multiple determinants in multi-reference methods [11].

Dynamic correlation is a short-range effect that results from electrons dynamically avoiding each other and thus lowering inter-electron repulsion. A simple example would be the Helium atom, which has two electrons in close proximity. It can be treated starting from a single-determinant reference and subsequently adding contributions from excited determinants either variationally or perturbatively. In cases with dynamic correlation, the actual wavefunction may have a good overlap (90%-95%) with the single-determinant wavefunction, with the remaining bit being the result of summing small contributions from many other determinants. Those small contributions are significant energetically because they allow the electrons to move in such a way as to avoid each other. These contributions are best treated by perturbative methods like MP2 [12].

Active Space Methods

Active space methods solve the Schroedinger equation within a subspace of the $\binom{M}{N}$ determinant complete basis. That subspace is known as the active space, and CI methods use the matrix elements of the full electronic Hamiltonian, and the overlap within that space to compute the c coefficients. The relatively small number of determinants needed to treat static correlation motivates the use of active space methods.

For example, in Complete-Active-Space Self-Consistent-Field (CASSCF), one picks a subset of the M orbitals M_s and number of electrons N_s, and within the resulting $\binom{M_s}{N_s}$ space of determinants, alternately solves for the CI coefficients c and the optimal orbitals $\{\phi_i\}$ under a given set of CI coefficients.

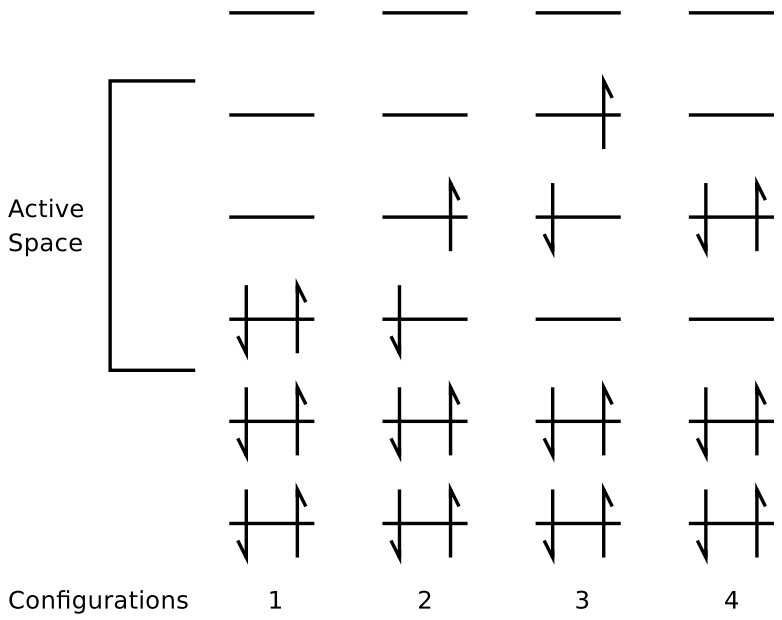

Figure 1-3: Some CASSCF(2,3) configurations

In figure 1-3 we have shown some possible configurations under CASSCF(2,3), where 2 electrons are placed in any of the $\binom{3}{1}^2$ possible configurations with the same total spin.

We develop a DFT-based active space CI method for treating both dynamic and static correlation in chapter 3.

1.2 Density Functional Theory

1.2.1 The Hohenberg-Kohn Theorems

Most of the difficulties in conventional wavefunction-based electronic structure stem from the complexity of the many-body wavefunction $\Psi(\vec{r})$. It is, however, possible to avoid the many-body wavefunction. Density Functional Theory (DFT) is the study of electronic structure with single-particle density as the independent parameter. The single-particle density is obtained from the many-body wavefunction by integrating out all but one position variable.

$$\rho(\mathrm{x}_1) = \int \Psi^\dagger(\mathrm{x}_1, \mathrm{x}_2, \cdots, \mathrm{x}_\mathrm{N})\Psi(\mathrm{x}_1, \mathrm{x}_2, \cdots, \mathrm{x}_\mathrm{N})\mathrm{dx}_2\mathrm{dx}_3\cdots\mathrm{dx}_\mathrm{N}$$

The single-particle density is a vastly simpler object than the many-body wavefunction, having only 3, as opposed to 3N, coordinates. Surprisingly, as proven by the Hohenberg-Kohn theorem [13], the single-particle density contains all the information of the many-body ground-state wavefunction. The crux of the Hohenberg-Kohn theorem is the idea that, even though electronic Hamiltonians are two-body operators, the difference between any two electronic Hamiltonians is a one-body operator.

We will now present a proof via *reductio ad absurdum* for the first Hohenberg-Kohn theorem, which states that there exists a one-to-one correspondence between densities ρ and external potentials $\mathbf{v_{ext}}$. We start by assuming the converse, that there exist two external potentials $\mathbf{v_{ext1}}$ and $\mathbf{v_{ext2}}$ which differ by more than a constant which give rise to two different wavefunctions Ψ_1 and Ψ_2 and two different energies E_1 and E_2 but the same density ρ. The expectation of $E_1 - E_2$ is given by

$$
\begin{aligned}
E_1 - E_2 &= \int \Psi_1^\dagger(\vec{r})\mathbf{H_1}\Psi_1(\vec{r})d\vec{r} - \int \Psi_2^\dagger(\vec{r})\mathbf{H_2}\Psi_2(\vec{r})d\vec{r} \\
&= \int \Psi_1^\dagger(\vec{r})\mathbf{H_1}\Psi_1(\vec{r})d\vec{r} - \int \Psi_2^\dagger(\vec{r})(\mathbf{H_2} - \mathbf{H_1} + \mathbf{H_1})\Psi_2(\vec{r})d\vec{r} \quad (1.13) \\
&= \int \Psi_1^\dagger(\vec{r})\mathbf{H_1}\Psi_1(\vec{r})d\vec{r} - \int \Psi_2^\dagger(\vec{r})\mathbf{H_1}\Psi_2(\vec{r})d\vec{r} \\
&- \int \Psi_2^\dagger(\vec{r})(\mathbf{H_2} - \mathbf{H_1})\Psi_2(\vec{r})d\vec{r} \\
&= \int \Psi_1^\dagger(\vec{r})\mathbf{H_1}\Psi_1(\vec{r})d\vec{r} - \int \Psi_2^\dagger(\vec{r})\mathbf{H_1}\Psi_2(\vec{r})d\vec{r} \\
&- \int \rho(\vec{r})(v_{ext2}(\vec{r}) - v_{ext1}(\vec{r}))d\vec{r} \quad (1.14)
\end{aligned}
$$

By the variational principle, we know that

$$\int \Psi_1^\dagger(\vec{r})\mathbf{H_1}\Psi_1(\vec{r})d\vec{r} - \int \Psi_2^\dagger(\vec{r})\mathbf{H_1}\Psi_2(\vec{r})d\vec{r} < 0 \quad (1.15)$$

and so

$$E_1 - E_2 < -\int \rho(\vec{r})(v_{ext2}(\vec{r}) - v_{ext1}(\vec{r}))d\vec{r} \quad (1.16)$$

We could, however, also have chosen to do the same proof for the expectation of $E_1 - E_2$, which would merely have swapped the labels 1 and 2, giving us

$$E_1 - E_2 > \int \rho(\vec{r})(v_{ext1}(\vec{r}) - v_{ext2}(\vec{r}))d\vec{r} \quad (1.17)$$

Combining inequalities 1.16 and 1.17, we get the contradiction

$$E_1 - E_2 > E_1 - E_2$$

Thus it must not be possible for two external potentials differing by more than a constant to give rise to the same density. This proves the existence of a mapping from densities $\rho(\vec{r})$ to external potentials $v_{ext}(\vec{r})$. The converse mapping is simply solving the Schroedinger equation for external potential $v_{ext}(\vec{r})$ and integrating the resulting

wavefunction to obtain the density $\rho(\vec{r})$. This is the first Hohenberg-Kohn theorem - the existence of a one-to-one map between the set of single-particle ground-state densities and the external potentials which generate them.

Since the external potential defines the ground-state wavefunction from which every ground-state observable can be obtained, *the first Hohenberg-Kohn proof establishes the existence of density functionals for every property of the corresponding ground-state wavefunction.* This includes, crucially, its energy expectation under any other Hamiltonian. Using this fact, the second Hohenberg-Kohn theorem expresses the variational principle in a density functional form, proving the existence of a universal functional $G[\rho]$ which can be used to find the energy of any ground-state density under any other Hamiltonian as defined by external potential $v_{ext}(\mathrm{r})$

$$E_v[\rho] = \int v_{ext}(\mathrm{r})\rho(\mathrm{r})\mathrm{dr} + \frac{1}{2}\int \frac{\rho(\mathrm{r})\rho(\mathrm{r}')}{|\mathrm{r}-\mathrm{r}'|}\mathrm{dr}\mathrm{dr}' + \mathrm{G}[\rho] \tag{1.18}$$

where $G[\rho]$ is universal and only dependent on the density, and $E_v[\rho]$ is variational. Even though it is proven to exist, however, the explicit form of the energy functional $G[\rho]$ is not known. There are, instead, numerous attempts at approximations to the energy functional. One of the key approaches, in which the work of this thesis is couched, is the Kohn-Sham formalism [14].

1.2.2 The Kohn-Sham Formalism

To derive the Kohn-Sham formalism, one begins by considering the set of non-interacting Hamiltonians

$$\mathbf{H_s} \;=\; -\frac{1}{2}\nabla^2 + \mathbf{v_{ext}} \tag{1.19}$$

Notice that the Hohenberg-Kohn theorem also applies for this set of non-interacting Hamiltonians $\mathbf{H_s}$, and therefore a one-to-one mapping exists between the non-interacting ground-state densities ρ and v_{ext} which give rise to them. A density functional of the non-interacting kinetic energy, $T_s[\rho]$ then exists. All the ground states to Hamiltoni-

ans 1.19 are single determinants, and T_s can be computed exactly from the orbitals that make up the determinant

$$\begin{aligned} \rho(\mathrm{r}) &= \sum_i \int \phi_i^\dagger(\mathrm{r})\phi_\mathrm{i}(\mathrm{r}) \\ T_s[\rho] &= \sum_i \int \phi_i^\dagger(\mathrm{r})\,\frac{1}{2}\,\nabla^2\phi_\mathrm{i}(\mathrm{r})\mathrm{dr} \end{aligned}$$

Using T_s, Kohn and Sham define E_{xc}, the exchange-correlation energy, as such:

$$G[\rho] = T_s[\rho] + E_{xc}[\rho] \tag{1.20}$$

Substituting $G[\rho]$ into equation 1.18 then gives

$$E_v[\rho] = T_s[\rho] + \int v_{ext}(\mathrm{r})\rho(\mathrm{r})\mathrm{dr} + \frac{1}{2}\int \frac{\rho(\mathrm{r})\rho(\mathrm{r}')}{|\mathrm{r}-\mathrm{r}'|}\mathrm{drdr}' + \mathrm{E_{xc}}[\rho] \tag{1.21}$$

Extremizing $E_v[\rho]$ with respect to Kohn-Sham orbitals $\phi_i(\mathrm{r})$ and using the Euler-Lagrange equations then gives the Kohn-Sham equations

$$\begin{aligned} \mathbf{H}_{\mathrm{KS}}\,\phi_i(\mathrm{r}) &= \epsilon_i\phi_i(\mathrm{r}) \\ \mathbf{H}_{\mathrm{KS}} &= \frac{dE_v[\rho]}{d\phi_i(\mathrm{r})} \\ &= -\frac{1}{2}\,\boldsymbol{\nabla^2} + \mathbf{v_{ext}} + \mathbf{J} + \mathbf{v_{xc}}[\rho] \\ \mathbf{v_{xc}}[\rho] &= \frac{dE_{xc}[\rho]}{d\rho} \end{aligned}$$

Kohn-Sham DFT is a search over N-body single determinant space, and is solved using highly similar techniques to Hartree-Fock, like that depicted in fig. 1-2. The Kohn-Sham wavefunction is the exact ground-state solution to a non-interacting Hamiltonian, the Kohn-Sham Hamiltonian. The resulting density is assumed to also be a fully-interacting ground-state density corresponding to some other external po-

tential v_{ext}(r). This is the assumption of v-representability. This is a requirement inherited from the Hohenberg-Kohn theorem, which is the proof of a one-to-one mapping only within a subset of all possible ground-state densities - densities which originate from the ground state under some $\mathbf{v_{ext}}$. Examples of densities which are not v-representable include one-electron excited state densities, and also other specific examples invented to explore this assumption [15, 16]. In the absence of a rigorous proof, however, KS-DFT has been applied to many ground-state molecular systems and found to work quite well empirically. This suggests that non v-representable densities must be quite rare in practice. We explore this issue further in chapter 4.

Given v-representability, Kohn-Sham DFT (KS-DFT) is in principle an exact formulation of many-body quantum mechanics. However, just like the case for the energy functional $E_v[\rho]$, the expression for $E_{xc}[\rho]$, the exchange-correlation functional, is not known. The achievement of KS-DFT lies in the non-interacting kinetic energy $T_s[\rho]$ being a good approximation to the exact kinetic energy, making $E_{xc}[\rho]$ much smaller in magnitude than $G[\rho]$, and correspondingly easier to approximate. Despite this, the development of exchange-correlation functionals remains an active field of research, and the quality of the exchange-correlation functional used has a big effect on the efficacy of KS-DFT.

1.2.3 Constrained Density Functional Theory (CDFT)

KS-DFT searches for the lowest energy solution amongst all possible single-determinant Kohn-Sham wavefunctions. Constrained DFT is a search that operates only over the space of Kohn-Sham wavefunctions that satisfy the specified density constraints [17]. Constraints come in the form of

$$\int \mathbf{w}_c(\mathrm{r})\rho(\mathrm{r})\mathrm{dr} - \mathrm{N_c} = 0 \tag{1.22}$$

where $\mathbf{w}_c$ is a space dependent weight function, ρ(r) is the electron density and N_c is the target value of the constraint operator. Spin indices have been suppressed for clarity. Possible constraints are any function of position, i.e. dipole and multipole moments and the total electron density on a subset of the atoms. Some operators like

the momentum operator cannot be expressed in this form.Constraints are imposed using Lagrange multipliers, such that instead of finding the minimum of $E_v[\rho]$ we find the extrema of $W[\rho, V_c]$:

$$W[\rho, V_c] = E_v[\rho] + V_c \left(\int \mathbf{w}_c(\mathrm{r})\rho(\mathrm{r})\mathrm{dr} - \mathrm{N_c} \right)$$

We only show one constraint here, but the extension to multiple constraints is straightforward. The resulting Kohn-Sham equations then look like they have an extra external potential $V_c\mathbf{w}_c(\mathrm{r})$ added. This potential is a function of the density, and CDFT introduces no new assumptions over those already needed for KS-DFT.

$$\begin{aligned} \frac{\delta W[\rho, V_c]}{\delta \rho} &= \mathbf{H}_{CDFT} = \mathbf{H}_{\mathrm{KS}} + V_c\mathbf{w}_c & (1.23) \\ \mathbf{H}_{CDFT}\,\phi_i(\mathrm{r}) &= \epsilon_i\,\phi_i(\mathrm{r}) & (1.24) \end{aligned}$$

The derivative with respect to V_c must also be zero when the constraint is satisfied:

$$\begin{aligned} \frac{dW[\rho, V_c]}{dV_c} &= \frac{d\rho}{dV_c}\cancelto{0}{\frac{\delta W[\rho, V_c]}{\delta \rho}} + \frac{\partial W[\rho, V_c]}{\partial V_c} \\ &= \int \mathbf{w}_c(\mathrm{r})\rho(\mathrm{r})\mathrm{dr} - \mathrm{N_c} = 0 & (1.25) \end{aligned}$$

Note that we have made use of the fact that $\delta W[\rho, V_c]/\delta\rho = 0$ (Equation 1.23). Second derivatives come from first-order perturbation theory:

$$\begin{aligned} \frac{d^2W[\rho, V_c]}{dV_c^2} &= \int \mathbf{w}_c(\mathrm{r})\frac{\mathrm{d}\rho(\mathrm{r})}{\mathrm{dV_c}}\mathrm{dr} \\ &= 2\sum_{i\in\mathrm{occ}}\sum_{a\in\mathrm{virt}} \frac{|\int \phi_i(\mathrm{r})\mathbf{w}_\mathrm{c}(\mathrm{r})\phi_\mathrm{a}(\mathrm{r})\mathrm{dr}|^2}{\epsilon_i - \epsilon_a} & (1.26) \end{aligned}$$

where indices i and a run over the occupied and unoccupied orbitals respectively, and $\epsilon_{i,a}$ are the Kohn-Sham eigenvalues. Equation 1.23 is solved as an eigenproblem using

numerical linear algebra routines, while equation 1.25 is solved using root-searching algorithms, with the help of the analytic second derivative equation 1.26.

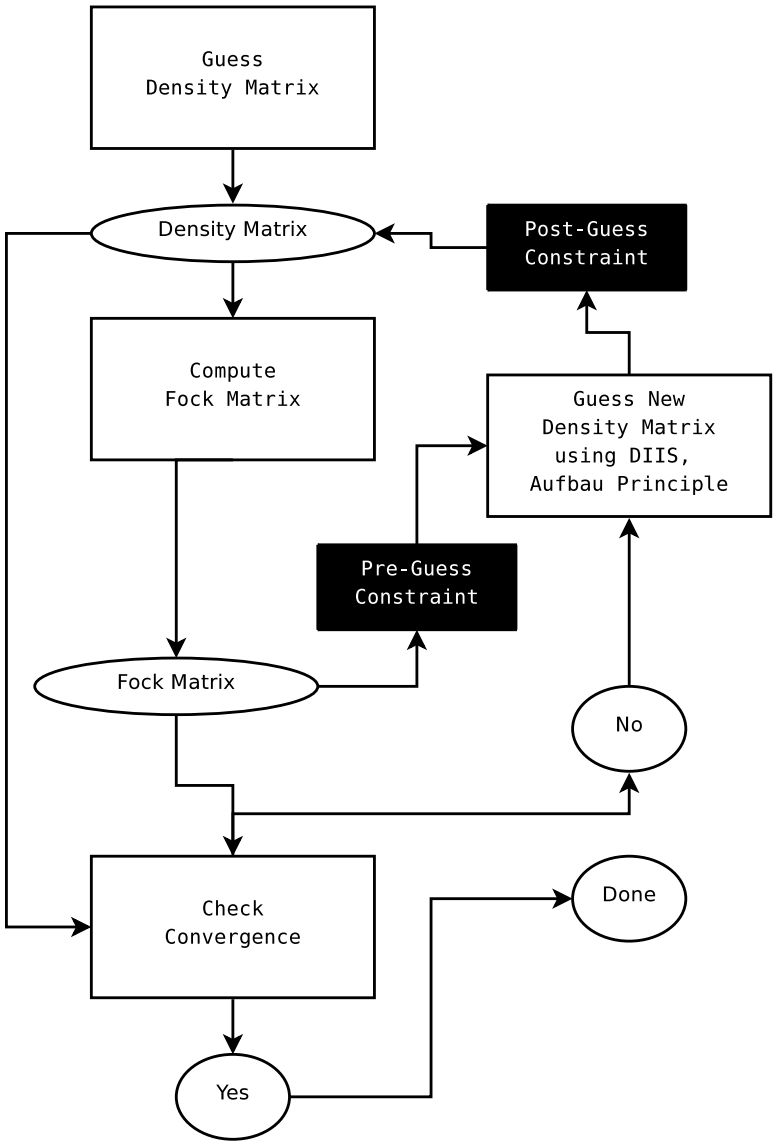

Figure 1-4: Algorithm for Solving the CDFT equations

Figure 1-4 illustrates the algorithms we use to solve the CDFT equations. within each of the black boxes are additional iterations which add the right multiple of the constraint matrix to the output Fock matrix, set such that the resulting density matrix built from the Fock matrix eigenvectors satisfies the constraints in equation 1.25.

Possible Constraints

Formally, the constraint $\mathbf{w}_c$ can be any function of the α- and β- densities, but in our implementation is limited to linear combinations of α- and β- atomic populations. We have implemented two definitions for the assignment of atomic populations, Becke weights and Lowdin populations. The Becke weights use the atomic center assignments of density that is used in the Becke quadrature [18], whereas Lowdin weights are basis-dependent projection operators obtained from diagonalizing the overlap matrix in the AO basis and assigning the resulting orthogonal basis functions to the AO basis atomic centers. In either case, the resulting populations sum to the total density of the atom and the population operators are Hermitian.

Previous work in the group has applied CDFT to the computation of long-range charge-transfer states [19], electron transfer coupling coefficients and reorganization energies [20, 21], all through the use of different constraints. We will use CDFT in chapter 3 to construct diabatic states, compute their electronic couplings, and use that information to construct a more accurate ground state.

1.2.4 Time-Dependent Density Functional Theory (TDDFT)

So far, we have only talked about ground-state densities. There is, however, also a formulation of time-dependent quantum mechanics based on the single-particle density. As described earlier, the basis of the Hohenberg-Kohn theorem is the fact that differences within the space of fully-interacting electronic Hamiltonians are all one-particle operators. Analogously, within the space of time-dependent fully-interacting electronic Hamiltonians, if we disallow magnetic fields, any difference is also a time-dependent one-particle potential. For time-dependent Hamiltonians of the form

$$\mathbf{H}(t) = \mathbf{T} + \mathbf{v_{ext}}(t) + \mathbf{v_{ee}}$$

the Runge-Gross theorem [22] states that, given initial ground-state wavefunction $\Phi(0)$, there exists a one-to-one correspondence between the time-dependent potential $\mathbf{v_{ext}}(t)$ and the time-dependent density $\rho(t)$. The corresponding Kohn-Sham formalism to the Runge-Gross theorem is the time-dependent Kohn-Sham (TDKS) equation,

which expresses the evolution of Kohn-Sham orbitals in response to a time-dependent external potential:

$$\partial_t \phi_i(t) = -i \cdot \mathbf{H}_{\mathrm{KS}}[\{\rho(\tau)\}_{\tau<t}, t]\phi_i(t) \tag{1.27}$$

Just like the case for the ground-state Kohn-Sham equations, the time-dependent Kohn-Sham orbitals give the same density as the exact wavefunction, but otherwise are not to be attributed any physical meaning. Notice the density dependence in equation 1.27 is of all densities before time t.

Time-Dependent Density Functional Response Theory (TDDFRT)

TDDFT is usually used in its linear response form, linear TDDFRT. We follow the treatment presented in Ref. [23]. Consider, to first order, the effect of a perturbation of time-dependent external potential at time t, $\delta\mathbf{v_{ext}}(t)$ on the TDKS density matrix at time t', $\rho(t') = \rho_0 + \delta\rho(t')$. The system starts out at $t = -\infty$ in the ground state ρ_0, is subject to perturbation $\delta\mathbf{v_{ext}}(t)$, and obeys the TDKS equations

$$\begin{aligned} \mathbf{H}_{\mathrm{KS}}[\rho, t] &= -\frac{1}{2}\nabla^{\mathbf{2}} + \mathbf{v_{ext}} + \delta\mathbf{v_{ext}}(t) + \mathbf{J}[\rho] + \mathbf{v_{xc}}[\rho] \\ \partial_t \rho(t) &= -i[\mathbf{H}_{\mathrm{KS}}[\rho(t), t], \rho(t)] \end{aligned} \tag{1.28}$$

The response of a system at time t' to a perturbation at time t is purely a function of $\tau = t' - t$ and of the density at t, $\rho(t)$. This time-translation invariance makes it preferable to work in frequency space, so we assume the following monochromatic forms for $\delta\mathbf{v_{ext}}(t)$ and $\delta\rho(t')$.

$$\begin{aligned} \delta\mathbf{v_{ext}}(t) &= \delta\tilde{\mathbf{v}}_{\mathbf{ext}}(\omega)e^{-i\omega t} + \delta\tilde{\mathbf{v}}^{\dagger}_{\mathbf{ext}}(\omega)e^{i\omega t} \\ \delta\rho(t') &= \delta\tilde{\rho}(\omega)e^{-i\omega t} + \delta\tilde{\rho}^{\dagger}(\omega)e^{i\omega t} \end{aligned}$$

To first order, the TDKS equation of motion (Eq. 1.28) then results in

$$\left\{ \begin{bmatrix} A(\omega) & B(\omega) \\ B(\omega) & A(\omega) \end{bmatrix} - \omega \begin{bmatrix} 1 & 0 \\ 0 & -1 \end{bmatrix} \right\} \begin{bmatrix} \delta\tilde{\rho}(\omega) \\ \delta\tilde{\rho}^{\dagger}(\omega) \end{bmatrix} = \begin{bmatrix} \delta\tilde{\mathbf{v}}_{\mathbf{ext}}(\omega) \\ \delta\tilde{\mathbf{v}}^{\dagger}_{\mathbf{ext}}(\omega) \end{bmatrix} \tag{1.29}$$

$$\begin{aligned} A_{iajb}(\omega) &= (\epsilon_a - \epsilon_i)\delta_{ij}\delta_{ab} + B_{iabj}(\omega) \\ B_{iajb}(\omega) &= \int \phi_i(\mathrm{x})\phi_{\mathrm{a}}(\mathrm{x}) \left(\frac{1}{\mathrm{r} - \mathrm{r}'} + \tilde{\mathrm{f}}_{\mathrm{xc}}(\omega, \mathrm{x}, \mathrm{x}') \right) \phi_{\mathrm{b}}(\mathrm{x}')\phi_{\mathrm{j}}(\mathrm{x}')\mathrm{dxdx}' \end{aligned} \tag{1.30}$$

where ϕ_i are the Kohn-Sham orbitals from the ground-state and ϵ_i are the Kohn-Sham eigenvalues. $\tilde{f}_{xc}(\omega, \mathrm{x}, \mathrm{x}')$ is the frequency-dependent exchange-correlation kernel, and represents the change in $\mathbf{v_{xc}}$ at one time in response to a change in the density at another. Up until this point, the treatment has been exact, given the restriction of sticking to purely electric fields. Note that this means we are unable to treat magnetic phenomena like EPR or electronic circular dichroism.

Under the adiabatic approximation, $\mathbf{v_{xc}}$ is assumed to depend only on the density at the same time, which in frequency space translates to $\tilde{\mathrm{f}}_{\mathrm{xc}}$ having no frequency dependence:

$$\tilde{\mathrm{f}}_{\mathrm{xc}}(\omega, \mathrm{x}, \mathrm{x}') = \tilde{\mathrm{f}}_{\mathrm{xc}}(0, \mathrm{x}, \mathrm{x}') = \frac{\delta\mathbf{v_{xc}}[\rho](\mathrm{x})}{\delta\rho(\mathrm{x}')} = \frac{\delta^2\mathrm{E}_{\mathrm{xc}}[\rho]}{\delta\rho(\mathrm{x})\delta\rho(\mathrm{x}')} \tag{1.31}$$

When the LHS of equation 1.29 is zero

$$\begin{bmatrix} A(\omega) & B(\omega) \\ B(\omega) & A(\omega) \end{bmatrix} \begin{bmatrix} \delta\tilde{\rho}(\omega) \\ \delta\tilde{\rho}^{\dagger}(\omega) \end{bmatrix} = \omega \begin{bmatrix} 1 & 0 \\ 0 & -1 \end{bmatrix} \begin{bmatrix} \delta\tilde{\rho}(\omega) \\ \delta\tilde{\rho}^{\dagger}(\omega) \end{bmatrix},$$

a finite $\delta\tilde{\mathbf{v}}_{\mathbf{ext}}(\omega)$ gives rise to an infinite $\delta\tilde{\rho}(\omega)$ - these are the poles of the response matrix

$$\begin{bmatrix} A(\omega) & B(\omega) \\ B(\omega) & A(\omega) \end{bmatrix}^{-1},$$

and the corresponding ω are the excited state energies of the system, with $\delta\widetilde{\rho}(\omega)$ being the Kohn-Sham transition density matrices, which in turn give the exact transition densities.

1.2.5 Approximate Exchange-Correlation Potentials

As mentioned earlier, the exact form for $E_{xc}[\rho]$ is not known, even in principle. In order to use KS-DFT, we must have a way of approximating $E_{xc}[\rho]$. Unlike wavefunction-based approaches, there is no exact space which is truncated to produce approximations - functionals are picked to satisfy both computability constraints and also to satisfy criteria that the exact functional is known to satisfy, and maybe also to produce the correct result for a model system. In this subsection, we introduce the exchange-correlation functionals which we use in our work.

The Local Spin Density Approximation (LSDA) The uniform electron gas is a fictitious system where a negative sea of electrons exactly neutralizes a uniform background of positive charge. It is parameterized by only two parameters, the alpha density ρ_α and the beta density ρ_β, and so, assuming the form

$$E_{xc}[\rho_\alpha, \rho_\beta] = \int f_{xc}^{LSDA}(\rho_\alpha(\mathrm{r}), \rho_\beta(\mathrm{r}))\mathrm{dr}$$

it is possible to formulate functional $f_{xc}^{LSDA}(\rho_\alpha, \rho_\beta)$ which gives the exact exchange and correlation energies for every possible uniform electron gas. The resulting functionals are the LSDA exchange and correlation functionals. The exchange functional was derived by Slater as an approximation to Hartree-Fock exchange [2], whereas the correlation functional is an interpolation based on accurate Monte-Carlo simulations [24].

The LSDA works very well in situations where the electron density varies slowly, outperforming semi-empirical functionals for solids and jellium surfaces, but tends to overbind electrons in molecules and atoms [25].

Generalized Gradient Approximations (GGAs) One of the earliest attempts to go beyond the LSDA was the gradient expansion approximation (GEA), a trun-

cated expansion based on slowly varying electron gas densities. This functional was found to have worse performance than the LSDA when used on molecules.

This was found to be due to a violation of certain exact conditions called the exchange-correlation hole sum rules [26, 27, 28]. By modifying the GEA functional to satisfy the exchange-correlation hole sum rules, the first GGAs like PW86 [27] were formulated. GGAs are of the form

$$E_{xc}[\rho_\alpha, \rho_\beta] = \int f_{xc}(\rho_\alpha(\mathrm{r}), \rho_\beta(\mathrm{r}), |\nabla\rho_\alpha(\mathrm{r})|, |\nabla\rho_\beta(\mathrm{r})|)\mathrm{dr}$$

and make use of both density and gradient to determine functional values. Later GGAs like PW91 [29] and PBE [30] were derived by first coming up with a model for the exchange-correlation hole, and then deriving the resulting functional. The judicious selection of exact conditions to satisfy is crucial - of particular note is the Becke88 [31] exchange GGA functional, which gives the right asymptotic exchange potential for finite systems, on top of satisfying the exchange hole sum rules.

GGAs correct for the tendency of LSDA to overbind and overestimate bond energies, performing better than LSDA in predicting total energies, atomization, barriers and geometries [32, 33, 34, 35].

The Adiabatic Connection and Hybrid Functionals Consider the set of Hamiltonians

$$\mathbf{H}_\lambda = \mathbf{T} + \mathbf{v}^\lambda_{\mathbf{ext}} + \lambda \cdot \mathbf{v}_{\mathbf{ee}}$$

The Kohn-Sham and the full Hamiltonians are instances of this set, with $\lambda = 0$ and $\lambda = 1$ respectively. For a given density $\rho(\mathrm{r})$, assume that there exists a $\mathbf{v}^\lambda_{\mathbf{ext}}$ for every value of λ that gives rise to $\rho(\mathrm{r})$ as its ground-state density, with corresponding wavefunctions Ψ_λ. Then, using the Hellman-Feynman theorem, one finds an expression for the exchange-correlation energy $E_{xc}[\rho]$ [36]:

$$E_{xc}[\rho] + E_J[\rho] \;=\; \int_0^1 \Psi^\dagger_\lambda(\vec{r})\mathbf{v}_{\mathbf{ee}}\Psi_\lambda(\vec{r})d\vec{r} \tag{1.32}$$

This process is known as the adiabatic connection. At $\lambda = 0$, the integrand of equation 1.32 is $\propto \mathbf{J} - \mathbf{K}$, and the wavefunction Ψ_0 is the Kohn-Sham Slater determinant. This implies that if we were to evaluate integral 1.32 by quadrature, the sum would include some component from $\mathbf{K}$ evaluated on the Kohn-Sham orbitals. This logic guided Becke to postulate the half-and-half functional in Ref. [37] and the B3PW91 functional in Ref. [38]. These are the hybrid functionals, some linear combination of GGAs and the Hartree-Fock exchange as evaluated using the Kohn-Sham orbitals. In the case of B3PW91, the coefficients of the linear combination were determined empirically by fitting to experimental results [38]. The resulting functional is

$$E_{xc}^{\mathrm{B3PW91}} = E_{xc}^{LSDA} + a_0(E_x^{\mathrm{exact}} - E_x^{\mathrm{LSDA}}) + a_x(E_x^{\mathrm{Becke88}} - E_x^{\mathrm{LSDA}}) + a_c(E_c^{\mathrm{PW91}} - E_c^{\mathrm{LSDA}})$$

where $a_0 = 0.20, a_x = 0.72, a_c = 0.81$.

Currently, the most popular hybrid functional is B3LYP, which uses the same coefficients as B3PW91 but replaces the PW91 correlation functional with the LYP correlation functional. By incorporating exact exchange, B3LYP is able to get an accuracy of 2-3 kcal/mol within the G2 test set. This is very close to chemical accuracy, $\approx$ 1 kcal/mol. Also because of the exact exchange component, hybrid functionals exhibit a lower level of self-interaction error (SIE) proportional to the amount of exact exchange [39]. We discuss SIE further below.

One might think to just use exact exchange and only approximate correlation. The problem with this approach lies in the inability of a delocalized exchange hole, in combination with a localized correlation hole, to give rise to a good approximation to the exact exchange-correlation hole (Ref. [10] chapter 6.6). Hybrid functionals hence represent a compromise between accurate exchange and accurate correlation.

Advantages and Flaws of Approximate Exchange-Correlation Functionals

The choice to use DFT is often motivated by its efficiency. DFT is as cheap as Hartree-Fock theory for most purposes because of the way commonly used xc potentials

are designed - $E_{xc}[\rho]$ are formulated such that the resulting $\mathbf{v_{xc}}[\rho] = \frac{dE_{xc}[\rho]}{d\rho}$ can be evaluated point-by-point on a spatial grid. The consequence of this is that the computation required to calculate $\mathbf{v_{xc}}$ scales linearly with system size. This is what makes KS-DFT so efficient.

KS-DFT's efficiency in treating electronic correlation allows it to be used on systems for which conventional wavefunction methods are simply too expensive. This cheapness, however, comes at a price - we know of many characteristics of the exact xc functional which that commonly used approximations do not satisfy. The inaccuracies are discussed below.

Lack of Derivative Discontinuity We first define the energy of densities that do not integrate to integers as being the result of ensembles of integer densities. In Ref. [40], Perdew et al. show that the lowest energy mixture for a density that integrates to $M + \omega$ electrons, where M is an integer and $0 \leq \omega \leq 1$, is the mixture of $(1 - \omega)$ of the lowest energy M-electron density and ω of the $(M + 1)$-electron density, giving rise to the energy

$$E_{M+\omega} = (1 - \omega)E_M + \omega E_{M+1}$$

This means that the energy as a function of N is a series of straight lines with discontinuities on the first derivative at integer values. As a consequence of this, the Kohn-Sham HOMO eigenvalue is in fact discontinuous at integer N:

$$\epsilon_{HOMO} = \begin{cases} -I_Z & (Z - 1 < N < Z) \\ -A_Z & (Z < N < Z + 1) \end{cases}$$

where I_Z and A_Z are the ionization and electron affinities of the Z-electron system. This property is not present in approximate non-hybrid exchange-correlation functionals [40, 41, 42]. It is partly present in hybrid functionals because of the orbital-dependence of exact exchange. The derivative discontinuity problem is most evident in the separation of ionic diatomics, like LiH, which dissociates to erroneous partial charges. Under LSDA, LiH dissociates to $Li^{+0.25}H^{-0.25}$ instead of the correct

Li^0H^0 [40]. In solid state applications, the lack of a derivative discontinuity causes underestimates in band gap predictions, which at times makes semi-conductors and insulators look like metals [43]. For example, it causes LSDA to predict a silicon band gap that is 50% too small [44].

Spatial Locality The local nature of exchange-correlation approximations means that charge transfer and charge transport cannot be treated correctly using perturbation theory [45].

As noted earlier, other than the exact exchange component of hybrid functionals, common approximate exchange-correlation potentials can all be evaluated on a grid. This means that the TDDFRT exchange-correlation kernel is not only local in time due to the adiabatic approximation, but also local in space. Equation 1.31 then becomes

$$\tilde{\mathrm{f}}_{\mathrm{xc}}(0, \mathrm{x}, \mathrm{x}') = \tilde{\mathrm{f}}_{\mathrm{xc}}(0, \mathrm{x})\delta(\mathrm{x} - \mathrm{x}')$$

The potential at a given location $\mathbf{v_{xc}}[\rho](\mathrm{r})$ only depends on properties of the density at the same point. This property is purely an ad-hoc simplification, and not given by the original Kohn-Sham derivation.

The simplification of spatial locality leads to erroneous predictions for charge-transfer under linear response TDDFT [45, 46]. Consider the $B_{iajb}(\omega)$ term of TDDFRT in equation 1.30. The ia and jb indices refer to excitations $\phi_i \rightarrow \phi_a$ and $\phi_j \rightarrow \phi_b$. Note that for long-range charge transfers, where there is little overlap between these excitation pairs, the $B(\omega)$ term effectively goes to zero, and the excitation is then determined solely by the $A(\omega)$ contribution, the difference in orbital eigenvalues. For well-separated molecules, this difference is not distance dependent at all, and so does not give rise to the correct $\frac{1}{R}$ factor. Charge transfer excitations are hence underestimated by TDDFRT. The exact exchange component of hybrid functionals is non-local, adding a multiple of the term

$$A^X_{iajb}(\omega) = -\int \phi_i(\mathrm{x})\phi_\mathrm{j}(\mathrm{x})\left(\frac{1}{\mathrm{r}-\mathrm{r}'}\right)\phi_\mathrm{a}(\mathrm{x}')\phi_\mathrm{b}(\mathrm{x}')\mathrm{dxdx}'$$
$$B^X_{iajb}(\omega) = -\int \phi_i(\mathrm{x})\phi_\mathrm{b}(\mathrm{x})\left(\frac{1}{\mathrm{r}-\mathrm{r}'}\right)\phi_\mathrm{a}(\mathrm{x}')\phi_\mathrm{j}(\mathrm{x}')\mathrm{dxdx}'$$

to $A_{iajb}(\omega)$ and $B_{iajb}(\omega)$. $A^X_{iajb}(\omega)$ has the correct $\frac{1}{R}$ dependence and allows hybrid functionals to perform better, but as a whole still exhibit the same problem.

Self-Interaction Error (SIE) This is the tendency of individual electrons to feel an erroneous repulsion from their own densities [47, 48]. Notice that even though the inter-electron interaction is pairwise between the $\frac{N(N-1)}{2}$ pairs of electrons, the sums in Hartree-Fock Coulomb (equation 1.6) and exchange (equation 1.7) energies run over all N^2 orbital indices. This transformation is allowed because the $j = k$ terms in the Hartree-Fock Coulomb and exchange terms are equal and opposite in sign to each other. This is the transformation that allows the Coulomb energy to be evaluated purely from the classical electron density. It is, however, a problem for DFT because DFT exchange is not evaluated exactly. Electrons hence experience a spurious repulsion from themselves.

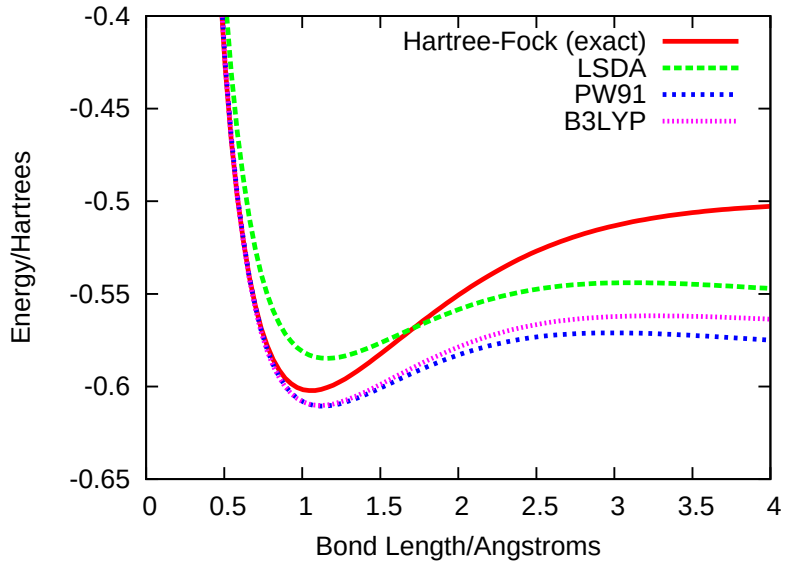

Figure 1-5: H_2^+ Energies in cc-PVTZ basis

Consider the example of one-electron system H_2^+. Hartree-Fock does not suffer at all from SIE, and is used to find the exact energy in this example. The error in the energy difference between the equilibrium and dissociated states comes from there being a larger SIE in the equilibrium state, when the electron density is more compact. Note that due to the inclusion of some exact exchange, hybrid functionals suffer less from SIE.

Lack of Static Correlation Wavefunctions which are well-described by the sum of multiple determinants exhibit long-range correlations which are treated with multiple-reference methods under wavefunction theories [11]. The Kohn-Sham Slater wavefunction is a single determinant by definition, and in principle is able to represent the multiple determinant wavefunction just fine. This non-interacting v-representability has been demonstrated for the specific case of dissociating H_2, where the wavefunction in the dissociated limit is the sum of two determinants, and yet can be represented by a single determinant KS wavefunction [49]. Using approximate xc functionals, however, static correlation is usually underestimated by DFT, especially when compensating effects from SIE are eliminated [50].

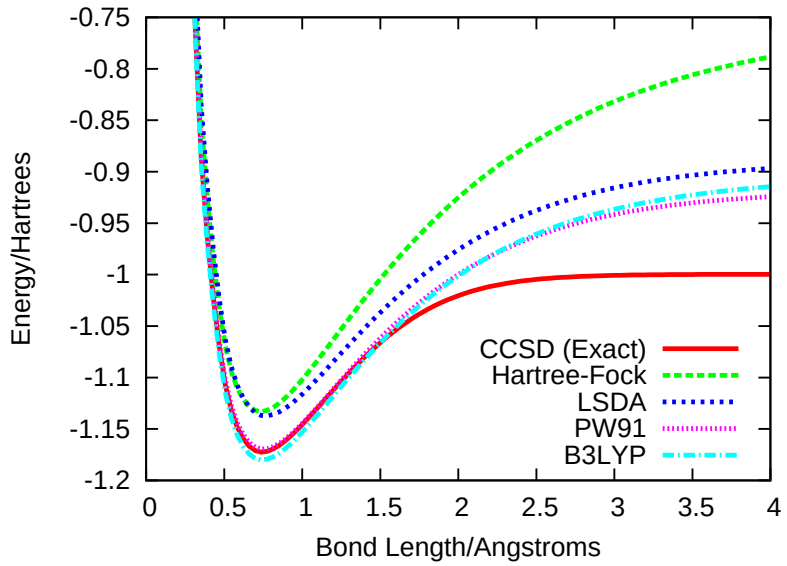

Figure 1-6: H_2 Energies in cc-PVTZ basis

Consider the 2-electron example of H_2. In 2-electron systems, the coupled-cluster singles-doubles (CCSD) method is exact. None of the other methods have static

correlation, and in the case of Hartree-Fock this results in charge-separation terms $H^{-\uparrow\downarrow}$-H^{+} and H^{+}-$H^{-\uparrow\downarrow}$ which cause the energy to go up with distance. Note that PW91, a GGA, and B3LYP, a hybrid functional, get pretty good energies at the equilibrium distance due to their ability to treat dynamic correlation.

There is much work on new xc functionals which address these systemic inaccuracies [51, 52, 53]. In this work, however, no new xc functionals will be presented. Instead, we focus on developing methods to extract physical properties of interest using the DFT formalism. We do not ignore the artifacts described above; instead of trying to tackle them directly, we design our procedures so as to minimize their effects.

1.3 Structure of this Dissertation

This dissertation will be structured as follows - chapters are arranged in accordance to physical properties of interest. Each chapter begins with an introduction to the significance of the property being studied, followed by a description of the state of the art, then a description of the methodology which we have developed. An account of results from applying the methodology to physical systems follows. The chapter then concludes with rationalizations of the failures and successes of the approach and, if appropriate, possible future directions.

Chapter 2 covers the work that we have done to simulate conductance in single molecules. We numerically integrate the time-dependent Kohn-Sham (TDKS) equations in a Gaussian basis to simulate the flow of charge across a polyene molecule, and characterize the corresponding current-voltage characteristics of the molecule. Chapter 3 describes a configuration interaction method based on constrained density functional theory, the advantage of which is its ability to treat both dynamic and static correlation at a modest computational cost. We apply this method to the computation of molecular dissociation curves of small diatomic molecules. Chapter 4 details explorations into the ability of DFT to treat isolated excited states - we devise a method that uses non-Aufbau occupation within the Kohn-Sham formalism to determine the energy of excited stationary states. This method is applied to the

Rydberg states of hydrogen and lithium atoms under various functionals.

Chapter 2

Molecular Conductance using Real-Time Time-Dependent Density Functional Theory

Note: The bulk of this chapter has been published in Ref. [54].

2.1 Introduction

Molecular electronics represent the next length-scale in the miniaturization of electronics as embodied in Moore's Law [55]. The pertinent physics in molecular electronics differs from that of molecules in bulk solids, and experiments probing the nature of single-molecule devices involving metal-molecule-metal (MMM) junctions have been performed in an attempt to understand more about them [56, 57, 58, 59, 60, 61, 62, 63, 64, 65, 66, 67, 68, 69, 70, 71, 72, 73, 74, 75, 76, 77, 78, 79]. In this chapter, we describe the development of DFT-based methods used to simulate molecular-scale conductors.

2.1.1 The Landauer-Büttiker Model

We start by examining charge transport under the Landauer-Büttiker model [80, 81, 82, 83, 84]. The Landauer formula expresses the conductance Γ as a sum of M channels which each have transmittance T_i.

$$\Gamma = \frac{1}{2\pi} \sum_{i}^{M} |T_i^2|$$

The Landauer-Büttiker model is an elastic electron transport model - electrons only exchange momentum with the channel, and are either transmitted through or reflected from the channel without a change in energy. Under the Landauer-Büttiker model, the metal leads to which the channel is connected exist in a state of grand canonical equilibrium, possesing well-defined chemical potentials and driving electron transport through the channel by virtue of the difference in chemical potential between the two leads. The resistance is quantized as a function of chemical potential difference, with step increases in conductance corresponding to the activation of new quantum channels. When applying the Landauer-Büttiker model to MMM experiments, treatments that interpret the channels as purely molecular scattering coefficients have been pursued [85, 86, 87, 88, 89]. Under such interpretations, the molecule acts as a potential off which electrons of the bulk scatter.

2.1.2 Non-Equilibrium Green's Function (NEGF) Methods

Beyond scattering theory, the non-equilibrium Green's function [90] can also be used to obtain a Landauer-like expression for electron transport through junctions. The NEGF contains the information needed to treat conductance exactly, but obtaining the exact NEGF is as difficult as solving the many-body Schroedinger equation. Therefore, instead of computing the exact NEGF, various approximations to the NEGF have been developed [91, 92, 93, 94, 95, 96, 97, 98, 99, 100, 101, 102, 103, 104].

DFT-based NGEF models use ground-state DFT to provide the effective single-particle potential for the scattering formalism. They divide the system into three regions, the left lead L, right lead R and molecule M, with the corresponding division of the DFT Fock matrix

$$\mathbf{F}_{tot} = \begin{pmatrix} \mathbf{F}_L & \mathbf{F}_{LM} & 0 \\ \mathbf{F}_{LM}^{\dagger} & \mathbf{F}_M & \mathbf{F}_{MR} \\ 0 & \mathbf{F}_{MR}^{\dagger} & \mathbf{F}_R \end{pmatrix},$$

For any given energy level, an effective Hamiltonian over the molecular basis functions is built:

$$\mathbf{F}_{eff} = \mathbf{F}_M - \mathbf{F}_{LM}^{\dagger}[\mathbf{F}_L - E\mathbf{I}]^{-1}\mathbf{F}_{LM} - \mathbf{F}_{MR}^{\dagger}[\mathbf{F}_L - E\mathbf{I}]^{-1}\mathbf{F}_{MR}$$

$\mathbf{F}_{eff}$ is then used as an effective one-body Hamiltonian for computing the NEGF. Since the ground-state Fock matrix is used, the assumption implicit in this procedure is that the steady state is a small perturbation from the ground state of the system.

There remain persistent discrepancies between theoretical prediction and experimental measurement of molecular conductance. One finds that the best experiments and theories differ by two orders of magnitude in predicting the conductance of simple junctions.

2.1.3 Time-Dependent Density Functional Theory

TDDFT can be used to study molecular conductance by simulating the evolution of the electron density $\rho(t)$ under a time-dependent potential $v(t)$. By formulating the appropriate potential $v(t)$, the charge transport observed can be taken to represent the flow of charge in the molecule in response to a voltage bias. This approach is supported by formal justification for TDDFT conductance simulations [105, 106, 107], the study of the effect of existing DFT approximations on conductance [108, 109] and protocols for simulating current flow using TDDFT [110, 111, 112, 113]. Our work is most directly preceded by that described in Refs. [110, 112, 113].

As described in the introduction chapter, time-dependent density functional theory is an exact reformulation of many-body quantum mechanics. As such, barring approximations at the DFT level, one would expect such an approach to be exact.

Difficulties with using TDDFT

There are two main obstacles that must be surmounted in order to use TDDFT to conduct full numerical simulations of molecular conductance.

Computational Expense The first difficulty is that of overcoming the computational expense of simulating the systems in real time. The conductance of a molecule in theory is a local molecular property that is independent of the leads, and simulations should in principle model molecules as open systems that lose and gain electrons

from their environment. In practice, however, large closed systems that include the environment are often used instead. Using a closed system to represent an open one places lower bounds on the size of the system used - the simulated system has to be large enough for results to approach convergence with respect to the infinite-size limit [105]. There is also the issue of temporal convergence - experimental timescales are typically much longer than electronic timescales, and hence experimental measurements are of steady-state properties. Therefore, for simulation results to be comparable to experiment, they must allow time for the system to reach steady state. These lower bounds on system size and simulation time impose considerable computational expense on the simulateur.

Despite this expense, however, simulations of credible size (e.g. 50-100 atoms) and time spans (femtoseconds) can now be done [114, 115, 116, 117, 118]. It has also been previously shown that one can attain a quasi-steady state in a simple metal wire using TDDFT [112]. Key to making these simulations practical is the efficient integration of the time-dependent Kohn-Sham (TDKS) equations [119, 120, 121].

Voltage Identification The second major obstacle to TDDFT conductance simulations is the difficulty of assigning the voltage value to a given current simulation. This is not a problem within the Landauer formalism, since the leads are always near equilibrium, the voltage is simply the difference between two well-defined chemical potential values. Differences in effective single-particle energy levels are used in some modern theories to define voltage, the choices being the difference between Fermi-levels conditioned on direction of propagation [122, 91, 123, 124, 125], or Fermi-levels of regions deep within the leads, away from the conducting molecule [94, 95, 96, 97, 98, 99, 100, 101]. The use of Fermi-levels in DFT is not fully justified, as the idea of a Fermi level is only valid for non-interacting particles. KS orbital energies (other than the HOMO), which are used as proxies for Fermi energies, are known to be meaningless [40, 41, 42, 126], and as a result, when computing biases by subtracting two KS orbital energies from each other, one is in fact using an uncontrolled approximation. This difficulty is specific to the DFT formalism, and different in nature from those faced in identifying the experimental voltage with microscopic

reality.

2.2 Methodology

2.2.1 Integrating the TDKS equations

These are the TDKS equations:

$$\mathbf{H}_{\mathrm{KS}}[\rho(t),t]\cdot\phi_i(t) = i\frac{d\phi_i(t)}{dt} \tag{2.1}$$

where $\rho(t) \equiv \sum_i^{occ} |\phi_i(t)|^2$. They describe the evolution of a density in response to time-dependent external potential. Under the KS formalism, an effective non-interacting mean-field Hamiltonian $\mathbf{H}_{\mathrm{KS}}[\rho(t),t]$ is computed from the density $\rho(t)$, and it is under this Hamiltonian that the KS orbitals $\phi_i(t)$ evolve. Under the *adiabatic* approximation [127], the KS Hamiltonian at time t, $\mathbf{H}_{\mathrm{KS}}[\rho(t),t]$ only depends on the density at the same time $\rho(t)$ and the time t itself. We only concern ourselves with adiabatic TDDFT functionals, so this will remain true for the rest of this chapter.

The formal solution to the TDKS equations is:

$$\begin{aligned} \phi(t+dt) &= \mathbf{U}(t+dt,t)\cdot\phi(t) \\ \mathbf{U}(t+dt,t) &\equiv T\exp\{-i\int_t^{t+dt}\mathbf{H}_{\mathrm{KS}}[\rho(\tau)\tau]d\tau\} \end{aligned} \tag{2.2}$$

Notice T, the time ordering operator, which reorders operators such that they always go from later to earlier times from left to right.

$\mathbf{H}_{\mathrm{KS}}[\rho(t),t]$ is composed of three main parts,

$$\mathbf{H}_{\mathrm{KS}}[\rho(t),t] = -\frac{1}{2}\nabla^2 + v_{ext}(t) + v_{Jxc}[\rho(t)]$$

the kinetic energy ($-\frac{1}{2}\nabla^2$) the external potential (v_{ext}) and the inter-electron Coulomb-exchange-correlation potential (v_{Jxc}). Note that only v_{ext} has an explicit time dependence. The kinetic energy operator is time-independent, whereas the

Coulomb-exchange-correlation potential is time-dependent only through the density $\rho(t)$. The implicit time-dependence of the Coulomb-exchange-correlation potential is an important detail which we will revisit later.

The one-particle density matrix (1PDM) $\mathbf{P}(t)$ and the KS orbitals $\phi_i(t)$ are equivalent ways of representing the states of the single-determinant KS wavefunction, with the 1PDM being slightly more general due to its ability to represent ensembles of single-determinant states as well. The 1PDM evolves as such:

$$\mathbf{P}(t+dt) \quad = \quad \mathbf{U}(t+dt,t)\cdot\mathbf{P}(t)\cdot\mathbf{U}^{\dagger}(t+dt,t). \tag{2.3}$$

with $\mathbf{U}$ defined in 2.2. Note that $\mathbf{P}$ is the 1PDM of the Kohn-Sham reference wavefunction, and not the 1PDM of the true wavefunction. We choose to use the 1PDM to represent the system both because it gives rise to more elegant equations and also because for insulators the 1PDM in a spatially local basis is sparse, i.e. the number of nonzero elements eventually scales linearly with system size for large systems [128, 129, 130]. This would allow a linear-scaling implementation of real-time TDDFT to be done in the future.

During a simulation, the total propagation interval $[t, t+\delta T]$ is broken up into T/dt timesteps of size dt. For each time step there are three primary operations: 1) constructing $\mathbf{H}_{\mathrm{KS}}$ 2) constructing $\mathbf{U}(t+dt,t)$ and 3) evolving the 1PDM using Eq. 2.3.

Sophisticated schemes may involve each of these operations multiple times and in a different ordering. For the moderate-sized systems we apply our methods to, the computational effort is dominated by the first step, that of computing the KS Hamiltonian $\mathbf{H}_{\mathrm{KS}}$. Under our scheme, $\mathbf{H}_{\mathrm{KS}}$ is computed a fixed number of times for each timestep, and so efficiency is attained by reducing the number of steps T/dt taken by increasing the size of each timestep dt. Step 2 and 3, under our implementation, are computed using standard computational dense linear algebra routines. To obtain a linear-scaling protocol, one would need to replace all the linear algebra with corresponding sparse matrix algorithms [131].

Time-Ordering

By dividing the propagation interval into timesteps, we assure the correct time-ordering between different timesteps. However, as we use longer individual timesteps, the time-ordering of operators within each timestep becomes important. This can be accomplished by using the Magnus expansion for the time-ordered exponential $T\exp$:

$$T\exp\{-i\int_t^{t+dt}\hat{A}(\tau)d\tau\} \;=\; \exp(\hat{\Omega}_1+\hat{\Omega}_2+\hat{\Omega}_3+\cdots)$$

$$\begin{aligned}
\Omega_1 &= -i\int_t^{t+dt} d\tau\hat{A}(\tau)\\
\Omega_2 &= \int_t^{t+dt} d\tau_1\int_t^{\tau_1} d\tau_2[\hat{A}(\tau_1),\hat{A}(\tau_2)]\\
\Omega_3 &= i\int_t^{t+dt} d\tau_1\int_t^{\tau_1} d\tau_2\int_t^{\tau_2} d\tau_3([\hat{A}(\tau_1),[\hat{A}(\tau_2),\hat{A}(\tau_3)]]+[[\hat{A}(\tau_1),\hat{A}(\tau_2)],\hat{A}(\tau_3)])\\
&\vdots
\end{aligned}$$

where the subscript n in Ω_n indicates the order to which the expansion is correct. For example,

$$T\exp\{-i\int_t^{t+dt}\hat{A}(\tau)d\tau\}\approx\exp(\hat{\Omega}_1+\hat{\Omega}_2+O(dt^3))=\exp(\hat{\Omega}_1+\hat{\Omega}_2)+O(dt^3)$$

Discretization

We have, at this point, converted the time-ordered exponential into a a normal exponential of some integral terms. Next, we discretize the integrals so that they can be implemented as a finite sum on the computer. Blanes *et al.* [132] showed that the operators Ω_n can be efficiently approximated to order $\mathrm{O}(dt^{2N})$ using Gauss-Legendre quadrature and evaluating the integrand $\hat{A}(t)$ at N time points. The first order term Ω_1 is approximated as

$$\int_t^{t+dt} \hat{A}(\tau)d\tau \approx \sum_i^N w_i \hat{A}(\tau_i) + O(dt^{2N+1})$$

where w_i and τ_i are the weights and grid points from the N^{th}-order Gauss-Legendre quadrature. Blanes *et al.* showed that, using the same grid points, τ_i, it was possible to construct the higher order Ω_n terms as well. For example, to second order,

$$\begin{aligned}
\tau_1 &= t + dt/2, \\
\hat{A}_i &= \hat{A}(\tau_i), \\
\hat{\Omega}_1 &\approx -i\hat{A}_1 \cdot dt + O(dt^3) \\
\hat{\Omega}_2 &\approx 0 + O(dt^3) \\
T\exp\{-i\int_t^{t+dt} \hat{A}(\tau)d\tau\} &\approx \exp(\hat{\Omega}_1 + \hat{\Omega}_2) + O(dt^3) \\
&= \exp(\hat{\Omega}_1) + O(dt^3)
\end{aligned} \tag{2.4}$$

and to fourth order,

$$\begin{aligned}
\tau_1 &= t + \left(\frac{1}{2} - \frac{\sqrt{3}}{6}\right) \cdot dt, \\
\tau_2 &= t + \left(\frac{1}{2} + \frac{\sqrt{3}}{6}\right) \cdot dt, \\
\hat{A}_i &= \hat{A}(\tau_i), \\
\hat{\Omega}_1 &\approx -i\left(\hat{A}_1 + \hat{A}_2\right) \cdot \frac{dt}{2} + O(dt^5), \\
\hat{\Omega}_2 &\approx \left[\hat{A}_1, \hat{A}_2\right] \cdot \frac{\sqrt{3}dt^2}{12} + O(dt^5) \\
\hat{\Omega}_3, \hat{\Omega}_4 &\approx 0 + O(dt^5) \\
T\exp\{-i\int_t^{t+dt} \hat{A}(\tau)d\tau\} &\approx \exp(\hat{\Omega}_1 + \hat{\Omega}_2 + \hat{\Omega}_3 + \hat{\Omega}_4) + O(dt^5) \\
&= \exp(\hat{\Omega}_1 + \hat{\Omega}_2) + O(dt^5)
\end{aligned}$$

By evaluating the operator $\hat{A}$, in our case $\mathbf{H}_{\mathrm{KS}}$, N times within the timestep, we

obtain a unitary approximation which is correct to $O(dt^{2N})$.

Predictor-Corrector

The implicit time-dependence of the $\mathbf{U}$ integrand is a significant problem for Magnus integrators. There is a circular dependency which needs to be resolved. The objective of each timestep is to find $\rho(t+dt)$ from $\rho(\tau)$ at $\tau \leq t$. This requires the evaluation of $\mathbf{U}(t, t+dt)$, which in turn involves evaluating $\mathbf{H}_{\mathrm{KS}}[\rho(\tau), \tau]$ for $\tau \in [t, t+dt]$. Since we do not know $\rho(\tau)$ for $\tau > t$, this is a problem.

Previous applications of the Magnus propagator to TDDFT [121] used iterative techniques to determine $\rho(\tau)$ for $\tau > t$. Unfortunately, such an approach requires many, e.g. 5-10, $\mathbf{H}_{\mathrm{KS}}$ builds per timestep, and consequently increases the computational cost of each timestep significantly. Instead of iterating to self-consistency, we use a predictor-corrector scheme:

1. Use extrapolation to *predict* $\mathbf{H}_{\mathrm{KS}}[\rho(\tau), \tau]$ for $\tau \in [t, t+dt]$ from $\mathbf{H}_{\mathrm{KS}}[\rho(\tau), \tau]$ for $\tau < t$

2. Use the approximate $\mathbf{H}_{\mathrm{KS}}[\rho(\tau), \tau]$ and $\rho(t)$ to find $\rho(\tau)$ for $\tau \in [t, t+dt]$.

3. The $\rho(\tau)$ for $\tau \in [t, t+dt]$ are then is used to construct a *corrected* $\mathbf{H}_{\mathrm{KS}}[\rho(t), t]$ for $\tau \in [t, t+dt]$.

4. The *corrected* $\mathbf{H}_{\mathrm{KS}}[\rho(t), t]$ for $\tau \in [t, t+dt]$ are used to compute $\mathbf{U}(t, t+dt)$, which is then used to propagate the $\rho(t)$ to $\rho(t+dt)$.

The predictor step does not involve computing new $\mathbf{H}_{\mathrm{KS}}$, and is hence inexpensive. Also, since we are extrapolating integrands, the extrapolation only needs to be correct to $O(dt^{2N-1})$ for the Magnus expansion to be accurate to $O(dt^{2N})$. The predictor step alone is either dissipative or unstable, and without the corrector step would eventually fail. We use the Magnus expansion for the both the predictor and corrector steps, taking full advantage of the radius of convergence of the Magnus expansion [133] at a modest cost.

In detail, the second order algorithm is illustrated in Fig. 2-1. The component steps are:

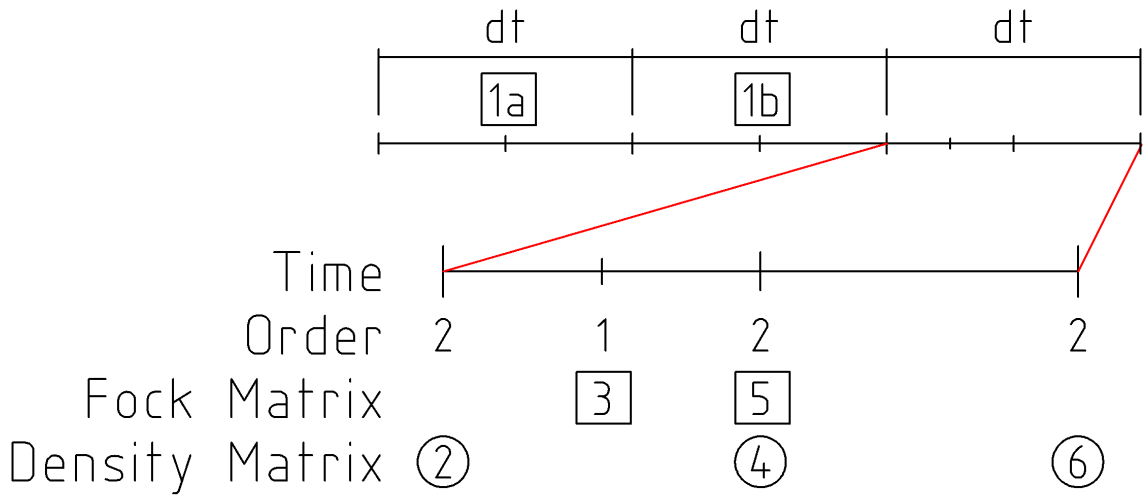

Figure 2-1: Predictor-Corrector routine for the 2^{nd} order Magnus integrator. The order row shows the time order (in dt) to which the matrices in the same column are correct to.

1. (Predictor) $\mathbf{H}_{\mathrm{KS}}$ matrices stored from previous time steps, 1a and 1b, are used to extrapolate $\mathbf{H}_{\mathrm{KS}}$ matrix 3 to order $O(dt)$: $\mathbf{H}_{\mathrm{KS}}(3) = -\frac{3}{4}\mathbf{H}_{\mathrm{KS}}(1a)+\frac{7}{4}\mathbf{H}_{\mathrm{KS}}(1b)$.

2. (Predictor) Using 3, the density matrix 2 is propagated to 4 using Eq. 2.4. This is correct to $O(dt^2)$.

3. (Corrector) Density matrix 4 is used to compute the $\mathbf{H}_{\mathrm{KS}}$ matrix 5 .

4. (Propagation) $\mathbf{H}_{\mathrm{KS}}$ matrix 5 is used to propagate the density matrix 2 to density matrix 6 using Eq. 2.4. This is correct to $O(dt^2)$.

5. (Update) For the next step, $\mathbf{H}_{\mathrm{KS}}$ matrix 1b becomes 1a, $\mathbf{H}_{\mathrm{KS}}$ matrix 5 becomes 1b, and density matrix 6 becomes 2. Other matrices are discarded, and the process starts again from step 1.

We have also derived the analogous 4^{th} and 6^{th} order Magnus expansions using Mathematica [134]. Since our results (see below) indicate these propagators are not preferable unless relatively high accuracy is desired, we only present the (quite involved) 4^{th}, 6^{th} and 8^{th} order predictor-corrector schemes in the appendix.

2.2.2 Numerical Validation

We implemented the Magnus integrators described above in a local version of the program NWChem [135]. For simplicity, we assume the nuclei are fixed and that the time dependence is generated by a (user-specified) sum of pulses of the form

$$\hat{v}_k(r,t) = \alpha_k \hat{O}_k(r) \frac{1}{\sqrt{2\pi}\sigma_k} e^{\frac{(t-t_k)^2}{2\sigma_k^2}} \cos(\omega_k t + \phi_k)$$

where $\hat{O}_k$ is an arbitrary operator. Our implementation uses the existing optimized subroutines to construct $\mathbf{H}_{\mathrm{KS}}$ as needed. Since intuition and numerical experiments dictate that this will be the rate limiting step, this allows us to easily produce efficient, flexible code. Note that, for hybrid functionals like B3LYP [136], NWChem follows the standard prescription of using the Hartree-Fock-like nonlocal form for v_{xc}. This is technically outside the domain of Kohn-Sham DFT - which requires a local v_{xc} - but we do not expect any significant errors from this well-tested approximation. The predictor and propagation phases of the calculation are formulated in terms of standard matrix operations (multiplication, inversion and diagonalization) in the atomic orbital(AO) basis, which are inexpensive for systems with less than a few thousand basis functions. For example, in the AO basis the propagator becomes

$$\mathbf{U}(t) = exp(\mathbf{S^{-1}} \cdot \Omega(t)) = \mathbf{S^{-1/2}} \cdot exp(\mathbf{S^{-1/2}} \cdot \Omega(t) \cdot \mathbf{S^{-1/2}}) \cdot \mathbf{S^{1/2}}$$

where $\mathbf{S}$ is the AO overlap matrix. $\mathbf{U}(t)$ is computed exactly by: 1) Computing $\mathbf{S^{1/2}}$ and $\mathbf{S^{-1/2}}$ (only needs to be done once for all times) 2) diagonalizing $\mathbf{S^{-1/2}} \cdot \Omega(t) \cdot \mathbf{S^{-1/2}}$ 3) exponentiating $\mathbf{S^{-1/2}} \cdot \Omega(t) \cdot \mathbf{S^{-1/2}}$ in the eigenbasis and 4) pre- and post- multiplying the result by $\mathbf{S^{-1/2}}$ and $\mathbf{S^{1/2}}$. There are no approximations due to Chebyshev expansions or Trotter factorizations of the propagator and thus all the Magnus propagators are rigorously unitary.

Our first task is to determine what timesteps are appropriate for these Magnus propagators. The value of having a large critical timestep is perhaps best illustrated by plotting the wall time required to propagate the 1PDM with a given accuracy. In

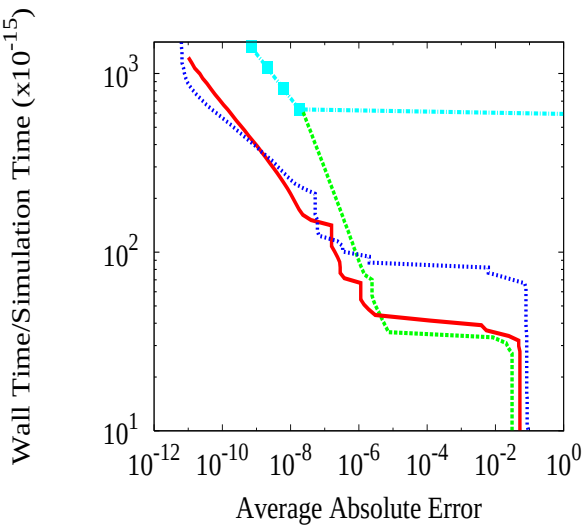

Figure 2-2: Minimum wall time required to obtain a prescribed average absolute error in the final density matrix of methane (B3LYP/6-31G*, 120 a.u of propagation) using various approximate propagators: 2^{nd} order Magnus (green dashed), 4^{th} order Runge-Kutta (teal dot-dashed with squares), 4^{th} order Magnus (red solid) and 6^{th} order Magnus (blue dotted).

Figure 2-2, we present an illustration of this type for methane in a 6-31G* basis [137] using the B3LYP functional [136]. We begin with the molecule in its ground state and apply a dipole pulse along one of the C_2 axes with a Gaussian envelope in time (intensity $\alpha_k = .1$, width $\sigma_k = 5$, center $t_k = 50$, all in a.u.) and evolve the system for 120 a.u. At the end of each simulation, we measure the error

$$Error = \frac{1}{K^2} \sum_{i,j} |P_{ij}^{exact}(t_f) - P_{ij}^{approx}(t_f)|$$

where K is the number of basis functions and the "exact" density matrix is obtained using 6^{th} order Magnus with a very small time step. It is clear from the figure that for very high accuracy the higher order methods outperform the low-order methods. If one was interested in obtaining near-machine precision results, the high order propagators are the clear choice. However, more typically, we are interested in the most economical way to obtain results of reasonable accuracy (e.g. with errors of order 10^{-4} in the 1PDM). As can be seen in Figure 2-2, the *low order* methods are often more efficient for moderate accuracy. While 4^{th}- and 6^{th}- order Magnus are always more

precise than 2^{nd} order for a fixed timestep, 2^{nd} order Magnus is often *more efficient* (i.e. requires the least wall time) due to the fact that it requires one half (one third) as many $\mathbf{H}_{\mathrm{KS}}$ builds as 4^{th} (6^{th}) order Magnus. As a result, for moderate accuracy, 2^{nd} order Magnus can actually be the propagator of choice. We have also compared these Magnus expansions to the commonly used 4^{th} order Runge-Kutta (RK4) integrator. RK4 abruptly diverges even for fairly small time steps of .2 a.u., resulting from the loss of normalization in the Kohn-Sham wavefunctions (see Fig. 2-2). On the other hand, Magnus integrators are convergent for every time step, and with these larger timesteps, Magnus propagators are 15-20 times more efficient than RK4 for these systems. The results from this and other test cases indicate that 2^{nd} order Magnus with a time step of 1-2 a.u. is usually the most efficient way to propagate the density within an error of 10^{-4}-10^{-5}.

2.3 Application: Conductance of a molecular wire

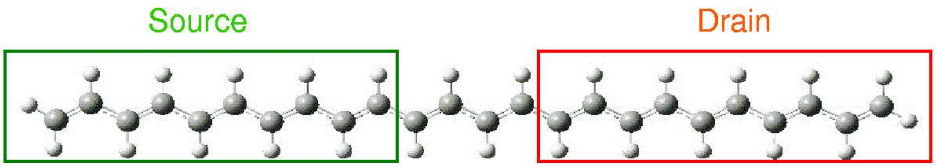

Figure 2-3: Schematic of the source-wire-drain geometry used in the present simulations. The bias is applied to the left and right groups of atoms, which act as a source and drain for electrons, respectively. For different wire lengths (e.g. 50 carbons versus 100) the wire length is kept fixed and the size of the source and sink are varied.

We now outline how TDDFT can be used to compute the conductance of a short, four-carbon segment of a polyacetylene wire where the role of the reservoirs is played by the semi-infinite left- and right- strands of the wire . Now, as stated previously, TDDFT is only able to handle the dynamics of *closed* quantum systems, so we must make a finite model of the infinite wire if we hope to make any progress. We will therefore focus our attention on oligomers of the form $\mathrm{C}_N\mathrm{H}_{N+1}$–$\mathrm{C}_4\mathrm{H}_4$-$\mathrm{C}_N\mathrm{H}_{N+1}$ (see Figure 2-3) with the implicit assumption that N must be chosen "large enough." Our choice of these model systems is inspired by previous work on short carbon wires

embedded in jellium layers [87, 110]. The resulting calculations on these simple wires are intended to illustrate the important points that will arise for more complicated junctions.

We will further restrict our attention to only one particular functional (B3LYP [136]) and one particular basis set (6-31G* [137]). There are undoubtedly interesting variations on these results with different model chemistries. However, our emphasis here is on the changes that must be applied *independent of the model chemistry* in order to extract transport properties from the dynamics. Thus B3LYP/6-31G* simply serves as a good model chemistry and could be replaced with any other combination of functional and basis set. Further, since we are interested in treating elastic conduction, the nuclei are held fixed throughout each calculation at their optimal positions at *zero bias*.

2.3.1 Voltage Definitions

We focus on potential-driven (rather than current-driven) conduction. In this case, there are at least two different prescriptions one can use to simulate conduction using TDDFT, depending on whether the current is driven by a chemical potential bias (μ) or a voltage bias (V). In the V case, the TDDFT prescription is to begin with the system at equilibrium with no external potential and then turn on a voltage V_L (V_R) in the left(right) lead such that V=V_L-V_R. The resulting voltage bias will drive a current from left to right for positive V. The μ case is somewhat more complicated. Here, one considers that the system is connected to two reservoirs (L and R) that are held at constant chemical potential (μ_L and μ_R). If the leads are large enough, this can be accounted for by equilibrating the system with each lead held fixed at its own chemical potential (μ_L or μ_R). Then, at time zero, the constraining chemical potential is removed allowing current to flow from regions of high chemical potential to low. Depending on the experiment, either scheme could be the more appropriate model, but the μ- and V- biased prescriptions tend to give very similar I-V curves [138]. We expect differences to primarily manifest themselves in the distinct transient dynamics of μ- and V- biased junctions [139] and the convergence of the two prescriptions

toward the thermodynamic limit. Since both of these issues are germane to the task of making the simulations "large enough" and "long enough" to mimic experiments, we will examine both prescriptions in what follows.

No matter which bias scheme one chooses, there is necessarily some ambiguity about how one defines the potential. The only piece of experimental information we have is that, when averaged over a macroscopic volume deep in the leads, there is a constant shift of the potential on the left relative to the right. This leads to any number of different *microscopic* potentials that satisfy this condition. Step-like potentials [97, 112], ramp potentials [94, 110], and potentials defined in terms of localized orbitals [96, 98, 100, 101] all give qualitatively similar I-V curves. In this paper, we propose to use atomic Löwdin populations [140] to define the potential in the following way. First, we note that the Löwdin population (N^X) for a given set of atoms (X) can be written as the trace of an operator matrix with the one particle density matrix ($\mathbf{P}$):

$$N^X \equiv Tr\mathbf{P}\mathrm{W}^{\mathrm{X}} \tag{2.5}$$

where $\mathbf{W}^{\mathrm{X}}$ is given by

$$W_{ij}^X \equiv \sum_{\alpha \in X} S_{i,\alpha}^{1/2} S_{\alpha,j}^{1/2} \tag{2.6}$$

and the summation runs only over atomic orbitals centered on atoms in the fragment X. It has been shown that $\mathbf{W}^{\mathrm{X}}$ is a projection operator [141], so the atomic populations are always non-negative. Next, we define the the bias potentials $\mathbf{V}^{\mathrm{B}}$ ($B = L, R$) to be simply a constant V_B times the appropriate Löwdin operator:

$$\mathbf{V}^{\mathrm{B}} \equiv V_B \mathbf{W}^{\mathrm{B}}.$$

This choice is motivated by previous studies within our group, which show that using this population definition within constrained DFT leads to a consistent treatment of long-range charge transfer excited states [142, 19] and low-lying spin states [143].

Given this definition of the potential, both the μ- and V-biased cases can be simulated using an appropriate time dependent potential $\hat{V}(t)$. For the chemical potential, $\hat{V}(t) = \mathbf{V}^{\mathrm{B}}\theta(-t)$, while for the voltage bias, $\hat{V}(t) = \mathbf{V}^{\mathrm{B}}\theta(t)$ where $\theta(t)$ is the Heaviside step function. In both cases, the system is equilibrated to the ground state at $t = -\infty$ (or, equivalently, at time t=$-\epsilon$) and then propagated forward in time using TDDFT. Because the system always begins in the ground state, there are no ambiguities about initial wavefunction dependence in either case. We note that the function used to turn the potential on or off in time is arbitrary. However, the average currents presented below are insensitive to the choice of the switching function as long as $f(t)$ changes from 0 to 1 within ≈ 15 a.u. Slower switching results in a partial depletion of the finite reservoirs before the bias is completely established.

In principle, the current through the device also needs to be defined. In the experiment, the current is measured deep in the leads and in a finite system it is not clear where the dividing surface should be placed in a simulation to best mimic the experiment. However, because we have chosen to define our bias in terms of a particular (albeit arbitrary) population definition, the definition of the current is uniquely determined via the continuity equation:

$$\frac{1}{2}\int_L \vec{I}\cdot\vec{n}d\sigma_L - \frac{1}{2}\int_R \vec{I}\cdot\vec{n}d\sigma_R = \frac{d}{dt}\frac{(N^L - N^R)}{2} \tag{2.7}$$

where σ_R and σ_L are the surface elements associated with the boundaries of the left and right leads. The left hand side is the current we seek: the average of the current out of the left hand lead (first term) and the current into the right hand lead (second term). The surface implied by the use of Löwdin populations is extremely complicated to define, and hence the left hand side is extremely difficult to evaluate. On the other hand the right hand side is just the time derivative of the Löwdin populations, easily obtainable from TDDFT. Further, since our bias couples directly to N^L and N^R it is most natural to think of the fluctuations in these variables as generating all the dynamics. For the present case, we use the right side of Eq. 2.7 to define the current through the junction in our simulations. Indeed, for any given definition of

the potential, Eq. 2.7 gives a unique prescription for the current through the device region. This equivalence is part of a deep connection between current and number fluctuations in electrical junctions [144].

2.3.2 Current Averaging

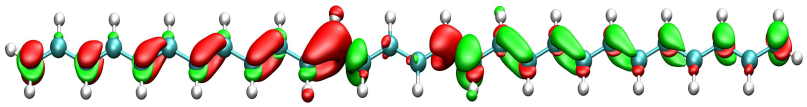

Figure 2-4: Initial density corresponding to a chemical potential bias in polyacetylene. Red indicates charge accumulation and green charge depletion relative to the unbiased ground state. At time t=0 the bias is removed and current flows from left to right.

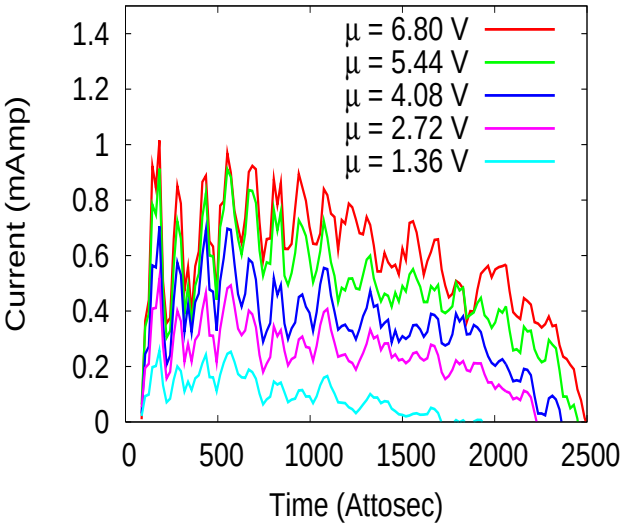

Figure 2-5: Transient current through the central four carbons in $C_{50}H_{52}$ at a series of different chemical potential biases. There is an increase in current as voltage is increased, along with large, persistent fluctuations in the current. The currents are converged with respect to time step and the apparent noise is a result of physical fluctuations in particle flow through the wire.

We first study the molecular wire $C_{50}H_{52}$ under a chemical potential bias. The electronic energy of the molecule is minimized while the left (right) $C_{23}H_{24}$ segments are subject to a bias of $+\mu$ ($-\mu$) in the Löwdin potential. An example of one such initial state is illustrated in Figure 2-4 for a short wire. At time zero, the bias is removed and

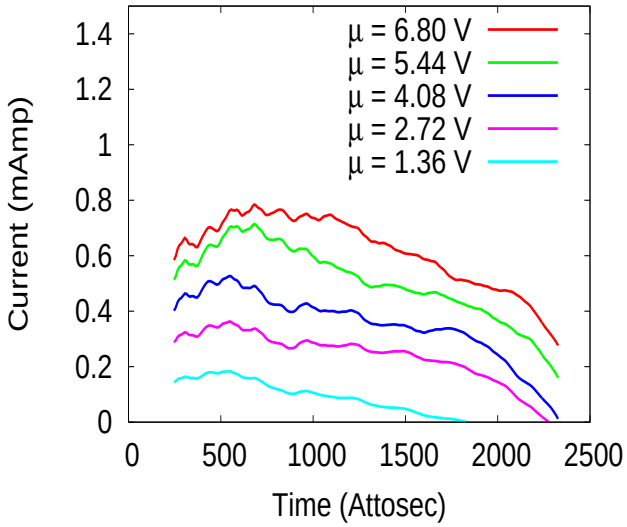

Figure 2-6: Transient current through the central four carbons in $C_{50}H_{52}$ at a series of different chemical potential biases smoothed over a time window of width $\Delta t = .36 fs$. The average currents are now move clearly visible. The slow decay of the current at later times results from the partial equilibration of the finite left and right leads.

the electrons are allowed to relax. Figure 2-5 shows the resulting current at a series of different voltage biases. Several important points follow from this figure. First, even for this wire length, the left and right chemical potentials equilibrate *very rapidly*, as evidenced by the fact that the current pinches off within about 2.5 fs. Second, there is clearly a general trend toward increasing current as we increase the bias, reflecting the current-voltage relationship for this wire. Finally, significant transient current fluctuations ('noise') hinder the identification of the average current based on in these calculations.

The noisiness of the data can be overcome by realizing that experimental measurements are made on a much coarser timescale than the timestep of our simulation. A better approximation to the experimental current can be made by *averaging* Eq. 2.7 over a relatively wide time interval Δt:

$$I_{avg} \equiv \frac{(N^L(t) - N^R(t)) - (N^L(t - \Delta t) - N^R(t - \Delta t))}{2\Delta t}. \tag{2.8}$$

This expression physically corresponds to the gedanken experiment where an apparatus with finite time resolution Δt checks the number bias twice in succession and

then uses the mean value theorem to approximate the derivative. This process will *ignore* fluctuations that occur on a timescale faster than Δt resulting in qualitatively smoothed current profiles. Figure 2-6 shows the transient currents obtained when one applies Eq. 2.8 (with $\Delta t = .36fs$) to $C_{50}H_{52}$ at various biases. As expected, the transient fluctuations are suppressed and one can now see the earmarks of smoothly increasing current in these molecular wires. It is somewhat remarkable that these molecules are able to attain a quasi-steady state so quickly (faster than 1 fs), and similar observations have been made previously for a simple gold wire [112]. We attribute this fast relaxation in molecular wires to the nearly perfect coupling between the "leads" and the "wire". Strong system-bath coupling leads to a very short lifetime for transient states and quick relaxation.

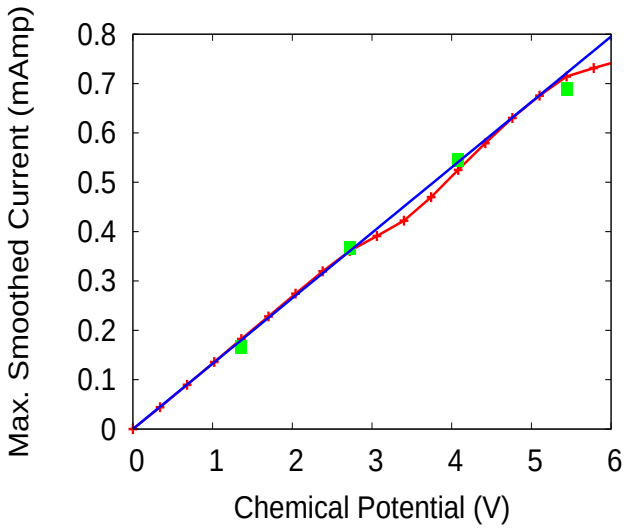

Figure 2-7: Maximum smoothed current through the central four carbons in $C_{50}H_{52}$ as a function of chemical potential bias (red pluses). For comparison, we also present the analogous result for the central carbons in $C_{100}H_{102}$ (green squares) demonstrating convergence of the calculation with respect to lead size. The blue line is a linear fit to the $C_{50}H_{52}$ data at low bias indicating that polyacetylene is an Ohmic resistor with a conductance of $\approx .8G_0$

If we interpret the maximum smoothed currents in Figure 2-6 as the appropriate steady-state current for each voltage, we obtain the current-voltage relation shown in Figure 2-7. From this graph it is clear that the current through the wire increases in very nearly linear fashion over a very wide range of voltages. There is a leveling off in current at large voltages that results from an essentially complete depletion

of the valence states of the central part of the wire. Perhaps surprisingly, while the conduction is quasi-Ohmic, the conductance is *not* one quantum of conductance ($G_0 \approx 74.5\mu S$). Instead, the low-bias behavior is better approximated by a conductance of .8 G_0. Initially, one might suspect that this is a finite size effect; that is to say that if the leads were "long enough" the conductance would approach G_0. To check this we have run similar calculations changing the size of the leads in the wire, keeping our attention on the conductance of the central four carbons. As an example, Figure 2-7 also shows a few I-V points for $C_{100}H_{102}$. We have considered only a few voltages because of the increased computational burden per voltage point. However, even this sparse set of data allows us to conclude that the differences between the C_{50} and C_{100} data are quite small and have little influence on the conductance. Thus, our approach of using larger and larger finite systems has indeed converged to the open system limit, but with a finite wire resistance.

In order to understand the origin of the conductance in this wire, we return to the original Landauer picture. Because the "leads" have an essentially perfect connection with the "molecule" in these polyacetylene wires, the appropriate picture involves strong coupling between the leads and the molecule. This coupling *broadens* the molecular levels to the point where the I-V curve becomes featureless. Recall that, in the weak coupling limit, the current displays a staircase structure as a function of bias, and so Figure 2-7 should be interpreted as the limiting case where this staircase pattern is "smeared out" yielding a smooth I-V characteristic. Thus, the conductance of the central four carbons should not be viewed as coming from a single quantum state, but from the superposition of a number of broadened states. The numerical value of the conductance thus reflects the density of states available in this wire.

2.3.3 Comparison to NEGF results

Assuming that the dynamics described so far approximate the steady state of the infinite system limit, the present approach is equivalent to the NEGF method [106]. Thus, as a test, we can compare the real-time DFT results with those obtained via DFT-NEGF. We use Lorentzian broadening on the finite lead to simulate the infinite

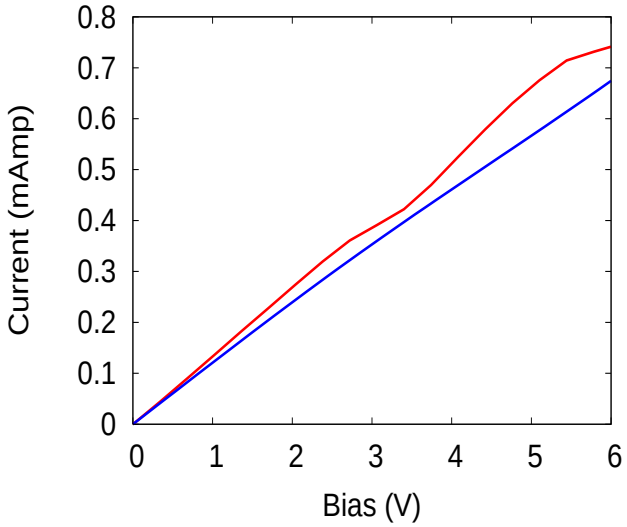

Figure 2-8: Maximum smoothed current through the central four carbons in $C_{50}H_{52}$ as a function of chemical potential bias using real-time TDDFT (top red line) and an NEGF approach described in the text (bottom blue line). The two calculations are nearly identical at low bias and differ somewhat at higher biases due to the lack of self-consistency in the NEGF results.

size limit [99]. We do this by first using Löwdin's symmetric orthogonalization [140] on $\mathbf{H}_{\mathrm{KS}}$, partitioning the molecule in exactly the same way as the real-time TDDFT simulation. We then add a small imaginary component, $\epsilon = .055$, to the eigenvalues of the orthogonalized $\mathbf{H}_{\mathrm{KS}}$ matrix, broadening the energy distributions of the lead states so that they now resemble the continuum present in infinite-sized leads. The value of ϵ was set by maximizing the current, consistent with our practice of picking the maximum current from the smoothed real-time TDDFT trajectories. Using the broadened density of state profile, we then computed the current using techniques outlined in Ref. [99]. The NGEF approach we use is not self-consistent, because $\mathbf{H}_{\mathrm{KS}}$ is computed using the ground-state electron density. However, the results obtained should be comparable to real-time TDDFT insofar as the self-consistent density resembles the ground-state density at low biases.

The NEGF results obtained for $C_{50}H_{52}$ are presented in Figure 2-8, alongside real-time TDDFT results from the previous section. The two techniques agree almost completely at low bias, and give qualitatively similar results at larger biases. Much of the difference can be attributed to the lack of self-consistency in the NGEF procedure

- at greater biases, the self-consistent density deviates more from the ground-state, leading to greater differences between self-consistent and ground-state results.

These results support our assertion that the real-time TDDFT simulations are informative of the open-system limit - enlarging the leads does not change the conductance curve (Fig. 2-7), and the results are consistent with NEGF calculations (Fig. 2-8) in the low-bias limit. We are hence able to conclude that even at relatively small lead sizes, our system already reflects the electron transport dynamics present in the large lead limit. This gives us reason to believe that a simulation of a metal-molecule-metal with finite metal leads would also be relevant to the experimental infinite metal lead setup. As we explain later in this chapter, however, we anticipate additional challenges for this latter case because of the physical relevance of *noise* in the simulation.

2.3.4 Voltage Biased Case

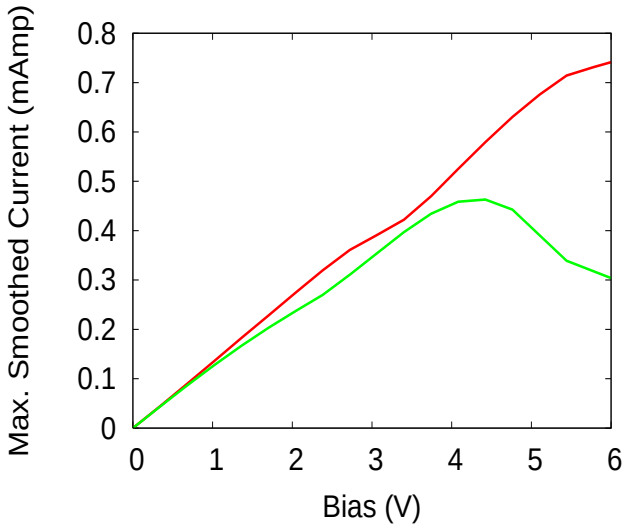

Figure 2-9: Maximum smoothed current through the central four carbons in $C_{50}H_{52}$ as a function of chemical potential bias (top red line) and voltage bias (bottom green line). The results are quite similar until 4 V, at which point the bias is so large that the finite width of the valence band for polyacetylene causes the conductance to plateau in the voltage biased case.

The preceding results were all obtained using a chemical potential bias. We have also investigated the effects of using a voltage bias to generate the conductance and find that the results are qualitatively no different. To illustrate this point, the current-

voltage plot for $C_{50}H_{52}$ using both μ and V biases is shown in Figure 2-9. Clearly, the differences between the two schemes are small until a bias of about 4 V, at which point the voltage biased results show some negative differential resistance. A brief inspection reveals that the plateau at high bias again results from the finite width of the polyacetylene valence band, which apparently has a somewhat larger influence in the voltage biased case.

2.3.5 Transient Fluctuations

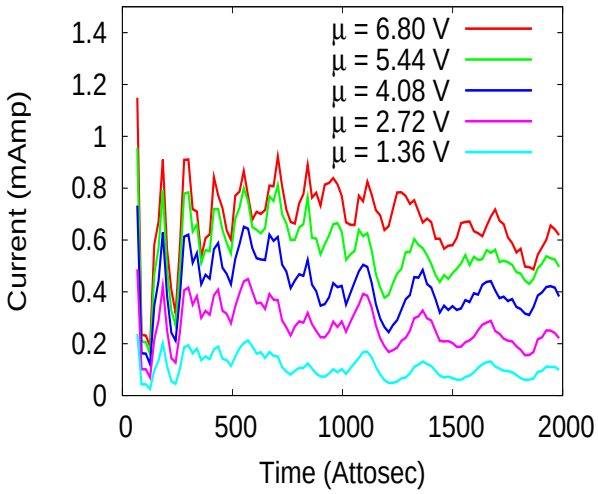

Figure 2-10: Transient current through the central four carbons in $C_{100}H_{102}$ at a series of different chemical potential biases. The current fluctuations previously observed with smaller reservoirs in $C_{50}H_{52}$ persist and are therefore not associated with a finite size effect.

Note that the fluctuations in the current shown in Fig. 2-5 *are not numerical noise*. These fluctuations are present even at smaller timestep sizes, and reflect deterministic variations of the current in the wire. Furthermore, the fluctuations are also converged with respect to lead size, and not due to the finite size of the leads. For example, examining the current fluctuations with larger reservoirs in $C_{100}H_{102}$ one notices that the magnitude of the variations in the current apparently approach a constant value rather than falling to zero (See Figure 2-10). This fact indicates that these fluctuations are characteristic of some physical current noise in the wire. We can easily quantify this noise from the transient current traces shown in Fig. 2-10 by simply computing

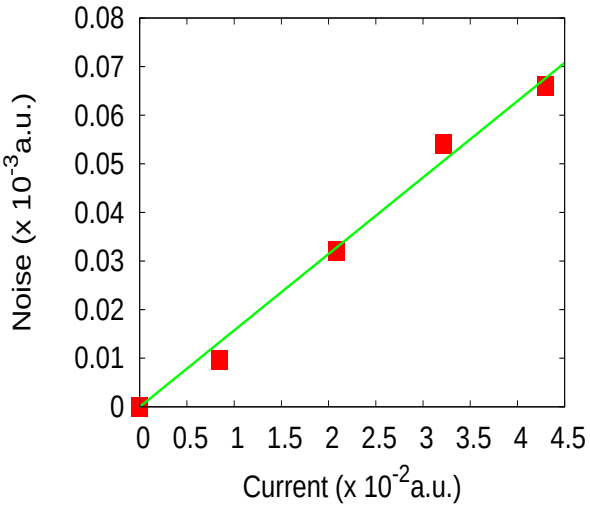

Figure 2-11: Statistical noise in the current through the central four carbons in $C_{100}H_{102}$. The data (squares) can be fit to a sub-Poissonian distribution (line).

the statistical uncertainty:

$$S(I) = \int \langle \hat{I}(t) - \bar{I} \rangle^2 dt \tag{2.9}$$

where $\bar{I}$ is the average current for the given voltage and the integration runs over the quasi-steady state currents shown in Figure 2-10. We find that it is somewhat more difficult to converge the noise than the conductance - somewhat longer time windows, and hence somewhat longer wires, are required to obtain accurate noise compared to the conductance. This is consistent with the experimental situation, where successively higher moments of the electron counting distribution are progressively more difficult to obtain [145]. However, if we average over a window of 70 a.u. ($\approx$ 1.7 fs), we obtain reasonably stable results for the noise in $C_{100}H_{102}$, as shown in Figure 2-11. Clearly the noise increases linearly with increasing current, but the slope is much less than 1, indicating a sub-Poissonian process. It is not clear what the origin of this noise is. It may be that the application of the bias leads to a finite population of one or more molecular excited states which then keeps the system from relaxing to a steady state. Alternatively, this could be the result of the interference of incoming and outgoing waves within the molecule. We have not successfully isolated

the origin of these fluctuations, and a case can be made for either picture.

Even without a molecular interpretation, the noise does give us some important clues about real time transport simulations. There is a large body of work that discusses the rich history of conductance noise in quantum transport [146, 147, 148, 149, 145, 150, 151, 152]. In particular *shot noise* describes the instantaneous, quantum fluctuations of the current about its mean value:

$$S \equiv \int \langle (I(t) - \bar{I})^2 \rangle. \tag{2.10}$$

where the average $\langle ... \rangle$ is taken over a time long compared to the characteristic time $\tau_0 \equiv e/\bar{I}$. Despite the mathematical similarity, the temporal noise (Eq. 2.9) is *not* shot noise (Eq. 2.10). Shot noise arises from quantum uncertainty of the current for identically prepared systems, whereas our simulations reflect temporal uncertainty in the average current. However, for the ideal case of single-electron transport through a junction of transmittance T, the shot noise is is also sub-Poissonian [146, 147]:

$$S \equiv e(1-T)\bar{I}$$

If we use this expression to fit the temporal noise in polyacetylene, we obtain $T \approx .98$, as compared to the numerically observed conductance of $.8G_0$. This discrepancy is to be expected on two grounds. First, because of the finite timestep, our simulations actually reflect the noise *power* over a particular interval rather than the noise itself. Second, shot noise involves *two particle* correlations while the noise we consider involves fluctuations in a one particle observable. These two quantities are in fact related via the fluctuation-dissipation theorem [153]: by considering the response of the system to all possible potential perturbations, two particle observables such as $\langle \hat{I}^2 \rangle$ can be obtained without further approximation. By restricting ourselves to spatially uniform bias potentials, we recover only a fraction of the associated fluctuations and observe an attendant reduction in the noise. Hence the analogy with shot noise can only be used for qualitative analysis of the temporal fluctuations in our simulations.

A characteristic of shot noise is its tendency to increase as transmittance is re-

duced. This suggests that for molecular junctions, which typically have much lower conductances (typically $.01G_0$), the temporal noise will be much more significant. In contrast, a purely metallic wire would experience no shot noise in the large lead limit because it is a perfect conductor. This explains the observation that for a gold wire [112] the current-versus-time plots smoothly approach a plateau, while for polyacetylene, which only reduces the conductivity by 20%, noise already becomes important. Thus, it seems likely that the transient currents in a $.01G_0$ junction may be dominated by shot noise over quite large time intervals, making the interpretation of real-time simulations much more challenging.

2.4 Conclusions

In this chapter, we have demonstrated the feasibility of performing real-time TDDFT simulations of the transient current dynamics through a molecular wire at finite bias. These results were made possible by an efficient algorithm for integrating the TDKS equations in a localized basis that allows us to take very large time steps. Taking polyacetylene as our prototypical example, we have shown that one can make a consistent definition of current and bias within TDDFT and obtain quantitative predictions of the current at finite bias by averaging the instantaneous current over a microscopic time window. Further, we have verified that these currents are converged with respect to the size of the reservoirs and that the results agree with the corresponding NEGF current-voltage character. Finally, we have investigated the temporal current noise and shown that for these wires, the noise does not decay to zero as the wire length is increased, but approaches a finite value. We argue that this noise is likely to be more significant in junctions that have low transmittance, which implies that real-time conductance simulations of MMM junctions -which have much lower transmittances than an isolated wire - may be quite challenging. In the near term, we plan to use TDDFT to study the conductance properties of some simple MMM junctions. The translation of this framework to such devices is straightforward in principle: one constructs a supersystem that contains enough metal atoms to mimic the 'bulk' properties of the leads and propagates the system under an appropriate bias until a reliable

average current can be extracted. Novel challenges that will need to be addressed for MMM junctions include the sensitivity of SCF convergence for metallic systems, the uncertain structure of the metal-molecule interface and the expected increase in noise due to the low transmittance of the junction. The points raised here – efficient integration of the TDKS equations, consistent definition of the bias potential, the importance of smoothing to obtain the relevant current – will facilitate study of these more technologically relevant devices.

For our time-dependent simulations, the average current provides an important validation of the model; by comparing to other predictions of the DC current, we can verify that our simulation is "large enough" and "long enough". However, once the model has been validated, the average current is only one of a host of properties a real-time simulation gives access to. Electroluminescence, finite bias impedances, driven rectification and current triggered molecular dynamics can all be treated within the framework described here. Hence, this "microcanonical" picture of electron transport dynamics opens up a huge array of physical processes for theoretical study and we are currently in the process of analyzing some of these effects. In particular, it may be possible to predict the shot noise in a molecular junction without further approximation using TDDFT in conjunction with the fluctuation dissipation theorem [154].

Finally, in regards to current voltage predictions, it has been pointed out that there are significant errors in the DFT currents at low bias due to improper cancellation between self-interaction errors [109] and static electron correlation [93, 100]. We have shown that for time-independent problems, the balance between static correlation and self-interaction can be controlled by applying physically motivated constraints to the electron density [142, 143, 19]. That approach, which we have dubbed Configuration Interaction Constrained Density Functional Theory, is described in the next chapter. The analogous time-dependent approach, which constructs reference states using constraints, and represents the time-evolution of the system within the space of those states, could be used to study conductance in the future.

Chapter 3

Dissociation Curves using Constrained Density Functional Theory Configuration Interaction

Note: The bulk of this chapter has been published in Ref. [1].

3.1 Introduction

Electron correlation is the difference between an exact treatment of electronic structure and the physics present in Hartree-Fock, where mean-field inter-electron Coulomb repulsion and Pauli exclusion have been accounted for. It affects important observables including ground state geometries, reaction barriers and dissociation energies.

Diatomic molecules experience a varying ratio of static to dynamic correlation depending on how long the interatomic distance is. At distances close to the equilibrium, the electrons are at a close distance to each other and experience strong Coulomb repulsion - this corresponds to dynamic correlation. At distances far from equilibrium, near the dissociative limit, the near-degeneracies in energies lead to significant static correlation. Correlation energies in diatomic molecules are dominated by one of the two forms of correlation depending on distance of separation, making dissociation curves ideal for contrasting dynamic correlation with static correlation.

DFT is able to treat dynamic correlations well, but tends to fail when static correlation becomes important. In this chapter, we develop a method where constrained DFT (CDFT) is used to construct an active space where dynamic correlation has

been accounted for, within which a new solution is constructed thus adding in static correlation. We demonstrate the efficacy of the method by computing dissociation curves for a few small diatomics, where we contrast our approach with the failures of conventional DFT near dissociation [155]. We show that our method is able to accurately treat both dynamic and static correlation dominated regimes of the dissociation curve more efficiently than wavefunction-based methods. The difference in efficiency is significant as it makes future treatment of bond breaking and formation in larger systems possible.

3.2 State of the Art

Under *ab initio* wavefunction-based methods, static correlation can be treated by using multiple reference (MR) methods [11], which use a multiple determinant reference state, and dynamic correlation can be treated by the use of perturbation theory on an uncorrelated single-determinant reference state [156, 157].

Density functional theory is in principle capable of treating both forms of correlation, but in reality DFT approximations deal with dynamic correlation a lot better than static correlation [50]. It is for this reason that DFT tends to have good accuracy [158, 159, 10] when dynamic correlation dominates, i.e. near equilibrium geometries, and fares worse at geometries far from equilibrium.

Cases where most DFT functionals fail to describe dissociation correctly include H_2^+, where it erroneously predicts a barrier to dissociation / association [160]. DFT also predicts the dissociation of LiF into partially charged atoms, whereas in reality it dissociates into neutral atoms [161, 162, 163]. In the case of neutral H_2, unrestricted DFT gets the energy correct but with a broken-symmetry spin density, instead of the correct symmetric spin density of a pure singlet [164, 165].

Improvements have been attempted while staying within the DFT formalism. It is DFT's ability to compute dynamic correlation cheaply that makes it attractive as a starting point for methods attempting to treat both types of correlation. Staying strictly within DFT, there are many ways in which multireference character is introduced, including the use of non-integer occupation numbers [166], an ensem-

ble of single-determinants [167, 168] and time-dependent density functional theory [169]. There have also been attempts to combine DFT with wavefunction-based MR methods like MCSCF [170], CASSCF [171], VB [172] and MRCI [173, 174]. A key difficulty with mixing wavefunction and DFT-based methods is that of avoiding double-counting, since there is no clear separation between dynamic and static correlation terms. There are also issues with using a density functional reference. Firstly, the KS orbitals provided by DFT have no physical significance [40, 41, 42, 126], and using them as a reference for perturbation is an uncontrolled approximation. Secondly, the accuracy of DFT is often attributed to the cancellation of error afforded by many of the approximations - in this case, the effect of missing static correlation is cancelled in part by the erroneous self interaction error (SIE) of DFT functionals. If we were to treat static correlation more accurately without accounting for SIE, the results would likely be worse.

3.3 Our Method: Constrained Density Functional Theory Configuration Interaction (CDFT-CI)

We formulate a new method in the configuration interaction (CI) tradition, using CDFT to construct an active space within which we compute the matrix elements of the full Hamiltonian, which we then solve to arrive at our final answer. We call this approach Constrained Density Functional Theory Configuration Interaction (CDFT-CI). The active space is picked in a way as to, one, ensure that important configurations have been covered, and two, ensure that static correlation and SIE are both minimized in the individual basis states. The states we have identified for this purpose are localized electronic states as defined via CDFT, technology previously developed within the group [142, 19], and described in the introduction chapter. These states are prime candidates for an active space because they experience both little SIE and little static correlation, and, as we will show later, can be systematically enumerated to form a complete space by allusion to Valence Bond (VB) theory [175], all without reference to orbitals.

3.3.1 Identifying an Active Space

As in other CI methods, we begin by identifying the active space which we use to represent the electronic state. The choice of active space is informed by previously formulated systematic approaches for finding energetically significant configurations, and also by the knowledge of deficiencies in existing DFT functionals.

There are a number of CI methods in wavefunction-based electronic structure, and they all come with prescriptions for picking an active space. Unfortunately, most of those prescriptions call for delocalized molecular orbital configurations as a basis, and CDFT does not do well for such configurations. There is, however, an exception in the case of VB theory [175]. VB theory identifies configurations which resemble ground states subject to spatial and spin density constraints, making them ideal for CDFT-CI. Moreover, it has been shown that active spaces under CASSCF can be systematically transformed into VB active spaces [176, 177]. For example, the CASSCF(2,2) active space for single bond breaking consists of the configurations $|\sigma\bar{\sigma}\rangle$, $|\sigma\bar{\sigma}^*\rangle$, $|\sigma^*\bar{\sigma}\rangle$ and $|\sigma^*\bar{\sigma}^*\rangle$, which corresponds to the VB active space with ionic terms $|L\bar{L}\rangle$, $|R\bar{R}\rangle$ and covalent terms $|L\bar{R}\rangle$, $|R\bar{L}\rangle$. These VB configurations can easily be identified with CDFT states that constrain spin charge density. Exploiting these facts, we adopt the following prescription for identifying CDFT-CI active spaces. First, we find the appropriate CASSCF(n,m) active space for the system we are studying. Second, we transform that space with a unitary transformation into a number of VB theory configurations. We then find the spatial and spin density constraint that corresponds to each VB active space state, and thus define the CDFT-CI active space. This prescription allows us to adapt the systematic enumeration of configurations that CASSCF offers to CDFT-CI. Note that when m and n are big, there may exist CASSCF(n,m) configurations that do not correspond to any CDFT constraint. In such cases, we have not solved the problem of finding a CDFT-CI active space. In the applications that follow, however, the procedure as defined here is sufficient.

As might have been noted, we go to considerable effort to obtain localized configurations for our active space. We are motivated to do so for two main reasons.

One, due to self-interaction error, available density functionals tend to underestimate the relative energy of fractionally charged states compared to integer charged states [47, 48]. This effect is best seen when an electron is delocalized between distant nuclei, like in the case of stretched H_s^+. Not only is there a large error in the energy of such radical dissociations [160], but that error also gets worse with larger distances [178, 179]. In the case of neutral, closed-shell molecules, the erroneous SIE can cause dissociated states to have the wrong density [161, 162, 163]. We are interested in describing dissociation accurately, and so it is important to avoid SIE by using localized configurations. Two, when stretching a singlet diatomic under Kohn-Sham DFT (KS-DFT), the dissociation energy obtained via common functionals misses the strong static correlation component present in the stretched system. In contrast to the KS-DFT ground state, broken-symmetry localized configurations have less static correlation and can be accurately treated by DFT [165]. Taking advantage of this fact, we use constraints to break the spin symmetry in each of our localized configurations, and then restore the right spin symmetry through configuration interaction later on.

The explicit enumeration of configurations has a drawback for treating extended systems. Even when the added molecules do not interact with the existing ones, they add multiplicatively to the active space basis. Let's say a molecule requires N active configurations to describe - to represent two such molecules placed far apart from each other, one would need to account for every possible combination of those N configurations, leading to the need to consider N^2 configurations. If one wishes to enforce size-consistency, the exponential growth of complexity with system size is not resolved with the CDFT-CI approach. However, the severity of the problem is reduced by the efficiency of DFT.

3.3.2 Computing Matrix Elements

Defining constraints for each configuration

$\mathbf{w}_c$ in Eq. 1.22 assigns part of the electron density measured at each spatial point to molecular fragment C, which is defined as a set of atomic centers. The sum total of

the densities assigned to every fragment results in the total density. For consistency, we require that our definition of $\mathbf{w}_c$ be the same throughout the CDFT-CI procedure. Previous work by our group [19, 20] showed that Becke's spatial weight functions [18], which assigns density to atomic centers, are a good choice for the atomic density assignment, and we use that definition here.

When fragments are far apart from each other, it is easy to assign N_c - one simply counts up the number of electrons in the constrained region, which due to the separation is usually a well-defined integer. When the individual fragments are close to each other, however, it is no longer so clear how many electrons should be in each fragment. In such cases, we use the following procedure to define N_c.

Depending on the configuration we are interested in, we first compute a reference promolecule density ρ_0 from a combination of molecular fragment densities

$$\rho_0(\mathrm{r}) = \sum_{\mathrm{a}} \rho_{\mathrm{a}}(\mathrm{r}). \tag{3.1}$$

where index a runs over the individual molecular fragments. The choice of fragment charges identifies the configuration we are trying to obtain. For example, for a molecule consisting of two fragments A and B, the promolecule density corresponding to the ionic configuration $\mathrm{A^+B^-}$ would be the combination of the $\mathrm{A^+}$ and the $\mathrm{B^-}$ densities, while the promolecule density corresponding to the covalent configuration $\mathrm{A{\uparrow}B{\downarrow}}$ would be the result of combining densities from the two open-shell fragments $\mathrm{A{\uparrow}}$ and $\mathrm{B{\downarrow}}$ that have $M_s = \pm\frac{1}{2}$ respectively. The atomic fragment densities we use are always spherically averaged.

Given a reference promolecule density ρ_0, we then constrain the expectation of all the fragment density operators $\mathbf{w}_c$ to give the same constraint value as in the promolecule density:

$$\begin{aligned} \int \mathbf{w}_C(\mathrm{r})\rho^{\mathrm{i}}(\mathrm{r})\mathrm{dr} - \mathrm{N_c^i} &= \int \mathbf{w}_C(\mathrm{r})\rho^{\mathrm{i}}(\mathrm{r})\mathrm{dr} - \int \mathbf{w}_{\mathrm{C}}(\mathrm{r})\rho_0^{\mathrm{i}}(\mathrm{r})\mathrm{dr} \\ &= \int \mathbf{w}_C(\mathrm{r})(\rho^{\mathrm{i}}(\mathrm{r}) - \rho_0^{\mathrm{i}}(\mathrm{r})) = 0, \end{aligned} \tag{3.2}$$

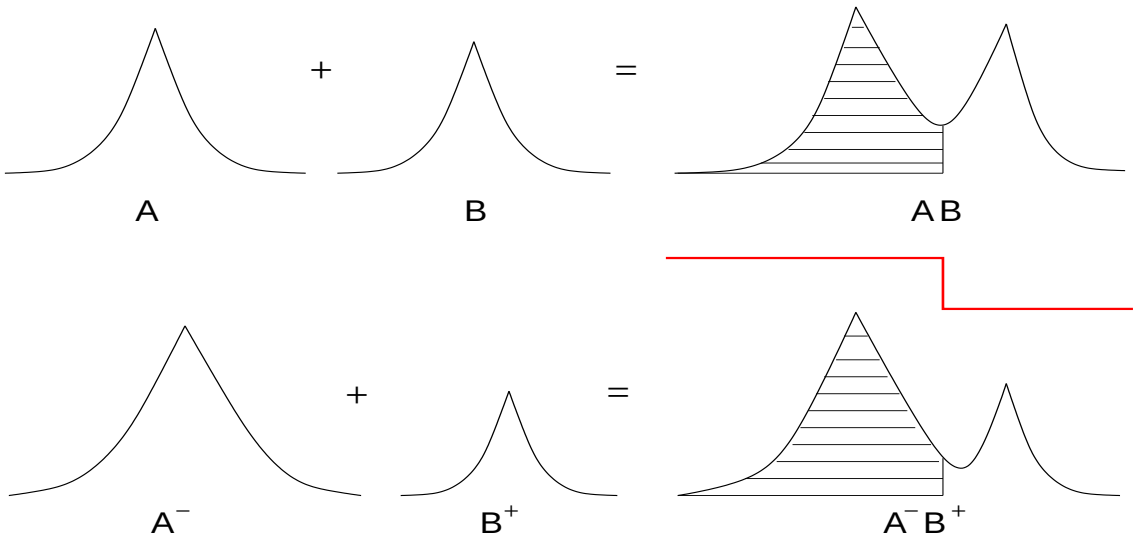

Figure 3-1: *Figure taken from Ref. [1]* Obtaining effective constraint value from promolecular densities. The constraints are on Fragment A. Integration over the striped area will give N_C^{eff}.

where the index i runs over the different configurations. Thus we determine the constraint values N_c^i. When the separation between fragments is large, the constraint $\mathbf{w}_C$ would only count density from molecular fragment C, and N_c^i would correspond to the integer number of electrons in that fragment. When the different fragments overlap, however, $\mathbf{w}_C$ would also count density from neighboring fragments in the promolecule density and a non-integer constraint value N_c^i would be obtained. Note that constraints defined in this way are continuous functions of interatomic distances - this is important for potential future work with force calculations. Later in this chapter, in the section on LiF, we test the sensitivity of our results to our definition of $\mathbf{w}_c$ by using another population definition.

Computing Matrix Elements

Each of the configurations is the result of enforcing constraints as in Eq. 1.22 with $\{\mathbf{w}_c, N_c^i\}$. Constraints are enforced using Lagrange multipliers V_c^i, so the resulting state $|i\rangle$ is an eigenstate of the Hamiltonian $\mathbf{H} = \mathbf{H}_0 + \sum_c V_c^i \mathbf{w}_c$ with the eigenvalue $E_i + \sum_c V_c^i N_c^i$ where $\mathbf{H}_0$ is the unconstrained Hamiltonian. Matrix elements in the basis of constrained states are computed as below:

$$
\begin{aligned}
\mathbf{H}_{ij} &= \langle i|\mathbf{H}_0|j\rangle \\
&= \frac{1}{2}(\langle i|\mathbf{H}_0 + \sum_c V_c^i \mathbf{w}_c - \sum_c V_c^i \mathbf{w}_c|j\rangle \\
&+ \langle i|\mathbf{H}_0 + \sum_c V_c^j \mathbf{w}_c - \sum_c V_c^j \mathbf{w}_c|j\rangle) \\
&= \frac{1}{2}((E_i + \sum_c V_c^i N_c^i + E_j + \sum_c V_c^j N_c^j)\langle i|j\rangle \\
&\quad -(V_c^i + V_c^j)\langle i|\mathbf{w}_c|j\rangle)
\end{aligned} \tag{3.3}
$$

where i and j are symmetrized to ensure Hermiticity of the resulting Hamiltonian. Two types of terms remain undetermined in Eq. 3.3 - the wavefunction overlap $\langle i|j\rangle$ and the coupling term from the constraint operator $\langle i|\mathbf{w}_c|j\rangle$. These terms cannot be computed from DFT, and must be approximated. We use the Kohn-Sham single-determinant wavefunction to compute these terms approximately - this approximation has previously been used in the group to compute electron transfer couplings [20], and is a natural choice for the case at hand.

For example, given two basis states

$$
\begin{aligned}
|\Psi_1\rangle &= |\phi_1^1, \phi_2^1, \phi_3^1| \\
|\Psi_2\rangle &= |\phi_1^2, \phi_2^2, \phi_3^2|,
\end{aligned}
$$

$$
\langle\Psi_1|\mathbf{S}|\Psi_2\rangle = \det(\sigma) = \begin{vmatrix}
\langle\phi_1^1|\mathbf{S}|\phi_1^2\rangle & \langle\phi_1^1|\mathbf{S}|\phi_2^2\rangle & \langle\phi_1^1|\mathbf{S}|\phi_3^2\rangle \\
\langle\phi_2^1|\mathbf{S}|\phi_1^2\rangle & \langle\phi_2^1|\mathbf{S}|\phi_2^2\rangle & \langle\phi_2^1|\mathbf{S}|\phi_3^2\rangle \\
\langle\phi_3^1|\mathbf{S}|\phi_1^2\rangle & \langle\phi_3^1|\mathbf{S}|\phi_2^2\rangle & \langle\phi_3^1|\mathbf{S}|\phi_3^2\rangle
\end{vmatrix}
$$

$$
\langle\Psi_1|\mathbf{w}_c|\Psi_2\rangle = \sum_{ij}(-1)^{i+j}\langle\phi_i^1|\mathbf{w}_c|\phi_j^2\rangle M_{ij}
$$

where M_{ij} is the determinant of σ with row i and column j removed.

Computing the Energy

This is the final CI step, and simply consists of diagonalizing the Hamiltonian $\mathbf{H}_{ij}$ obtained previously. The basis is non-orthogonal, so the generalized eigenvalue equation has to be solved.

$$\begin{aligned} |\Psi_{CI}\rangle &= \sum_i C_i |\Psi_i\rangle \\ \mathbf{H}_{ij} C_j &= \epsilon \mathbf{S}_{ij} C_j \end{aligned}$$

The ground-state energy ϵ is the smallest root of the secular equation

$$\det(\mathbf{H}_{ij} - \epsilon \mathbf{S}_{ij}) = 0$$

3.4 Application

Unless otherwise stated, calculations were all done in the 6-311G++(3*df*,3*pd*) basis set with the BLYP [180, 181] and B3LYP [38] functionals in a developmental version of Q-Chem [182]. Energies depicted in dissociation curves are zeroed at the value obtained from summing fragment energies computed with the same basis set and functional. The following notation is used to indicate the combinations of schemes and functionals computed - for the exchange-correlation functional B3LYP, RB3LYP and UB3LYP would be the restricted and unrestricted Kohn-Sham DFT results, respectively, and CB3LYP-CI would be the CDFT-CI result. CDFT calculations are always done in an unrestricted manner, with any resulting restricted ground-state only appearing in the final CI step.

3.4.1 $\mathbf{H}_2^+$

This system has only one electron, and is thus treated exactly by Hartree-Fock. As shown in figure 3-2, however, with both BLYP and B3LYP, Kohn-Sham DFT fails to capture even qualitative aspects of the potential curve, predicting a barrier at around 3 Å with the energy decreasing as a function of distance after the barrier.

This particular artifact is a well-known failure of DFT [160] and is blamed on self-interaction error [47, 48]. B3LYP performs slightly better than BLYP because of its exact exchange component, but still exhibits the same failure overall.

For this case, we used the minimal active space CAS(1,2), which prescribes the two active configurations H^+H and HH^+. At long distances, the CDFT-CI solution localizes the charge, making the resulting configuration simply that of a neutral atom and a proton, which is treated correctly by DFT. At short distances, the coupling term increases and gives the right mixture of the two configurations to reproduce the correct ground-state energy. As can be seen in Fig 3-2, this accuracy persists into the hard wall region. The promolecule definition for N_c^i is very important to this case because there is only one electron - requiring any local constraint to integrate to one would mean requiring the density to be zero everywhere else, and be unphysical to enforce.

Since H_2^+ does not have static correlation, this case demonstrates CDFT-CI's ability to fix SIE in DFT functionals. Even though exact exchange is not an explicit part of CDFT-CI, the local states used as a basis ensure that SIE stays constant at all distances, leading to an effective cancellation of error if we are to concern ourselves only with energy differences.

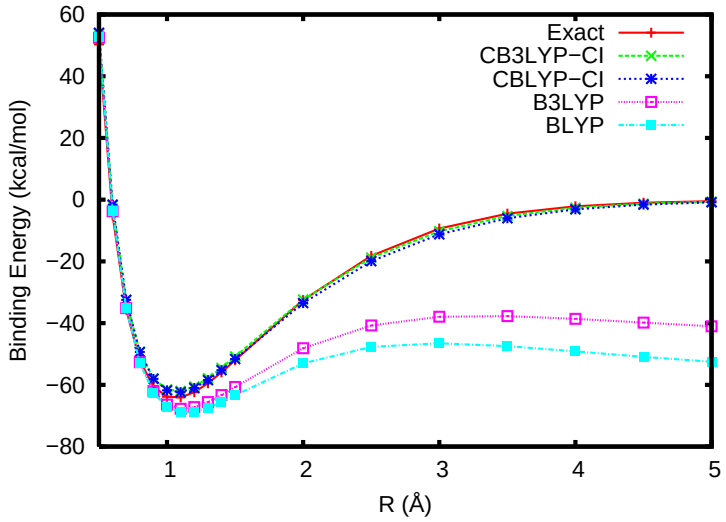

Figure 3-2: *Figure taken from Ref. [1]* Potential curves of H_2^+.

3.4.2 H_2

For this system, we use the aug-cc-pVQZ basis set and only present the B3LYP results because the BLYP results are largely identical. The potential curves for both restricted and unrestricted B3LYP are presented in Fig. 3-3. Unrestricted B3LYP gets the geometry and atomization energies correct, and the potential from unrestricted B3LYP dissociates correctly, albeit with a broken symmetry spin density [164, 165]. Restricted B3LYP preserves the correct spin symmetry, but dissociates to the wrong energy limit. The restricted and unrestriced B3LYP results diverge at the Coulson-Fisher at about 1.6 Å.

For this case, we use the CAS(2,2) active space transformed to the four localized states H↑H↓, H↓H↑, H^+H^- and H^-H^+. Using CAS(2,2), CDFT-CI dissociates H_2 correctly, and displays the correct spin symmetry for the ground state, being an equal mixture of H↑H↓ and H↓H↑.

CDFT-CI once again gives an accurate potential at all distances, doing no worse than restricted B3LYP at equilibrium bond lengths, and outperforming it at greater bond lengths. For a clearer comparison of unrestricted B3LYP and CDFT-CI B3LYP, we compare the errors from both directly in Fig. 3-4. The exact answer is obtained from a full CI calculation. The unrestricted B3LYP error has a maximum of 5 kcal/mol at 1.8 Å, while its CDFT-CI counterpart has a more slowly varying error which peaks no larger than 3 kcal/mol. For this case then, CDFT-CI is a better method for studying bond breaking compared to broken-symmetry DFT. The CDFT-CI error, however, approaches zero much slower than broken-symmetry DFT - we do not understand this, but also do not consider this a serious problem as the absolute magnitude of the error is small.

To judge the effect of dynamic correlation, we repeat the same calculation with CASSCF(2,2) (Fig. 3-3). CASSCF(2,2) gives the right symmetry and energy at dissociation, but badly underestimates the binding energy. We attribute this to the lack of dynamic correlation at the equilibrium geometry. Near the equilibrium, at 0.75 Å, CASSCF(2,2) has an error of 14 kcal/mol while CDFT-CI B3LYP only has

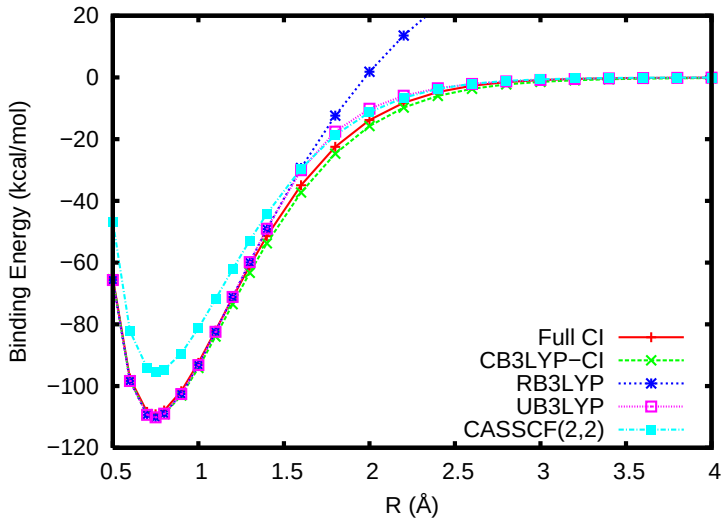

Figure 3-3: *Figure taken from Ref. [1]* Potential curves of H_2.

an error of 1 kcal/mol. This case demonstrates one of the motivating factors for CDFT-CI - DFT's ability to capture dynamic correlation.

3.4.3 LiF

The erroneous dissociation limit of highly ionic neutral molecules under DFT was known early on [161], and has recently attracted more attention [162, 163]. You can see this effect for the case of LiF in Fig. 3-5. Singly-bonded diatomic molecules should always dissociate to neutral atoms, whereupon the singlet and triplet states are degenerate. Hence, both singlet and triplet states of LiF should dissociate to the same limit at infinity. Under unrestricted B3LYP, however, singlet LiF dissociates into atoms with erroneous fractional charges and a negative energy at infinity. This is once again attributed to self-interaction error. Using the CAS(2,2) active space, transformed to the localized basis $Li\uparrow F\downarrow$, $Li\downarrow F\uparrow$, Li^+F^- and Li^-F^+, the singlet state under CDFT-CI once again dissociates correctly, while remaining accurate near equilibrium.

Because conducting a Full-CI for this system size is impossible, we use an optimized-orbital coupled-cluster doubles [183, 184] calculation with the OD(2) second-order correction in a CC-pVQZ basis for our comparison. The choice of unrestricted versus restricted Hartree-Fock as the reference state for the coupled-cluster calculation

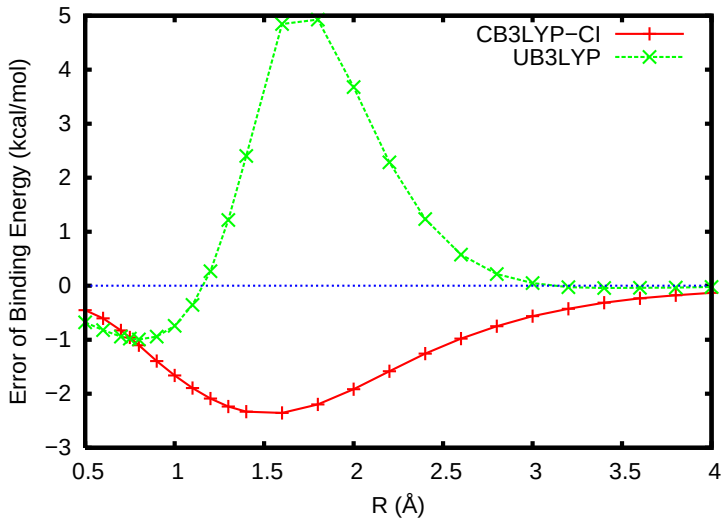

Figure 3-4: *Figure taken from Ref. [1]* Error comparison of UB3LYP and CB3LYP-CI. Errors are calculated against full CI results.

results in different energies [185]. We use the UHF reference, which gives the same energy as RHF up to 5 Å. Observe in Fig. 3-6 that CDFT-CI gives a very good equilibrium geometry and energy. At larger distances, however, the CDFT-MI results from BLYP and B3LYP differ. Assuming the OD(2) is a good proxy for full CI, it would appear that CDFT-CI B3LYP is better than CDFT-CI BLYP. However, overall both functionals perform pretty well.

We test sensitivity to the w_c definition by trying another definition for the density to atomic center mapping, the stockholder weight [186, 187]. The reference densities used to obtain the stockholder weights are spherically-averaged atomic densities in the 6-311G basis.

Ionic versus Covalent Components

With CDFT-CI, it is possible to identify the relative contributions of ionic and covalent terms in the ground state. We start by orthogonalizing the constraint operator $\mathbf{w}_c$ in the active space basis, much the same way it was previously done in the group to obtain diabatic states for electron transfer [20]:

$$\mathbf{w}_c\Psi_i = n_i\mathbf{S}\Psi_i \tag{3.4}$$

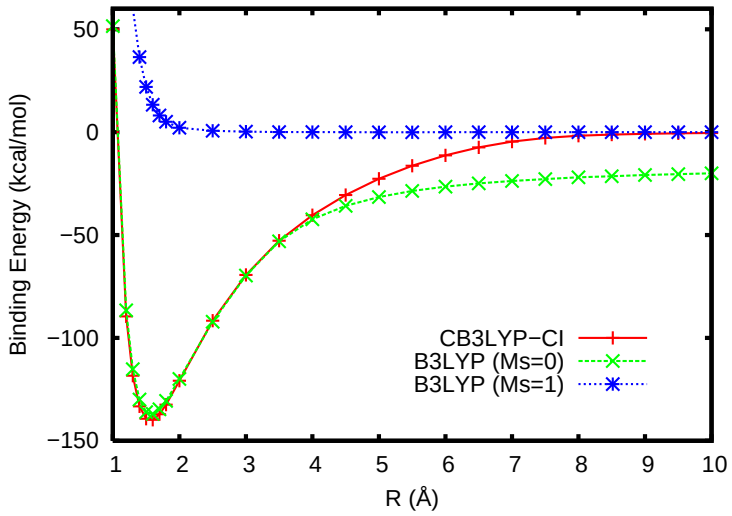

Figure 3-5: *Figure taken from Ref. [1]* Singlet potential curves of LiF by B3LYP and CB3LYP-CI as compared to the triplet curve by B3LYP. The M_s=0 curve of B3LYP is a broken-symmetry solution at large R and has a positive charge of 0.3 on Li at the dissociation limit.

where the resulting states Ψ_i are the best orthogonal representations of the starting active states, and have eigenvalues n_i which represent the ionicity of the states. For example, in the case of LiF, the constraint on Li has $n_i \approx 2, 3, 3, 4$. These values correspond to the Li^+F^-, LiF singlet/triplet, and Li^-F^+ states respectively. Taking the overlap of the ground state with each basis state gives us coefficients, which when squared sum to unity and individually represent the contribution from each configuration. The weights as a function of bond distance are plotted in Fig. 3-7. As expected, we see contributions from the ionic configuration Li^+F^- and the covalent states form most of the ground state at most distances. At short bond lengths, the ionic state is dominant, while the covalent states are dominant at long bond lengths. Configuration weights are smooth with respect to distance, and cross at 6.6 Å. A different way of estimating the crossing point is to ask when the difference in ionic energies, as determined by the difference between IP_{Li} and EA_F, offsets the electrostatic attraction between Li^+ and F^-. Under B3LYP, IP_{Li} is 0.2064 Hartree and EA_F is 0.1270 Hartree, giving the crossing point at 6.6 Å, exactly where we found it. This success is consistent with previous findings in the group that CDFT correctly predicts long-range charge transfer energies.

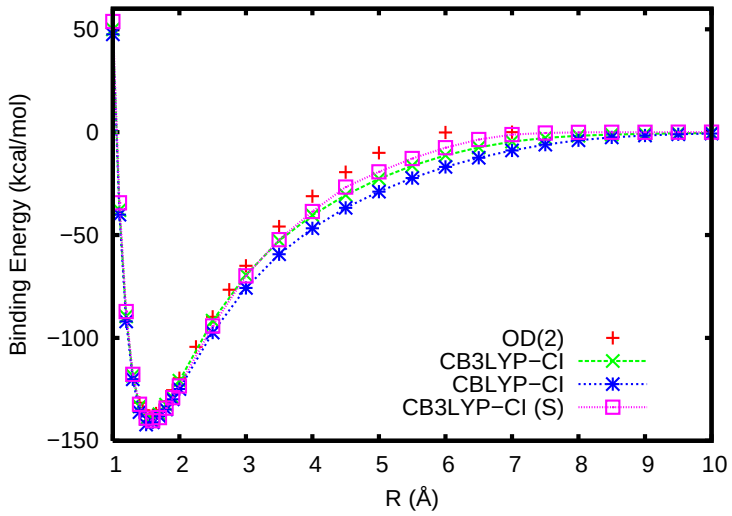

Figure 3-6: *Figure taken from Ref. [1]* CB3LYP-CI(S), CB3LYP-CI and CBLYP-CI potential curves as compared to OD(2). CB3LYP-CI(S) is the CB3LYP-CI using stockholder weights.

3.5 Conclusion

We have introduced a configuration interaction method based on spatial and spin constrained states. The active space states in our method have local spatial and spin density constraints and treat dynamic correlation while remaining low in self-interaction error and static correlation. Using this basis, we approximate the off-diagonal Hamiltonian matrix elements also using DFT, and at the end of the process add back static correlation by diagonalization. This is efficient and provides a good treatment of both dynamic and static correlation, enabling it to describe bond-breaking accurately. This is evident from the good results we've obtained for the dissociation potentials of H_2^+, H_2 and LiF.

There is a class of *ab initio* MR methods which perturb the ground state and use the perturbed states as an active space for configuration interaction. CDFT-CI is unique in this class because it is a purely DFT approach, using DFT to form both the active space and compute matrix elements. Other "perturb-then-diagonalize" approaches use perturbation theory, configuration interaction (in a bigger MO basis), coupled cluster and canonical transformations [188, 189, 190, 191]. CDFT-CI is more efficient than these techniques, and at the same time comparatively accurate for the

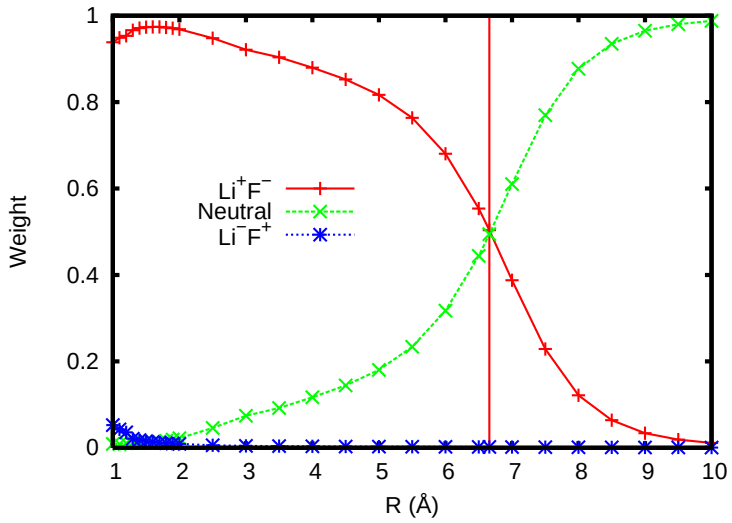

Figure 3-7: *Figure taken from Ref. [1]* Weights of configurations in the final ground state.

cases we have examined.

We attribute the success of the method to the nature of the active states chosen - the active states we use have local spin and charge density, which minimizes self-interaction error and static correlation. Avoiding the former controls an error endemic to DFT, while having low levels of static correlation in the active space reduces double-counting as static correlation is added later in the process. The dissociation curve from the equilibrium bond length to dissociation is described correctly by CDFT-CI, and this type of consistency is progress towards a reliable treatment of bond-breaking and bond-formation in chemical reactions of larger molecules. Best of all, CDFT-CI does this in a functional-agnostic manner, in theory with no greater reliance on cancellation of error between SIE and static correlation biases. This will enable it to take advantage of improvements in functionals which seek to reduce SIE [51, 52, 53].

3.6 Acknowledgements

This work was done in collaboration with Dr. Qin Wu, who is the first author on Ref. [1].

Chapter 4

Rydberg Energies using Excited-State DFT

4.1 Introduction

As described in the thesis introduction, the Hohenberg-Kohn (HK) theorem guarantees that all the properties of the ground state can be extracted from its one-particle density [13]. This existence proof has inspired the development of numerous functionals that approximate the ground state energy based on the density, and is the basis of density functional theory (DFT).

There is, however, no corresponding theorem for electronic excited states. The mapping from electronic excited states to densities is not unique [192] and thus a one-to-one mapping does not exist. This means that it is not possible to construct a functional which determines excited state energies from just their densities. However, this hasn't dissuaded the development of a number of ways of getting excited states in the DFT framework. The most widely used is time dependent DFT (TDDFT), where the Runge-Gross theorem [22] has proven the existence of a one-to-one mapping between the density trajectory and the time dependent potential. There are also approaches which target excited states directly, including but not limited to symmetry-based methods [193], methods based on ensembles [194] and methods that attempt to treat individual excited states [142, 195].

Even though excited state DFT (eDFT) lacks a completely rigorous foundation, it has been applied to a number of different systems of interest. A common approach is to use the Kohn-Sham orbitals from a ground state DFT calculation, but occupy

them differently and compute the energy of the resulting density using a ground state functional. This type of procedure has been used to treat excitons in conjugated polymers [196, 197], exciton-induced bond breaking at semiconductor surfaces [198], photoisomerization of aromatics [199], and solvatochromatic effects in dyes [200].

In this chapter, we attempt to do two things. Firstly, we try to apply the commonly used eDFT approach, which is usually limited to the treatment of HOMO-LUMO transitions, to the description of higher-lying excited states. We use standard semilocal functionals to treat atomic Rydberg states, and find that, even without any correction of the exchange correlation potential, we are able to obtain reasonable Rydberg excitation energies. We find this to be a result of, under eDFT, each Rydberg state experiencing its own effective potential - while each individual potential decays exponentially beyond a certain distance, the distance at which the erroneous exponential decay starts is pushed further and further out as one goes up the series of Rydberg states.

Secondly, we attempt to reconcile the formally exact DFT-based excited state approaches mentioned above with the eDFT procedure. Specifically, we note that many years ago, Levy and Perdew proved that all stationary densities of the exact functional, E_{cs}, (as defined by the Levy constrained search [201]) are physically significant and in fact stationary states under the full Hamiltonian [202]. This theorem applies to both minima (ground states) and saddle points (excited states) of the functional. In this article, we explore the connection between these Levy-Perdew (LP) stationary densities and the self-consistent solutions of the Kohn Sham (KS) eDFT equations. We find that the two approaches are *identical* as long as the eDFT solutions give the minimum KS kinetic energy. Thus, in certain situations one might conjecture that eDFT excited states could be rigorous approximations to the true excited states. We test this conjecture for the atomic Rydberg states computed herein and find that, in some cases, the eDFT solutions are minima of the KS kinetic energy. In particular, we find that that this occurs when the excited state density is not ground state v-representable. In these situations, there exists no potential for which the ground state density is equal to the density in question. For these densities, then, there must be

an excited state solution which gives the minimum kinetic energy, and it is this state that is rigorously predicted in eDFT. We thus find that eDFT plays a complementary role to constrained DFT [203, 142, 1] in terms of describing excited states in DFT: eDFT can only work if the density is *not* the ground state of some potential, while constrained DFT can only work if it *is*.

4.2 Ground State Kohn-Sham DFT

We start by clarifying what we mean by eDFT, both to clarify notation and also to specify the variant we employ (there are several in the literature). We start with ground-state Kohn-Sham DFT (KS-DFT) [14]. Under KS-DFT, the energy

$$E[\rho^\uparrow, \rho^\downarrow] \equiv T_s[\rho^\uparrow, \rho^\downarrow] + \int \rho(r) V_{ext}(r) dr + E_{Jxc}[\rho^\uparrow, \rho^\downarrow] \tag{4.1}$$

is minimized with respect to the spin densities, which are expressed as a sum of KS orbital densities

$$\rho^\uparrow \equiv \sum_i^{N^\uparrow} |\phi_i^\uparrow| \qquad \rho^\downarrow \equiv \sum_i^{N^\downarrow} |\phi_i^\downarrow|$$

where $\rho \equiv \rho^\uparrow + \rho^\downarrow$ and the KS kinetic energy is given by

$$T_s[\rho^\uparrow, \rho^\downarrow] \equiv \min_{\phi_i^\uparrow \to \rho^\uparrow} \sum_i^{N^\uparrow} \langle \phi_i^\uparrow | \hat{T} | \phi_i^\uparrow \rangle + \min_{\phi_i^\downarrow \to \rho^\downarrow} \sum_i^{N^\downarrow} \langle \phi_i^\downarrow | \hat{T} | \phi_i^\downarrow \rangle$$

Physically, T_s is the minimum kinetic energy possible for a single-determinant wavefunction that yields the given density, and the minimum is obtained for the optimal KS orbitals ϕ_i. Meanwhile, E_{Jxc} contains all the inter-electron interactions and must be approximated, in practice. Extremizing the energy expression (Eq. 4.1) with respect to $\rho^\uparrow, \rho^\downarrow$ subject to the normalization constraint gives

$$\begin{aligned} \delta \Bigg[T_s[\rho^\uparrow, \rho^\downarrow] + \int \rho(r) V_{ext}(r) dr + E_{Jxc}[\rho^\uparrow, \rho^\downarrow] \\ - \mu^\uparrow \left(\int \rho^\uparrow(r) dr - N^\uparrow \right) - \mu^\downarrow \left(\int \rho^\downarrow(r) dr - N^\downarrow \right) \Bigg] = 0 \end{aligned} \tag{4.2}$$

The corresponding Euler equation implies that the Kohn-Sham orbitals $\phi_i^{\uparrow,\downarrow}$ satisfy

$$\begin{aligned}\left(\hat{T}_s + \hat{V}_{ext} + \hat{V}_{Jxc}^{\uparrow}[\rho^{\uparrow}, \rho^{\downarrow}]\right) \cdot \phi_i^{\uparrow} &= \epsilon_i^{\uparrow} \cdot \phi_i^{\uparrow} \\ \left(\hat{T}_s + \hat{V}_{ext} + \hat{V}_{Jxc}^{\downarrow}[\rho^{\uparrow}, \rho^{\downarrow}]\right) \cdot \phi_i^{\downarrow} &= \epsilon_i^{\downarrow} \cdot \phi_i^{\downarrow}\end{aligned} \tag{4.3}$$

Solving the Kohn-Sham equations(Eqs. 4.3) requires a set of self consistent iterations, because V_{Jxc} depends on the density while the density depends on V_{Jxc} via the orbitals. For grounds states, this leads to the Kohn-Sham self-consistent field (KS-SCF) iterations:

1. Compute the potentials $V_{Jxc}^{\uparrow,\downarrow}$ from the density $\rho^{\uparrow,\downarrow}$.

2. Determine the orbitals that solve the KS equations (Eqs. 4.3) for the fixed potentials $V_{Jxc}^{\uparrow,\downarrow}$.

3. Choose the $N^{\uparrow}$ ($N^{\downarrow}$) lowest spin-$\uparrow$ (spin-$\downarrow$) orbitals (Aufbau occupation), and form new spin densities $\rho_{new}^{\uparrow}, \rho_{new}^{\downarrow}$from these orbitals.

4. If ρ_{new} is sufficiently similar to ρ, the procedure is done. Otherwise, start over from step 1 with ρ_{new}.

Due to Janak's theorem [204], the Aufbau occupation in step 3 implies that the converged KS-SCF solutions are energy minima - that is to say, they correspond to ground states.

4.3 Excited State Kohn-Sham DFT

In excited state DFT, we follow the KS prescription in all respects, except that we modify step 3 to allow non-Aufbau occupations. All calculations are still to be performed self-consistently, so that the potentials $V_{Jxc}^{\uparrow,\downarrow}[\rho^{\uparrow}, \rho^{\downarrow}]$ will be different for different excited states, because they will be evaluated using *different excited state densities*. Of the many non-Aufbau schemes possible, the simplest consists of occupying the orbitals as if the Hamiltonian were non-interacting, e.g. the first excited state would fill the N-1 lowest orbitals and the (N+1)-th lowest orbital, swapping the HOMO and

LUMO occupations as compared to ground state, while other excites states would correspond to HOMO $\leftrightarrow$ LUMO+1, HOMO-1 $\leftrightarrow$ LUMO,.... This scheme often works well for the lowest excited state, particularly if the HOMO and LUMO are of different symmetries [196, 197, 198, 199, 200]. However, for higher-lying states we find this simple approach rarely converges to a self-consistent solution. Changes in orbital energy levels between iterations often permute the order of the physical orbitals, leading what was, say, the LUMO+2 in the previous iteration to be LUMO+1. These erratic orbital ordering swaps lead to inconsistent orbital occupations and the resulting changes in the density from iteration to iteration then lead to non-convergence in most cases.

Explicitly designing for convergence, we devised a scheme that minimizes density difference relative to a reference density. The basic idea is that, within the self-consistent iterations one occupies the KS orbitals that have greatest overlap with a set of reference orbitals. Since we do not use energetic ordering, this removes the problem of erratic orbital occupation. In order to obtain good reference densities, we actually use an adiabatic connection between the non-interacting and interacting systems. Here, we reduce the electron-electron interaction terms by a factor λ and begin with the non-interacting limit ($\lambda = 0$) where exact excited states can be trivially obtained for any non-Aufbau configuration. We then use these orbitals as a starting point for a calculation at $\lambda = \epsilon$ (where $\epsilon << 1$). Once this calculation is converged, we use the $\lambda = \epsilon$ orbitals as a reference for a self-consistent $\lambda = 2\epsilon$ calculation,.... The solution is thus brought adiabatically from the non-interacting ($\lambda = 0$) to the fully-interacting ($\lambda = 1$) limit. This method is well-defined but probably sub-optimal - we leave the search for efficiency to future work.

4.4 State of the Art: Linear Response TDDFT

A cheap and accurate DFT-based excited-state method already exists in the form of time-dependent DFT (TDDFT) and thus an approach like eDFT should be thought of as a *supplement* to TDDFT, filling in the gaps where TDDFT is to cumbersome or existing functionals are not accurate enough. In particular, we note that TDDFT has

severe problems treating Rydberg excitations accurately [205, 206] and the reasons for this are well understood. Specifically, whereas the true exchange-correlation potential, V_{xc} should fall off as $-\frac{1}{r}$ at large distances from a molecule, the potential predicted with commonly used approximate functionals decays exponentially [207, 4]. Further, the LUMO in Kohn-Sham DFT systematically underestimates the electron affinity due to the lack of a derivative discontinuity, which is known to be present in the exact functional [40, 41, 42]. For localized, valence-like excitations, these are not serious problems. However, because most of the electron density for Rydberg states resides in the asymptotic region, they are extremely sensitive to the long range behavior of V_{xc}, leading to a systematic overestimate of Rydberg transitions. In the worst cases, the Rydberg states are so overestimated that they lie above the ionization threshold and are thus embedded the continuum. There are a number of ways to solve this problem within TDDFT. On the pragmatic side, one can simply replace the approximate V_{xc} with the correct $-\frac{1}{r}+\Delta E$ decay after some appropriate distance [207, 4]. The asymptotic form will have little influence on the valence excited states, but dramatically improves the Rydberg states. On the more formal side, it has recently been shown that many problems with Rydberg states in TDDFT can be circumvented via clever use of quantum defect theory [208]. Here we explore the idea that eDFT could provide a third route to Rydberg states in DFT.

4.5 Application

4.5.1 The Excited-State Exchange-Correlation Potential

To start with, we examine the simplest Rydberg states; the s-type eigenstates of the hydrogen atom. To further simplify matters, we will also use the known exact densities for the hydrogen Rydberg states our analysis, postponing all questions concerning self-consistency to the next section. Now, we want compare TDDFT and eDFT using the same functional in each case. The only difference is that in eDFT the functional is evaluated at the excited-state density, whereas the TDDFT potential is determined by the ground state. This leads to a different exchange-correlation potential in each case and – as we shall see – vastly different behavior for Rydberg states.

Electronic State	ϵ_{1s}	ϵ_{2s}	ϵ_{2p}	ϵ_{3s}	ϵ_{3p}	ϵ_{3d}
1s	-6.32	0.91	1.41	0.82	1.02	1.33
2s	-12.00	-1.80	-1.41	0.03	0.15	0.10
2p	-10.62	-1.30	-1.28	0.19	0.23	0.32
3s	-13.58	-2.43	-2.41	-0.84	-0.76	-0.55
3p	-13.10	-2.12	-2.34	-0.73	-0.76	-0.52
3d	-11.32	-2.20	-2.08	-0.51	-0.49	-0.53

Table 4.1: eDFT orbital eigenvalues of the hydrogen atom computed using LSDA exchange and the exact densities. Each row corresponds to a particular excited state, and the columns give the appropriate orbital eigenvalues. Note that, as one occupies more and more diffuse orbitals, the 1s orbital eigenvalue approaches the correct value of -13.6 eV, naturally correcting for the poor LSDA exchange-only estimate of the ionization energy of ϵ_{1s}=-6.3 eV.

As is well known, the failure of density functionals for Rydberg states stems from two qualitative problems: 1) the apparent ionization threshold of the atom or molecule must be adjusted [207, 4] to account for the derivative discontinuity of the xc-potential [40, 41, 42] and 2) the xc-potential should decay as $1/r$ at large distances, while commonly used functionals typically decay exponentially [209]. We first show analytically that the prescription of eDFT addresses both of these concerns *without modifying the xc functional*. To address the first point, Table 4.1 shows the computed Kohn-Sham eigenvalues (ϵ) for the $1s, 2s, 2p, 3s$ ... orbitals when the electron is considered as occupying any one of the $1s, 2s, 2p, 3s$... states. If we neglect self consistency considerations, then, the first row represents the *ground state* orbital eigenvalues, while subsequent rows represent the first, second, third... *excited state eigenvalues* as would be obtained from eDFT. Examining the data in the table, it is clear that the ground state HOMO *underpredicts* the ionization potential (IP) for hydrogen (e.g ϵ_{HOMO}=-6.3 eV which should be -13.6 eV). The result is that any Rydberg excitation that exceeds 6.3 eV will be embedded in a continuum; indeed TD-LSDA exchange predicts *no* bound excited states for hydrogen. However, looking at the subsequent columns in the table, we see that as one moves up from first, to second, to third ... excited states, the orbital energies shift so that the $1s$ orbital quickly approaches the correct IP. Note for example, that when the electron sits in the $3s$ orbital, the eigenvalue of the 1s orbital is -13.58 eV. Thus, the apparent ionization threshold in

eDFT is *not* related to the ground state orbital eigenvalues. We conclude that the eDFT prescription incorporates some of the effects of the derivative discontinuity on the orbital eigenvalues, pushing the IP high enough that Rydberg-like states should be bound.

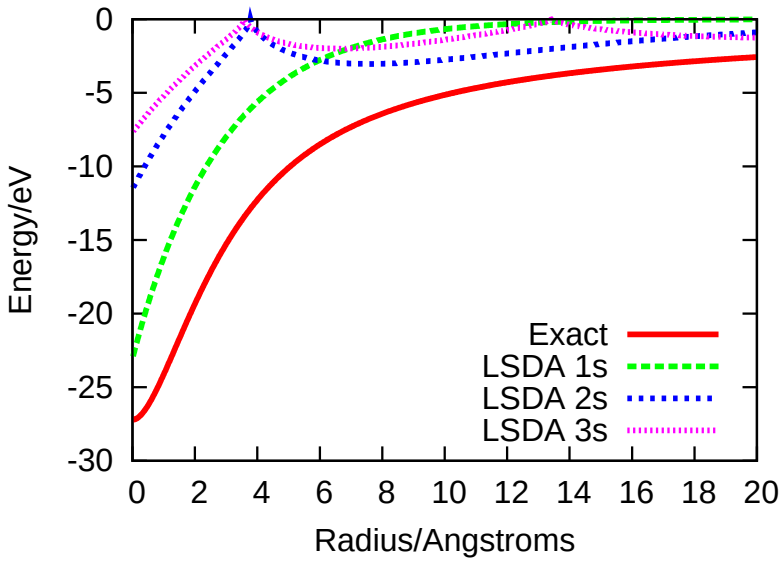

Figure 4-1: Hydrogen atom excited state exchange potentials (eV vs. Angstroms). The solid red line shows the exact exchange potential and the subsequent lines (moving upward at the origin) show the 1s, 2s and 3s LSDA exchange potentials from eDFT using the exact density. While none of the potentials individually has the correct decay, subsequent potentials decay more and more slowly.

Addressing the potentials, Figure 4-1 shows the LSDA exchange potentials that result from the 1s, 2s and 3s hydrogen orbitals. We present only the exchange potential for simplicity, since it is exchange (and not correlation) that determines the long-range behavior of V_{xc} Clearly, none of the potentials is particularly similar to the exact potential. They all decay too quickly in the asymptotic region, and once we get beyond the ground state, the potential even has nodes at finite values of r, corresponding to the nodes in the hydrogenic orbitals. However, hidden within this series of potentials is the information necessary for a Rydberg-like series, as we now show.

We focus on the region near the classical turning point ($r_{tp}(n) = 2n^2$), where the density will tend to be large. If we examine the large-n limit appropriate for Rydberg

states, we can use Erdélyi's asymptotic expansion of the Laguerre polynomials to facilitate simple analytic expressions for the exact density and density gradient [210]. We then get the following expressions for the exact hydrogen s-orbital density and gradient at the classical turning point $r_{tp}(n) = 2n^2$:

$$\lim_{n\to\infty} \rho_n(r)|_{r=2n^2} \approx \frac{n^{-17/3}}{2^{2/3}27\sqrt[3]{3}\pi\Gamma\left(\frac{5}{3}\right)^2} = \frac{0.00632}{n^{17/3}} \tag{4.4}$$

$$\lim_{n\to\infty} \partial_r\rho_n(r)|_{r=2n^2} \approx -\frac{n^{-7}}{2\sqrt{3}\pi} = \frac{-0.09188}{n^7}$$

$$\lim_{n\to\infty} \partial_r^2\rho_n(r)|_{r=2n^2} \approx \frac{\sqrt[3]{\frac{3}{2}}\Gamma\left(\frac{2}{3}\right)^2}{16\pi^3} n^{-25/3} = \frac{0.00423}{n^{25/3}}$$

Again, focusing on exchange, we take LSDA exchange

$$v_{LSDA}(\rho) = -\left(\frac{6}{\pi}\right)^{1/3} \rho^{1/3} \tag{4.5}$$

and equation 4.4, the LSDA exchange potential v_{LSDA} at the classical turning point is

$$\lim_{n\to\infty} v_{LSDA}(\rho_n(r)|_{r=2n^2}) \approx \frac{-\sqrt[9]{2}}{3^{7/9}n^{17/9}\left(\pi\Gamma\left(\frac{5}{3}\right)\right)^{2/3}} = \frac{-0.229}{n^{17/9}} \tag{4.6}$$

The dimensionless density gradient, $s = |\nabla\rho|/(2k_f\rho)$, where $\rho = k_F^3/3\pi^2$, as a function of the principle quantum number n and evaluated at r_{tp} is

$$\lim_{n\to\infty} s(r)|_{r=2n^2} = \frac{3^{17/18}\Gamma\left(\frac{2}{3}\right)^{8/3}}{2\sqrt[9]{2}\pi^{5/3}} n^{5/9} \approx 0.4351n^{5/9} \tag{4.7}$$

Under the same conditions, the PBE exchange functional [30] is

$$\lim_{n\to\infty} v_{PBE}(\rho, |\nabla\rho|) = -\frac{0.414}{n^{17/9}} \tag{4.8}$$

and the PW91 exchange functional [29] is

$$\lim_{n\to\infty} v_{PW91}(\rho, |\nabla\rho|) = F_x(\rho, |\nabla\rho|)\partial_\rho v_{lda}(\rho) + \partial_\rho F_x(\rho, |\nabla\rho|)v_{lda}(\rho) = -\frac{0.206}{n^{5/3}}$$

Under the same conditions, the Becke88 exchange functional [31] gives

$$\lim_{n\to\infty} v_{Becke88}(\rho,|\nabla\rho|) = \frac{-\frac{0.312}{\log^2(n)} - \frac{1.87}{\log^3(n)}}{n^{4/3}} + \frac{-0.229 + \frac{5.28}{\log^2(n)} + \frac{20.2}{\log^3(n)}}{n^{17/9}} + O\left(\frac{1}{n^2}\right)$$

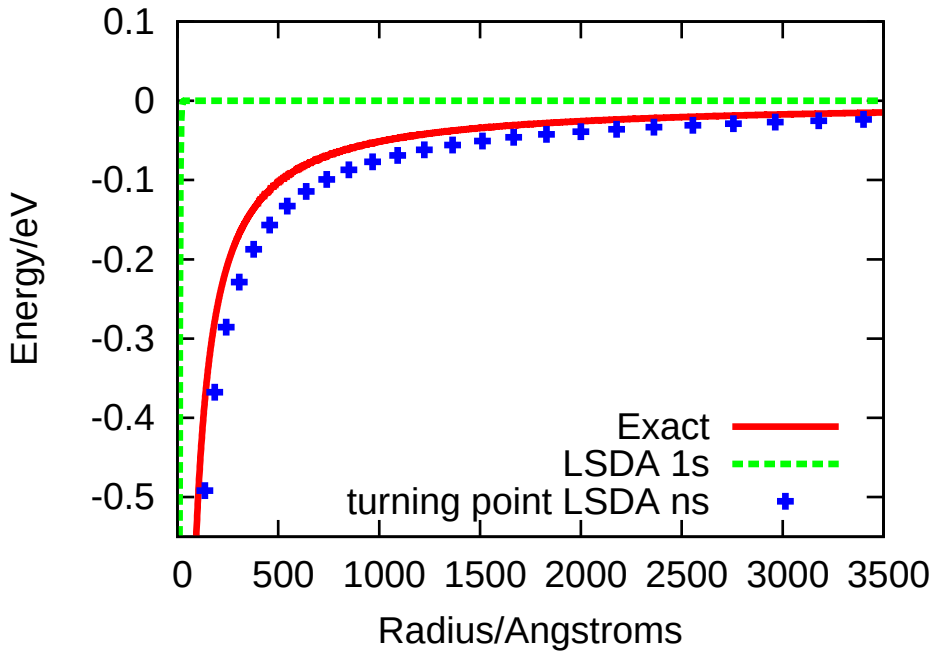

Figure 4-2: Exchange potentials for hydrogen. The dotted green line is the ground-state LSDA exchange potential [2]. The solid red line is the exact exchange potential. The blue crosses are the excited-state density LSDA exchange potential at the classical turning points $r = 2n^2$.

Comparing the approximate potentials to the exact exchange potential at the turning point,

$$v_x(r)|_{r=2n^2} = -\frac{0.5}{n^2} \tag{4.9}$$

we see that both the exact and the excited-state LSDA, Becke88, PBE and PW91 exchange potentials are polynomials in n. In contrast, the LSDA exchange potential of the exact ground-state density is

$$v_{LSDA}(\rho_1(r)|_{r=2n^2}) = -2\left(\frac{3}{\pi}\right)^{1/3} e^{-4n^2/3} = -1.97e^{-4n^2/3}$$

As evident from figure 4-2, the ground-state LSDA exchange potential bears little resemblance to the exact exchange potential, whereas the excited-state LSDA exchange is close to the exact value over a large range in n: the effective potential in eDFT shows a marked improvement over the ground state potential, and should be expected to give a more faithful description of Rydberg states. To understand why this is the case, note that within the adiabatic local density approximation, V_{xc} decays exponentially as a consequence of two factors: the exponential decay of the density and the local nature of the functional. In the the large r limit, any given excited-state V_{xc} also decays exponentially, for precisely the same reasons (cf Fig. 4-1). However, as n increases, the region of exponential decay for the excited state V_{xc} gets further and further from the nucleus. Thus, because each excited state sees its own xc potential, areas of significant density need not coincide with the asymptotic r region. Indeed, as shown above the regions of large density near the classical turning points experience an effective *polynomial* decay with distance; thus, for a given excited-state, the electron density never "sees" the exponential decay of the excited-state exchange potential.

4.5.2 Numerical Evaluation of Rydberg Energies

nl	E_{exact}	E_{LDA-X}	E_{LSDA}	E_{PW91}	E_{B3LYP}
2s	10.204	9.222 *(-0.982)*	9.502 *(-0.702)*	9.955 *(-0.250)*	9.985 *(-0.219)*
2p	10.204	9.195 *(-1.009)*	9.423 *(-0.782)*	9.830 *(-0.374)*	9.874 *(-0.330)*
3s	12.094	10.981 *(-1.113)*	11.374 *(-0.720)*	11.910 *(-0.185)*	12.625 *(0.531)*
3p	12.094	10.909 *(-1.185)*	11.261 *(-0.833)*	11.776 *(-0.318)*	11.806 *(-0.288)*
3d	12.094	10.912 *(-1.182)*	11.247 *(-0.847)*	11.745 *(-0.348)*	11.767 *(-0.327)*
4s	12.755	11.608 *(-1.147)*	12.062 *(-0.693)*	12.635 *(-0.120)*	NC
4p	12.755	11.563 *(-1.192)*	11.948 *(-0.808)*	12.496 *(-0.260)*	NC
4d	12.755	11.533 *(-1.222)*	11.947 *(-0.808)*	12.494 *(-0.262)*	NC
4f	12.755	11.534 *(-1.221)*	11.930 *(-0.826)*	12.469 *(-0.287)*	NC
5s	13.062	11.902 *(-1.159)*	12.391 *(-0.670)*	12.979 *(-0.082)*	NC
Avg		-1.141	-0.769	-0.248	-0.127
RMS		1.144	0.771	0.264	0.355

Table 4.2: Hydrogen Atom eDFT Excitation Energies (eV). *Italics* indicate difference from the exact energy. NC indicates no converged state was found. Average and Root Mean Square errors are also indicated.

So far, we have only examined the exchange-correlation potentials as calculated

from frozen densities. We test eDFT by self-consistently calculating the energies of atomic Rydberg states using the techniques described above. To begin with, we have computed the eDFT excitation energies of the hydrogen atom using several commonly used functionals [29, 136], with the excitation energy being given by the difference between self-consistent excited-state and ground-state energies. In order to obtain complete basis set-quality results, we utilize an uncontracted d-aug-cc-pV6Z basis, consisting of 100 uncontracted Gaussians [211], leading to absolute energies that are converged to within 0.05 eV in all cases. Our results are presented in Table 4.2. Examining the results, we see that each functional does, in fact yield a Rydberg-like series of self-consistent excited states. This is perhaps to be expected from the analysis of the potentials detailed in the previous section, but it is nonetheless comforting that self-consistency does nothing to spoil this property. We also note that, while the previous section focused solely on s-states for simplicity, our calculations reveal the presence of s-, p-, d- and f-type Rydberg states with similar accuracy. There is a systematic trend in these eDFT results toward underestimating the Rydberg energies by several tenths of an eV. This observation should be contrasted, however, with the fact that TDDFT with the same functionals predicts *no* bound Rydberg states, with all the Rydberg-like solutions being embedded in the continuum. Hence, from this perspective, eDFT provides a dramatic improvement to the TDDFT description of these states. On the other hand, these results could be seen as disappointing, since even something as simple as Hartree-Fock predicts the Rydberg series of hydrogen exactly.

In any case, we do see the expected Jacob's Ladder [212] trend in accuracy (Local<GGA<Hybrid), which suggests semi-systematic approach to the correct answer. On the other hand, we find that the ease of convergence is inversely related to accuracy: the LDA exchange only calculations are the easiest to converge (in that the adiabatic connection can be achieved with large steps in λ) while it was not even possible to converge some of the Rydberg states for B3LYP. The primary obstacle to convergence is that the high-lying states have a tendency to collapse to lower-lying solutions even when the connection is performed very slowly. We finally note that the

degeneracy of different l values for a given n is very nearly preserved by the eDFT predictions. Since this is a special property of the Coulomb potential, one cannot expect perfect fidelity from the approximate functionals, and the clustering of eDFT results into quasidegenerate groups is a relatively positive result.

nl	E_{HF}	E_{LDA-X}	E_{B3LYP}	E_{TDLDA}	E_{CS00}	$E_{Expt.}$
2p	1.842 *(0.020)*	1.576 *(-0.246)*	1.607 *(-0.215)*	1.972 *(0.150)*	1.971 *(0.149)*	1.822
3s	3.335 *(0.010)*	3.018 *(-0.308)*	3.278 *(-0.048)*	3.078 *(-0.247)*	3.151 *(-0.175)*	3.326
3p	3.798 *(0.018)*	3.304 *(-0.477)*	3.589 *(-0.191)*	NA	3.410 *(-0.371)*	3.780
3d	3.831 *(0.007)*	3.406 *(-0.418)* 3.161 *(-0.663)*	3.682 *(-0.142)* 3.583 *(-0.241)*	NA	3.502 *(-0.322)*	3.824
avg	0.013	-0.422	-0.167	-0.049	-0.180	
rms	0.014	0.446	0.180	0.205	0.271	

Table 4.3: Lithium Atom Excitation Energies (eV). *Italics* indicate difference from the experimental energy. E_{LDA-X} and E_{B3LYP} denote eDFT energies with the appropriate functional, while TDLDA and TDB3LYP are the corresponding TDDFT energies. $CS00$ [4] contains an asymptotic corrections to the B3LYP exchange potential. In the TDDFT columns NA indicates energy levels above the ionization energy. Experimental numbers from Ref. [5].

As a somewhat more complex test of our algorithm, we have examined the excited states of the Lithium atom. Our calculations employed an uncontracted aug-cc-pVQZ basis [211], which led to excitation energies correct to within 0.1 eV. Our results are presented in Table 4.3. Clearly, once again, eDFT gives relatively accurate Rydberg energies using standard functionals, even for states that TDDFT predicts are embedded in the continuum. Indeed, for B3LYP, the Rydberg energies are predicted with an accuracy approaching that achieved for valence states (e.g. within .2 eV). The eDFT predictions once again systematically underestimate the experimental results. Further, we note that, in our simulations the eDFT d-states typically broke symmetry. This splitting arises because the eDFT exchange-correlation potential is fully *state-specific* – each of the five d orbitals experiences its own (non-spherical) potential. It is thus possible these results could be improved by using a functional that treats degenerate members of a single term on an equal footing[213].

Hartree Fock gives an extremely accurate treatment of Rydberg states generally, and therefore it is not surprising that HF soundly outperforms eDFT for these ex-

citation energies. In order to get a ballpark feeling for the accuracy of these eDFT energies, we also compare them to asymptotically corrected (AC) Casida-Salahub (CS00) [4] TDDFT results. CS00 creates a clear Rydberg series, showing that there are bound 3p- and 3d- states for the lithium atom. However, the results are not significantly better than the eDFT predictions, although CS00 does preserve the degeneracy of the d-levels. While this may or may not be indicative of the quality of eDFT for more complicated Rydberg states, it suggests that eDFT might be a pragmatic means of obtaining Rydberg excitation energies in DFT.

Before moving on, we should offer the caveat that, even with the adiabatic connection algorithm outlined above, obtaining converged eDFT excited states for Li was *extremely* difficult. Some part of this difficulty was due to the very diffuse basis set required to obtain accurate energies. However, a large portion also arose from the inherent instability of solving the eDFT equations. Thus, while one would ideally like Rydberg excited states for several more atoms to make a quantitative comparison between AC functionals and eDFT, such a comparison is impractical with the present algorithm.

4.6 Discussion

4.6.1 Extrema of the ground state energy functional

Are the results above merely fortuitous, or is there some deeper reason why one should expect eDFT to provide good excitation energies from a delta SCF procedure? It is known that there is no universal functional that gives all excited state energies, but is it possible that there exists a universal functional that gives exact energies for a subset of excited state densities? We suspect that the answer to the latter question is 'yes' and based on a theorem proven by Perdew and Levy concerning extrema of the ground-state energy functional [202]. We review the theorem here for completeness and then proceed to explore its applicability to the present results.

Begin with a constrained search formulation of the ground state energy functional

$E_v[\rho]$

$$E_v[\rho] \equiv \min_{\Psi \to \rho} \langle \Psi | \hat{H}_v | \Psi \rangle$$

The absolute minimum of this functional is the ground state energy, E_0 , and it assumes this value at the ground state density ρ_0:

$$E_0 = E_v[\rho_0] = \min_{\rho} E_v[\rho].$$

Perdew and Levy proved that *every extreme density,ρ_i (maximum, minimum, saddle point) of E_v is the density of a stationary state of $\hat{H}_v$ and the value of E_v at that density is the lowest stationary state energy of that density.* Thus, while the minimum of E_v has a rigorous interpretation in connection with the ground state, all other extrema of E_v can just as rigorously be associated with excited states. Further, Perdew and Levy were able to show that no extremal density of E_v above the ground state could be pure-state v-representable – that is, the excited state densities found by this procedure must not be ground state densities for any other external potential [214, 215, 216]. Thus, *it may be possible to use the ground state functional to determine the energies of certain excited states, so long as the associated excited state density is not the ground state density of some other potential.* Further, it would seem likely that highly excited Rydberg densities would be likely candidates if one is searching for a non-pure state v-representable density. Hence, the Perdew-Levy theorem would seem to suggest (but not prove) that Rydberg excited states energies might be rigorously obtained from appropriate extrema of the ground state functional E_v

In order to flesh out the connection of the above theorem with eDFT, we employ a constrained-search formulation of KS theory [217]. Here, one defines the KS kinetic energy functional via:

$$T_s[\rho] \equiv \min_{\Psi \to \rho} \langle \Psi | \hat{T} | \Psi \rangle \tag{4.10}$$

and the Coulomb-exchange-correlation energy functional via

$$E_{xc} \equiv E_v[\rho] - T_s[\rho] - \int \rho(r)v(r)dr.$$

The Euler equation for an extremum of E_v being given by

$$\frac{\delta E_v}{\delta \rho} = \mu$$

one finds that, for the i^{th} extremal density,

$$\left.\frac{\delta T_s}{\delta \rho(r)}\right|_{\rho_i} + v_s[\rho_i](r) = \mu \tag{4.11}$$

Eq. 4.11 is precisely the Euler equation one would obtain for a system of *non-interacting* electrons moving in a potential v_s – this is the Kohn-Sham reference potential associated with the external potential v. We further note that, Eq. 4.11 holds *independent of whether one is speaking of a minimum, maximum or saddle point of* E_v. Thus, for every stationary density, ρ_i of E_v, there exists a noninteracting system that reproduces the exact density, and that system moves under the associated Kohn-Sham potential $v_s[\rho_i]$. Thus, there is a close connection between eDFT excited states – which by design are self-consistent solutions of Eq. 4.11 (cf Eq. 4.3 – and the densities that extremize E_v.

Now, Eq. 4.11 is a necessary but not sufficient condition for a given density to make E_v stationary. In order to satisfy Eq. 4.10, one must additionally have that the Kohn-Sham reference state minimizes the kinetic energy for the given density. The question therefore arises: do the Rydberg states determined in the previous section deliver the minimum kinetic energy for their density? If they do, then the associated eDFT energies are rigorous approximations to the correct Rydberg energies, within the approximations due to functional, basis set, etc. If there is a non-interacting reference with the same density but lower energy, then the states are likely artifacts and the agreement with true Rydberg results is likely fortuitous.

We have attempted to address this question for the Rydberg states above. For

the hydrogen atom, it is trivial to show that every eDFT solution delivers the lowest kinetic energy for its density. Since there is only one electron, there is only ever one wavefunction that maps to a given density (up to an overall phase) and thus there can only be one non-interacting system associated with each excited state density. Thus, the hydrogen atom excited state energies predicted above should be considered rigorous approximations.

The situation for lithium is more complicated, as for this three electron system there are always an infinite number of non-interacting states that map to a given density. In order to locate the minimum kinetic energy associated with each lithium density, we employed a direct minimization technique [218] that is essentially a refined version of the Zhao-Morrison-Parr (ZMP) procedure[219]. Specifically, for a given electron density ρ_{in}, one defines the following new functional of any determinantal wave function Ψ_{det} and the Lagrange multiplier function $v(\text{r})$

$$W_s\left[\Psi_{\text{det}}, v(\text{r})\right] = \sum_i^N \langle\phi_i|\hat{T}|\phi_i\rangle + \int d\text{r} v(\text{r}) \left\{\rho(\text{r}) - \rho_{\text{in}}(\text{r})\right\}, \tag{4.12}$$

where ϕ_i are the orbitals and $v(\text{r})$ can be regarded as the corresponding potential, which is expanded in a basis [218], with the expansion coefficients treated as variational parameters. The solution is found by optimizing W_s. When W_s is optimized, the difference between W_s and $T_s(=\sum_i^N \langle\phi_i|\hat{T}|\phi_i\rangle)$ shows how well the given density is reproduced. We note that the v-representability question arises here, as well. The above formalism is generally applicable any density, either from the ground state or excited states. Meanwhile, when building Ψ_{det}, one is not required to always use orbitals with lowest energies, i.e, one may leave a hole below the highest occupied orbital. In practice, we always stay in the Kohn-Sham scheme; that is, orbitals with lower energies are always occupied first. Hence, if the optimized potential does not reproduce W_s, ρ_{in}, then ρ_{in} is probably not noninteracting v-representable. With this caveat, we can state the results of our search quite succinctly: for all the s-type excited states in Table 4.3, we were able to find an alternate non-interacting ground state that gave a lower KS kinetic energy. For the p- and d- type states our ZMP

search was unsuccessful in locating a ground state that reproduces ρ_{in}. This result *does not prove conclusively* that the p- and d- densities are not noninteracting v-representable, as our search is only numerical and does not necessarily exhaustively cover the available density space. However, the results strongly suggest that the p- and d- densities are not noninteracting v-representable.

We thus conclude that the s-type excited states for lithium are accurate, at least in part, due to a cancellation of errors, because their kinetic energies are *not* what would be predicted by the constrained search. A cancellation of errors could be expected, however, as Rydberg states are essentially one-electron in nature, making the KS reference a fairly good description of these excitations. On the other hand, our results suggest that the p- and d-type Rydberg states may be more physically justified, since their densities appear to be not noninteracting v-representable. This may stem, in part, from the symmetry considerations present in the p- and d- excited states.

Given the intimate connection between the physical basis of eDFT and the pure state v-representability of the density, one immediately recognizes a connection between eDFT and constrained density functional theory [203]. In constrained DFT, one applies a constraint to the electron density in order to enforce some physical property of interest (e.g. dipole, charge localization) [1]. As we have recently shown, this technique can be used to good effect to obtain information about charge transfer excited states [142, 19, 21, 220] and spin states [221, 143]. In each case, the excited state in question can actually be obtained as the ground state of the system *under an alternative potential*. Taken together with our results here, one comes to the conclusion that these techniques are essentially complementary to one another; while constrained DFT works only when the excited density is pure state v-representable, eDFT appears to only apply when the excited density is *not* pure state v-representable. Thus, while neither of these techniques by itself provides complete coverage of the space of

[1] We note that, somewhat confusingly, a few authors have historically referred to what we here call excited state DFT, as constrained DFT, with the idea that eDFT involves a constraint on the occupation numbers. For our purposes, constrained DFT will refer *only* to constraints involving the density.

all possible excited states available in DFT, together they bring us a few steps closer to a rigorous basis for obtaining excited states as stationary states in DFT.

4.7 Conclusions

We have investigated both the practical and formal utility of excited state DFT (eDFT) calculations for electronic excited states, with particular emphasis on Rydberg states. Because the Kohn-Sham (KS) potential in eDFT is *different for each excited state* we find that eDFT gives a qualitatively correct asymptotic form of the effective potential, even for commonly used exchange correlation functionals for which the ground state potential has the incorrect form at large distances. We verify numerically that commonly used functionals – including LSDA, GGAs and hybrids – give accurate energies for the Rydberg states of the hydrogen and lithium atoms. While the errors in these cases are worse than Hartree-Fock, they are competitive with at least one asymptotically corrected hybrid functional [4]. Finally, we address the formal basis of eDFT for excited states. Based on a theorem due to Perdew and Levy [202] we note that all stationary energies of the exact functional correspond to eigenvalues of the true Hamiltonian. We further note that eDFT solutions correspond to stationary states *as long as they deliver the minimum kinetic energy for their density.* We test this criterion in the present cases, and find that for all the hydrogen states and all of the p- and d- states for lithium, the eDFT solution delivers the minimum kinetic energy for its density. Thus, in some cases, eDFT can be a rigorous way to obtain excited state energies in DFT.

Moving forward, there are several issues to be addressed. The primary obstacle to progress relates to convergence; even for these simple systems, we found it extremely difficult to converge the self-consistent field (SCF) iterations for eDFT, as high-lying solutions had a very strong tendency to collapse to lower-lying states. In order for eDFT to become in any way practical, then, one must determine a means of stabilizing the SCF iterations, perhaps using variations of existing SCF minimization strategies [8, 9, 222] adapted to locate saddle points. The second major issue is the necessity of testing to see if the converged eDFT solution delivers the minimum kinetic energy.

While not computationally costly, this procedure is far from standard and the option to minimize T_s is not available in most production codes. Do eDFT states that are not minima give appreciably worse results than those that do? Can one build in this constraint to the SCF iterations?

Finally, on the more speculative side, there are a number of directions one would like to take this result assuming the technical obstacles mentioned above can be overcome. The Perdew-Levy theorem suggests that eDFT provides a route to excited states whose densities *are not the ground state of some other potential* (i.e. they are not pure-state v-representable). This puts eDFT in a complementary position to constrained DFT, which is explicitly able to approximate excited states that *are the ground state of an alternative potential* [203]. Thus, while neither of these techniques together provides a complete set of excited states (as can be obtained in principle from TDDFT) together these two methods may cover a large fraction of the "interesting" low-lying excited states of atoms and molecules. For example, we have shown that constrained DFT provides a rigorous route to charge-transfer excited states [142, 19] while eDFT describes Rydberg states effectively. It would be interesting to see if some combination of these techniques could be used to obtain doubly excited states with DFT, which have proven elusive in TDDFT [223].

Chapter 5

Conclusion

Even though DFT is formally exact, existing approximations to the DFT energy functional suffer from numerous flaws. These flaws are broadly attributed to self-interaction error, the adiabatic approximation, and spatial locality of xc functionals.

The improvement of exchange-correlation functionals is an active field of research, and much of that work is geared towards ridding exchange-correlation functionals of the artifacts described above. It was realized pretty early on, however, that the success of DFT was in no small part due to the fortuitous cancellation of error between the different artifacts. As such, the independent elimination of single artifacts from the list often led to worse results in practice.

Our answer to this conundrum has been to tackle the xc functional artifacts indirectly - instead of developing functionals, we have focused on developing procedures which overcome some of the systematic flaws, but which would also work with an exact functional. It is our hope that in doing so, we are making progress in a direction orthogonal and complementary to that of functional developers.

Practically, this orthogonality facilitates the application of existing functionals to new problems. Intellectually, however, the successes and failures of our approaches can help to guide functional improvement. Wavefunction-based methods may seem to provide the ideal reference for DFT development by eliminating the uncertainty associated with the interpretation of experimental results. However, systems of interest to DFT practitioners are often too big for high quality wavefunction methods to be used. As such, alternative protocols for determining physical observables, like

the procedures described in this work, make available self-consistency checks and in doing so provide clues as to the nature of inaccuracies encountered.

Appendix A

Magnus and Runge-Kutta Munthe-Kaas Integrators

Both of these integrators are strictly unitary, with unitarity ensured by the use of numerical diagonalization routines.

A.1 Magnus Integrators

The 2nd order propagator is presented in Chapter 3. Here we present the 4th order Magnus integrator scheme.

$$\begin{aligned}
\hat{U}(t, t+dt) &\approx exp(\hat{\Omega}_1 + \hat{\Omega}_2) + O(dt^5) \\
\hat{\Omega}_1 &= -i \cdot (\hat{H}(\tau_1) + \hat{H}(\tau_2)) \cdot \frac{dt}{2} \\
\hat{\Omega}_2 &= [\hat{H}(\tau_1), \hat{H}(\tau_2)] \cdot \frac{\sqrt{3}\, dt^2}{12} \\
\tau_{1,2} &= t + (\frac{1}{2} \mp \frac{\sqrt{3}}{6}) \cdot dt
\end{aligned}$$

Like the 2nd order propagator, because of the implicit time-dependence of the Fock matrix we need to formulate a predictor-corrector scheme, which is depicted in figure A-1.

1. Polynomial extrapolation: 3rd order fock matrices stored from previous time steps, 1a, 1b and 1c, are used to extrapolate the fock matrices 3a and 3b.

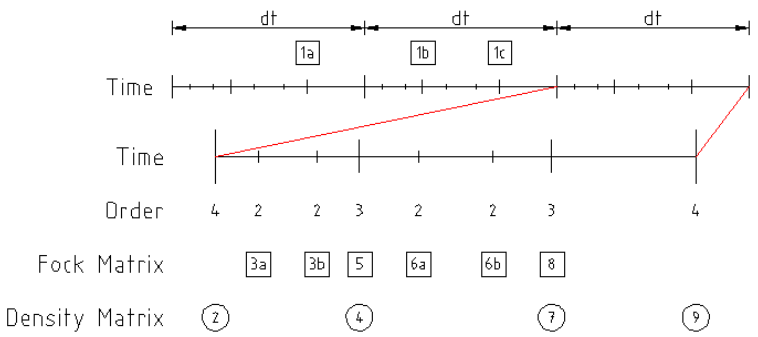

Figure A-1: Extrapolation routine for the 4th order Magnus integrator. The order row shows the time order (in dt) to which the matrices in the same column are correct to.

2. Magnus Integrator: using 3a and 3b, the density matrix 2 is propagated to 4.

3. Fockbuild: density matrix 4 is used to compute the fock matrix 5.

4. Polynomial extrapolation: fock matrices 1b, 1c and 5 are used to extrapolate fock matrices 6a and 6b.

5. Magnus Integrator: fock matrices 6a and 6b are used to propagate the density matrix 4 to density matrix 7.

6. Fockbuild: density matrix 7 is used to compute the fock matrix 8.

7. Magnus Integrator: fock matrices 5 and 8 are then used to propagate the density matrix 2 to density matrix 9.

A.2 RKMK Integrators

By using the ansatz

$$\Psi(t) \quad = \quad e^{\hat{\Omega}(t)} \cdot \Psi(t_0)$$

one can reformulate the schroedinger equation as a differential equation for $\hat{\Omega}(t)$, and then propagate $\hat{\Omega}(t)$ using Runge-Kutta. This is known as the RKMK [224]

propagator. The RKMK propagator uses the same number of fockbuilds as regular Runge-Kutta, but is unitary.

$$
\begin{aligned}
\partial_t e^{\hat{\Omega}(t)} &= dexp_{\hat{\Omega}(t)}\left(\partial_t \hat{\Omega}(t)\right) \cdot e^{\Omega(t)} \\
dexp_{\hat{A}} &= \frac{exp(ad_{\hat{A}}) - I}{ad_{\hat{A}}} \\
ad_{\hat{A}}(\hat{B}) &= [\hat{A}, \hat{B}] \\
\partial_t e^{\Omega(t)} \cdot \Psi(t_0) &= dexp_{\Omega(t)}\left(\partial_t \hat{\Omega}(t)\right) \cdot e^{\Omega(t)} \cdot \Psi(t_0) \\
\partial_t \Psi(t) &= dexp_{\Omega(t)}\left(\partial_t \hat{\Omega}(t)\right) \cdot \Psi(t) \\
-i\hat{F}(t) \cdot \Psi(t) &= dexp_{\Omega(t)}\left(\partial_t \hat{\Omega}(t)\right) \cdot \Psi(t) \\
dexp^{-1}_{\hat{\Omega}(t)}\left(-i\hat{F}(t)\right) &= \partial_t \hat{\Omega}(t) \\
dexp^{-1}_{\hat{A}} &= \frac{ad_{\hat{A}}}{exp(ad_{\hat{A}}) - I} \\
&= \sum_{j=0}^{\infty} \frac{B_j}{j!} ad^j_{\hat{A}}
\end{aligned}
$$

where B_j are the Bernoulli numbers.

Bibliography

[1] Q. Wu, C.L. Cheng, and T. Van Voorhis. Configuration interaction based on constrained density functional theory: A multireference method. *The Journal of Chemical Physics*, 127:164119, 2007.

[2] J. C. Slater. A simplification of the hartree-fock method. *Phys. Rev.*, 81(3):385–390, Feb 1951.

[3] R. Buchner, J. Barthel, and J. Stauber. The dielectric relaxation of water between C and C. *Chemical Physics Letters*, 306(1-2):57–63, 1999.

[4] Mark E. Casida and Dennis R. Salahub. Asymptotic correction approach to improving approximate exchange–correlation potentials: Time-dependent density-functional theory calculations of molecular excitation spectra. *The Journal of Chemical Physics*, 113(20):8918–8935, 2000.

[5] Leon J. Radziemski, Rolf Engleman, and James W. Brault. Fourier-transform-spectroscopy measurements in the spectra of neutral lithium, ^6i and ^7i (li i). *Phys. Rev. A*, 52(6):4462–4470, Dec 1995.

[6] J. C. Slater. *Phys. Rev.*, 34:1293, 29.

[7] A Szabo and N. S. Ostlund. *Modern Quantum Chemistry.* McGraw-Hill, New York, 1989.

[8] P. Pulay. *Chem. Phys. Lett.*, 73:393, 1980.

[9] P. Pulay. *J. Comp. Chem.*, 3:556, 1982.

[10] W. Koch and M. C. Holthausen. *A Chemist's Guide to Density Functional Theory.* Wiley VCH, Weinheim, 2001.

[11] R. Shepard. In K. P. Lawley, editor, *Advances in Chemical physics: ab initio methods in Quantum Chemistry-II*, volume 69, page 63. John Wiley & Sons Ltd., New York, 1987.

[12] C. Møller and M. S. Plesset. *Phys. Rev.*, 46:618, 1934.

[13] P. Hohenberg and W. Kohn. Inhomogeneous electron gas. *Phys. Rev.*, 136(3B):B864–B871, Nov 1964.

[14] W. Kohn and L. J. Sham. Self-consistent equations including exchange and correlation effects. *Phys. Rev.*, 140(4A):A1133–A1138, Nov 1965.

[15] M. Levy. Electron densities in search of Hamiltonians. *Physical Review A*, 26(3):1200–1208, 1982.

[16] H. Englisch and R. Englisch. Hohenberg-Kohn theorem and non-V-representable densities. *Physica A*, 121(1-2):253–268, 1983.

[17] P. H. Dederichs, S. Blügel, R. Zeller, and H. Akai. Ground states of constrained systems: application to cerium impurities. *Phys. Rev. Lett.*, 53(26):2512–2515, 1984.

[18] A. D. Becke. A multicenter numerical integration scheme for polyatomic molecules. *J. Chem. Phys.*, 88(4):2547–2553, 1988.

[19] Q. Wu and T. Van Voorhis. Constrained Density Functional Theory and Its Application in Long-Range Electron Transfer. *J. Chem. Theory Comput*, 2(3):765–774, 2006.

[20] Q. Wu and T. Van Voorhis. Extracting electron transfer coupling elements from constrained density functional theory. *The Journal of Chemical Physics*, 125:164105, 2006.

[21] Q. Wu and T. Van Voorhis. Direct Calculation of Electron Transfer Parameters through Constrained Density Functional Theory. *J. Phys. Chem. A*, 110(29):9212–9218, 2006.

[22] E. Runge and E. K. U. Gross. *Phys. Rev. Lett.*, 52:997, 1984.

[23] F. Furche. On the density matrix based approach to time-dependent density functional response theory. *The Journal of Chemical Physics*, 114:5982, 2001.

[24] SH Vosko, L. Wilk, and M. Nusair. Accurate spin-dependent electron liquid correlation energies for local spin density calculations: a critical analysis. *Canadian Journal of Physics*, 58(8):1200–1211, 1980.

[25] Viktor N. Staroverov, Gustavo E. Scuseria, Jianmin Tao, and John P. Perdew. Tests of a ladder of density functionals for bulk solids and surfaces. *Phys. Rev. B*, 69(7):075102, Feb 2004.

[26] Shang-Keng Ma and Keith A. Brueckner. Correlation energy of an electron gas with a slowly varying high density. *Phys. Rev.*, 165(1):18–31, Jan 1968.

[27] John P. Perdew and Wang Yue. Accurate and simple density functional for the electronic exchange energy: Generalized gradient approximation. *Phys. Rev. B*, 33(12):8800–8802, Jun 1986.

[28] John P. Perdew. Density-functional approximation for the correlation energy of the inhomogeneous electron gas. *Phys. Rev. B*, 33(12):8822–8824, Jun 1986.

[29] J.P. Perdew and W. Yue. Accurate and simple density functional for the electronic exchange energy: Generalized gradient approximation. *Physical Review B*, 33(12):8800–8802, 1986.

[30] J. P. Perdew, K. Burke, and M. Ernzerhof. *Phys. Rev. Lett.*, 77:3865–3868, 96.

[31] AD Becke. Density-functional exchange-energy approximation with correct asymptotic behavior. *Physical Review A*, 38(6):3098–3100, 1988.

[32] A. D. Becke. Density-functional thermochemistry. i. the effect of the exchange-only gradient correction. *J. Chem. Phys.*, 96:2155–2160, 1992.

[33] PHT PHILIPSEN, G. TE VELDE, and EJ BAERENDS. The effect of density-gradient corrections for a molecule-surface potential energy surface. Slab calculations on Cu (100) c (2 × 2)-CO. *Chemical physics letters*, 226(5-6):583–588, 1994.

[34] S. Tsuzuki and H.P. Lüthi. Interaction energies of van der Waals and hydrogen bonded systems calculated using density functional theory: Assessing the PW91 model. *The Journal of Chemical Physics*, 114:3949, 2001.

[35] R.J. Deeth and H.D.B. Jenkins. A Density Functional and Thermochemical Study of MX Bond Lengths and Energies in [MX˜ 6]ˆ 2ˆ-Complexes: LDA versus Becke88/Perdew86 Gradient-Corrected Functionals. *Journal of physical chemistry. A, molecules, spectroscopy, kinetics, environment & general theory*, 101(26):4793–4798, 1997.

[36] J. Harris. Adiabatic-connection approach to Kohn-Sham theory. *Physical Review A*, 29(4):1648–1659, 1984.

[37] A. D. Becke. A new mixing of hartree-fock and local density-functional theories. *J. Chem. Phys.*, 98(2):1372–1377, 1993.

[38] A. D. Becke. Density-functional thermochemistry. iii. the role of exact exchange. *J. Chem. Phys.*, 98(7):5648–5652, 1993.

[39] Y. Zhang and W. Yang. A challenge for density functionals: Self-interaction error increases for systems with a noninteger number of electrons. *The Journal of Chemical Physics*, 109:2604, 1998.

[40] J. P. Perdew, R. G. Parr, M. Levy, and J. L. Balduz, Jr. *Phys. Rev. Lett.*, 49:1691–1694, 1982.

[41] J. P. Perdew and M. Levy. *Phys. Rev. Lett.*, 51:1884–1887, 1983.

[42] L. J. Sham and M. Schluter. *Phys. Rev. Lett.*, 51:1888–1891, 1983.

[43] J. P. Perdew and M. Levy. Physical content of the exact kohn-sham orbital energies: Band gaps and derivative discontinuities. *Phys. Rev. Lett.*, 51:1884, 1983.

[44] R. W. Godby, M. Schlüter, and L. J. Sham. Accurate exchange-correlation potential for silicon and its discontinuity on addition of an electron. *Phys. Rev. Lett.*, 56(22):2415–2418, Jun 1986.

[45] Andreas Dreuw, Jennifer L. Weisman, and Martin Head-Gordon. Long-range charge-transfer excited states in time-dependent density functional theory require non-local exchange. *J. Chem. Phys.*, 119:2943–2946, 2003.

[46] Andreas Dreuw and Martin Head-Gordon. Failure of time-dependent density functional theory for long-range charge-transfer excited states: the zincbacteriochlorin-bacteriochlorin and bacteriochlorophyll-spheroidene complexes. *J. Am. Chem. Soc.*, 126:4007–4016, 2004.

[47] John P. Perdew and Mel Levy. Comment on "significance of the highest occupied kohn-sham eigenvalue". *Phys. Rev. B*, 56:16021–16028, 1997.

[48] Yingkai Zhang and Weitao Yang. A challenge for density functionals: Self-interaction error increases for systems with a noninteger number of electrons. *J. Chem. Phys.*, 109:2604–2608, 1998.

[49] Marten A. Buijse, Evert Jan Baerends, and Jaap G. Snijders. Analysis of correlation in terms of exact local potentials: Applications to two-electron systems. *Phys. Rev. A*, 40(8):4190–4202, Oct 1989.

[50] D. Cremer. Invited Paper-Density functional theory: coverage of dynamic and non-dynamic electron correlation effects. *Mol. Phys.*, 99(23):1899–1940, 2001.

[51] Y. Zhao, N. E. Schultz, and D. G. Truhlar. Design of Density Functionals by Combining the Method of Constraint Satisfaction with Parametrization for Thermochemistry, Thermochemical Kinetics, and Noncovalent Interactions. *J. Chem. Theory. Comput.*, 2(2):364–382, 2006.

[52] O. A. Vydrov, J. Heyd, A. V. Krukau, and G. E. Scuseria. Importance of short-range versus long-range Hartree-Fock exchange for the performance of hybrid density functionals. *J. Chem. Phys.*, 125:074106, 2006.

[53] A. J. Cohen, P. Mori-Sánchez, and W. Yang. Development of exchange-correlation functionals with minimal many-electron self-interaction error. *J. Chem. Phys.*, 126:191109, 2007.

[54] C.L. Cheng, J.S. Evans, and T. Van Voorhis. Simulating molecular conductance using real-time density functional theory. *Physical Review B*, 74(15):155112, 2006.

[55] GE Moore. Cramming more circuits on chips. *Electronics*, 19(4):114, 1965.

[56] R. P. Andres, T. Bein, M. Dorogi, S. Feng, J. I. Henderson, C. P. Kubiak, W. Mahoney, R. G. Osifchin, and R. Reifenberger. *Science*, 272:1323, 1996.

[57] T. A. Jung, J. K. Schlitter, J. K. Gimzewski, H. Tang, and C. Joachim. *Science*, 271:181, 1996.

[58] L. A. Bumm, J. J. Arnold, M. T. Cygan, T. D. Dunbar, T. P. Burgin, L. Jones II, D. L. Allara, J. M. Tour, and P. S. Weiss. *Science*, 271:1705, 1996.

[59] M. A. Reed, C. Zhou, C. J. Muller, T. P. Burgin, and J. M. Tour. *Science*, 278:252, 1997.

[60] B. C. Stipe, M. A. Rezaei, and W. Ho. *Science*, 280:1732, 1998.

[61] R. Martel, T. Schmidt, H. R. Shea, T. Hertel, and P. Avouris. *App. Phys. Lett.*, 73:2447–2449, 1998.

[62] J. Chen, M. A. Reed, A. M. Rawlett, and J. M. Tour. *Science*, 286:1550, 1999.

[63] G. Leatherman, E. N. Durantini, D. Gust, T. A. Moore, A. L. Moore, S. Stone, Z. Zhou, P. Rez, and Y. Z. Liu. *JPCB*, 103:4006–4010, 1999.

[64] H. Park, J. Park, A. K. L. Lim, E. H. Anderson, A. P. Alivisatos, and P. L. McEuen. *Nature*, 407:57–60, 2000.

[65] D. L. Gittins, D. Bethell, D. J. Schiffrin, and R. J. Nichols. *Nature*, 408:67, 2000.

[66] P. C. Collins, M. S. Arnold, and P. Avouris. *Science*, 292:706–709, 2001.

[67] X. D. Cui, A. Primak, X. Zarate, J. Tomfohr, O. F. Sankey, A. L. Moore, T. A. Moore, D. Gust, and G. Harris. *Science*, 294:571–574, 2001.

[68] P. L. McEuen, M. S. Fuhrer, and H. K. Park. *IEEE Trans. Nanotech.*, 1:78–85, 2002.

[69] W. J. Liang *et al. Nature*, 417:725, 2002.

[70] J. Park *et al. Nature*, 417:722, 2002.

[71] P. Avouris. *Acc. Chem. Res.*, 35:1026–1034, 2002.

[72] M. C. Hersam, N. P. Guisinger, J. Lee, K. Cheung, and J. W. Lydig. *Appl. Phys. Lett.*, 80:201, 2002.

[73] G. V Nazin, D. L. Wang, and W. Ho. *Science*, 302:77–81, 2003.

[74] A. Salomon, D. Cahen, S. Lindsay, J Tomfohr, V. B. Engelkes, and C. D. Frisbie. *Adv. Mat.*, 15:1881–1890, 2003.

[75] J. G. Kushmerick, J. Lazorcik, C. H. Patterson, R. Shashidhar, D. S. Seferos, and G. C. Bazan. *Nano. Lett.*, 4:639–642, 2004.

[76] X. Y. Xiao and N. J. Xu, B. Q. ant Tao. *Nano. Lett.*, 4:267–271, 2004.

[77] N. P. Guisinger, M. E. Greene, R. Basu, A. S. Baluch, and M. C. Hersam. *Nano. Lett.*, 4:55–59, 2004.

[78] R. L. McCreery. *Chem. Mater.*, 16:4477–4496, 2004.

[79] K. Kitagawa, T. Morita, and S. Kimura. *J. Phys. Chem. B*, 109:13906–13911, 2005.

[80] R. Landauer. *IBM J. Res. Dev.*, 1:223, 1957.

[81] R. Landauer. *Philos. Mag.*, 21:863, 1970.

[82] R. Landauer. *Z. Phys. B*, 21:247, 1975.

[83] M. Büttiker. *Phys. Rev. Lett.*, 57:1761, 1986.

[84] M. Büttiker. *Phys. Rev. B*, 38:9375, 1988.

[85] N. D. Lang. *Phys. Rev. B*, 52:5335–5342, 1995.

[86] N. D. Lang. *Phys. Rev. Lett.*, 79:1357–1360, 1997.

[87] N. D. Lang and P. Avouris. *Phys. Rev. Lett.*, 81:3515–3518, 1998.

[88] E. G. Emberly and G. Kirczenow. *Phys. Rev. B*, 58:10911–10920, 1998.

[89] J. Tomfohr and O. F. Sankey. *J. Chem. Phys.*, 120:1542–1554, 2004.

[90] L. P. Kadanoff and G. Baym. *Quantum Statistical Mechanics.* Benjamin/Cummings, New York, 1962.

[91] S. Datta. *Superlattices Microstruct.*, 28:253–278, 2000.

[92] T. N. Todorov. *J. Phys. Cond. Mat.*, 14:3049–3084, 2002.

[93] P. Delaney and J. C. Greer. *Phys. Rev. Lett.*, 93:036805, 2004.

[94] J. Taylor, H. Guo, and J. Wang. *Phys. Rev. B*, 63:245407, 2001.

[95] P. A. Derosa and J. M. Seminario. *J. Phys. Chem. B*, 105:471–481, 2001.

[96] Y. Xue, S. Datta, and M. A. Ratner. *Chem. Phys.*, 281:151–170, 2002.

[97] M. Brandbyge, J. L. Mozos, P. Ordejón, J. Taylor, and K. Stokbro. *Phys. Rev. B*, 65:165401, 2002.

[98] S. H. Ke, H. U. Baranger, and W. Yang. *Phys. Rev. B*, 70:085410, 2004.

[99] T. Tada, M. Kondo, and K. Yoshizawa. *J. Chem. Phys.*, 121:8050–8057, 2004.

[100] G. C. Solomon, J. R. Reimers, and N. S. Hush. *J. Chem. Phys.*, 121:6615, 2004.

[101] G. C. Solomon, J. R. Reimers, and N. S. Hush. *J. Chem. Phys.*, 122:224502, 2005.

[102] V. Mujica, M. Kemp, A. Roitberg, and M. A. Ratner. *J. Chem. Phys.*, 104:7296–7305, 1996.

[103] H. Ness and A. J. Fisher. *Phys. Rev. Lett.*, 83:452–455, 1999.

[104] T. Kostyrko and B. R. Bulka. *Phys. Rev. B*, 67:205331, 2003.

[105] M. di Ventra and T. N. Todorov. *J. Phys. Cond. Mat.*, 16:8025–8034, 2004.

[106] G. Stefanucci and C. O. Almbladh. *Europhys. Lett.*, 67:14, 2004.

[107] K. Burke, R. Car, and R. Gebauer. *Phys. Rev. Lett.*, 94:146803, 2005.

[108] N. Sai, M. Zwolak, G. Vignale, and M. di Ventra. *Phys. Rev. Lett.*, 94:186810, 2005.

[109] C. Toher, A. Filippetti, S. Sanvito, and K. Burke. *Phys. Rev. Lett.*, 95:146402, 2005.

[110] R. Baer, T. Seideman, S. Ilani, and D. Neuauser. *J. Chem. Phys.*, 120:3387–3396, 2004.

[111] S. Kurth, G. Stefanucci, C. O. Almbladh, A. Rubio, and E. K. U. Gross. *Phys. Rev. B*, 72:035308, 2005.

[112] N. Bushong, N. Sai, and M. di Ventra. *Nano. Lett.*, 5:2569–2572, 2005.

[113] X. F. Qian, J. Li, X. Lin, and S. Yip. *Phys. Rev. B*, 73:035408, 2006.

[114] K. Yabana and G. F. Bertsch. *Phys. Rev. B*, 54:4484–4487, 1996.

[115] K. Yabana and G. F. Bertch. *Int. J. Quantum Chem.*, 75:55–66, 1999.

[116] F. Calvayrac, P. G. Reinhard, E. Suraud, and C. A. Ullrich. *Phys. Rep.*, 337:493–578, 2000.

[117] K. Tada and K. Watanabe. *Phys. Rev. Lett.*, 88:127601, 2002.

[118] M. A. L. Marques, X. Lopez, D. Varsano, A. Castro, and A. Rubio. *Phys. Rev. Lett.*, 90:258101, 2003.

[119] O. Sugino and Y. Miyamoto. *Phys. Rev. B*, 59:2579–2586, 1999.

[120] R. Baer and R. Gould. *J. Chem. Phys.*, 114:3385–3392, 2001.

[121] A. Castro, M. A. L. Marques, and A. Rubio. *J. Chem. Phys.*, 121:3425–3433, 2004.

[122] M. P. Samanta, W. Tian, S. Datta, J. I. Henderson, and C. P. Kubiak. *Phys. Rev. B*, 53:R7626–7629, 1996.

[123] D. S. Kosov and J. C. Greer. *Phys. Lett. A*, 291:46–50, 2001.

[124] D. S. Kosov. *J. Chem. Phys.*, 120:7165–7168, 2004.

[125] D. S. Kosov. *J. Chem. Phys.*, 119:1–5, 2003.

[126] H. Appel, , E. K. U. Gross, and K. Burke. *Phys. Rev. Lett.*, 90:043005, 2003.

[127] E. K. U. Gross, J. F. Dobson, and M. Petersilka. *Top. Curr. Chem.*, 181:81–172, 1996.

[128] W. Kohn. *Phys. Rev. Lett.*, 76:3168–3171, 1996.

[129] R. Baer and M. Head-Gordon. Sparsity of the Density Matrix in Kohn-Sham Density Functional Theory and an Assessment of Linear System-Size Scaling Methods. *Phys. Rev. Lett.*, 79(20):3962–3965, 17 November 1997.

[130] P. E. Maslen, C. Ochsenfeld, C. A. White, M. S. Lee, and M. Head-Gordon. *J. Phys. Chem. A*, 102:2215–2222, Locality and sparsity of ab initio one particle density matrices and localized orbitals.

[131] M. Challacombe. *Comput. Phys. Comm.*, 128:93–107, 2000.

[132] S. Blanes, F. Casas, and J. Ros. Improved High Order Integrators Based on the Magnus Expansion. *BIT Numerical Mathematics*, 40(3):434–450, September 2000.

[133] S. Blanes, F. Casas, J. A. Oteo, and J. Ros. *J. Phys. A: Math. Gen.*, 31:259–268, 1998.

[134] Wolfram Research, Inc. *Mathematica, Version 5.2*. Wolfram Research, Inc. , Champaign, IL, 2005.

[135] High Performance Computational Chemistry Group, *NWChem, A Computational Chemistry Package for Parallel Computers, Version 4.6*(Pacific Northwest National Laboratory, Richland, Washington 99352, USA, 2004).

[136] A. D. Becke. Density-functional thermochemistry .3. the role of exact exchange. *J. Chem. Phys.*, 98:5648–5652, 1993.

[137] P. C. Hariharan and J. A. Pople. *Theor. Chim. Acta*, 28:213, 1973.

[138] M. di Ventra and N. D. Lang. *Phys. Rev. B*, 65:045402, 2001.

[139] I. V. Ovchinnikov and D. Neuhauser. *J. Chem. Phys.*, 122:024707, 2005.

[140] P. O. Löwdin. *J. Chem. Phys.*, 18:365, 1950.

[141] E. R. Davidson. *J. Chem. Phys.*, 46:3320, 1967.

[142] Q. Wu and T. Van Voorhis. Direct optimization method to study constrained systems within density functional theory. *Phys. Rev. A*, 72:024502, 2005.

[143] I Rudra, Q. Wu, and T. Van Voorhis. *J. Chem. Phys.*, 24:024103, 2006.

[144] M. Kindermann, Yu. V. Nazarov, and C. W. J. Beenakker. *Phys. Rev. Lett.*, 90:246805, 2003.

[145] L. S. Levitov and G. B. Lesovik. *JETP Lett.*, 58:230–235, 1993.

[146] V. K. Khlus. *Sov. Phys. JETP*, 66:1243, 1987.

[147] G. B. Lesovik. *JETP Lett.*, 49:592, 1989.

[148] C. W. J. Beenakker and M. Büttiker. *Phys. Rev. B*, 46:1889, 1992.

[149] M Büttiker. *Phys. Rev. B*, 46:12485–12507, 1992.

[150] M. Reznikov, M. Heiblum, H. Shtrikman, and D. Mahalu. *Phys. Rev. Lett.*, 75:3340–3343, 1995.

[151] A. Kumar, L. Saminadayar, D. C. Glattli, Y. Jin, and B. Etienne. *Phys. Rev. Lett.*, 76:2778–2781, 1996.

[152] C. W. J. Beenakker. *Rev. Mod. Phys.*, 69:731–808, 1997.

[153] A. L. Fetter and J. D. Walecka. *Quantum Theory of Many-Particle Systems.* McGraw-Hill, New York, 1971.

[154] F. Furche and T. Van Voorhis. *J. Chem. Phys.*, 122:164106, 2005.

[155] M. Fuchs, Y. M. Niquet, X. Gonze, and K. Burke. Describing static correlation in bond dissociation by Kohn–Sham density functional theory. *J. Chem. Phys.*, 122:094116, 2005.

[156] R. J. Bartlett and J. F. Stanton. Applications of post-hartree - fock methods: A tutorial. In *Reviews in computational chemistry*, volume 5, pages 65–169. VCH, New York, 1994.

[157] T. D. Crawford and H. F. Schaefer III. An Introduction to Coupled Cluster Theory for Computational Chemists. In *Reviews in Computational Chemistry*, volume 14, pages 33–136. VCH, New York, 2000.

[158] B. G. Johnson, P. M. W. Gill, and J. A. Pople. The performance of a family of density functional methods. *J. Chem. Phys.*, 98:5612–5626, 1993.

[159] W. Kohn, A. D. Becke, and R. G. Parr. Density functional theory of electronic structure. *J. Phys. Chem.*, 100:12974–12980, 1996.

[160] Thomas Bally and G. Narahari Sastry. Incorrect dissociation behavior of radical ions in density functional calculations. *J. Phys. Chem. A*, 101:7923, 1997.

[161] John P. Perdew. What do the kohn-sham orbital energies mean? how do atoms dissociate. In Reiner M. Dreizler, editor, *Density Functional Methods in Physics*, pages 265–308. Plenum Press, New York, 1985.

[162] A. D. Dutoi and M. Head-Gordon. Self-interaction error of local density functionals for alkali-halide dissociation. *Chem. Phys. Lett.*, 422(1-3):230–233, 2006.

[163] A. Ruzsinszky, J. P. Perdew, G. I. Csonka, O. A. Vydrov, and G. E. Scuseria. Spurious fractional charge on dissociated atoms: Pervasive and resilient self-interaction error of common density functionals. *J. Chem. Phys.*, 125:194112, 2006.

[164] O. Gunnarsson and B. I. Lundqvist. Exchange and correlation in atoms, molecules, and solids by the spin-density-functional formalism. *Phys. Rev. B*, 13:4274–4298, 1976.

[165] John P Perdew, Andreas Savin, and Kieron Burke. Escaping the symmetry dilemma through a pair-density interpretation of spin-density functional theory. *Phys. Rev. A*, 51:4531, 1995.

[166] J. C. Slater, J. B. Mann, T. M. Wilson, and J. H. Wood. Nonintegral Occupation Numbers in Transition Atoms in Crystals. *Phys. Rev.*, 184(3):672–694, 1969.

[167] M. Filatov and S. Shaik. A spin-restricted ensemble-referenced Kohn-Sham method and its application to diradicaloid situations. *Chem. Phys. Lett*, 304:429–437, 1999.

[168] P. R. T. Schipper, O. V. Gritsenko, and E. J. Baerends. Benchmark calculations of chemical reactions in density functional theory: Comparison of the accurate kohnsham solution with generalized gradient approximations for the h2 + h and h2 + h2 reactions. *J. Chem. Phys.*, 111:4056–4067, 1999.

[169] Y. Shao, M. Head-Gordon, and A. I. Krylov. The spin–flip approach within time-dependent density functional theory: Theory and applications to diradicals. *J. Chem. Phys.*, 118(11):4807, 2003.

[170] P. Borowski, KD Jordan, J. Nichols, and P. Nachtigall. Investigation of a hybrid TCSCF-DFT procedure. *Theo. Chem. Acc.*, 99(2):135–140, 1998.

[171] J. Gräfenstein and D. Cremer. Development of a CAS-DFT method covering non-dynamical and dynamical electron correlation in a balanced way. *Mol. Phys.*, 103(2):279–308, 2005.

[172] W. Wu and S. Shaik. VB-DFT: A nonempirical hybrid method combining valence bond theory and density functional energies. *Chem. Phys. Lett*, 301:37–42, 1999.

[173] Thierry Leininger, Hermann Stoll, Hans-Joachim Werner, and Andreas Savin. Combining long-range configuration interaction with short-range density functionals. *Chem. Phys. Lett.*, 275(3):151–160, 1997.

[174] S. Grimme and M. Waletzke. A combination of Kohn–Sham density functional theory and multi-reference configuration interaction methods. *J. Chem. Phys.*, 111(13):5645, 1999.

[175] J. Gerratt, D. L. Cooper, P. B. Karadakov, and M. Raimondi. Modern valence bond theory. *Chem. Soc. Rev*, 26:87–100, 1997.

[176] T. Thorsteinsson, D. L. Cooper, J. Gerratt, P. B. Karadakov, and M. Raimondi. Modern valence bond representations of CASSCF wavefunctions. *Theo. Chem. Acc.*, 93(6):343–366, 1996.

[177] T. Thorsteinsson and D. L. Cooper. Exact transformations of CI spaces, VB representations of CASSCF wavefunctions and the optimization of VB wavefunctions. *Theo. Chem. Acc.*, 94(4):233–245, 1996.

[178] J. Gräfenstein, E. Kraka, and D. Cremer. The impact of the self-interaction error on the density functional theory description of dissociating radical cations: Ionic and covalent dissociation limits. *J. Chem. Phys.*, 120(2):524, 2004.

[179] M. Lundberg and P. E. M. Siegbahn. Quantifying the effects of the self-interaction error in DFT: When do the delocalized states appear? *J. Chem. Phys.*, 122:224103, 2005.

[180] A. D. Becke. Density-functional exchange-energy approximation with correct asymptotic behavior. *Phys. Rev. A*, 38:3098–3100, 1988.

[181] Chengteh Lee, Weitao Yang, and Robert G. Parr. Development of the colle-salvetti correlation energy formula into a functional of the electron density. *Phys. Rev. B*, 37:785, 1988.

[182] Yihan Shao, Laszlo Fusti-Molnar, Yousung Jung, J. Kussmann, Christian Ochsenfeld, Shawn T. Brown, Andrew T. B. Gilbert, Lyudmila V. Slipchenko, Sergey V. Levchenko, Darragh P. O'Neill, Robert A. DiStasio Jr., Rohini C. Lochan, Tao Wang, Gregory J. O. Beran, Nicholas A. Besley, John M. Herbert, Ching Yeh Lin, Alex Sodt Ryan P. Steele Troy Van Voorhis, Siu Hung Chien, Vitaly A. Rassolov, Paul E. Maslen, Prakashan P. Korambath, Ross D. Adamson, Brian Austin, Jon Baker, Edward F. C. Byrd, Holger Daschel, Robert J. Doerksen, Andreas Dreuw, Barry D. Dunietz, Anthony D. Dutoi, Thomas R. Furlani, Steven R. Gwaltney, Andreas Heyden, So Hirata, Chao-Ping Hsu, Gary Kedziora, Rustam Z. Khalliulin, Phil Klunzinger, Aaron M. Lee, Michael S. Lee, WanZhen Liang, Itay Lotan, Nikhil Nair, Baron Peters, Emil I. Proynov, Piotr A. Pieniazek, Young Min Rhee, Jim Ritchie, Edina Rosta, C. David Sherrill, Andrew C. Simmonett, Joseph E. Subotnik, H. Lee Woodcock III, Weimin Zhang, Alexis T. Bell, Arup K. Chakraborty, Daniel M. Chipman, Frerich J.

Keil, Arieh Warshel, Warren J. Hehre, Henry F. Schaefer III, Jing Kong, Anna I. Krylov, Peter M. W. Gill, and Martin Head-Gordon. Advances in methods and algorithms in a modern quantum chemistry program package. *Phys. Chem. Chem. Phys*, 8:3172–3191, 2006.

[183] G. D. Purvis III and R. J. Bartlett. A full coupled-cluster singles and doubles model: The inclusion of disconnected triples. *J. Chem. Phys.*, 76:1910, 1982.

[184] C. D. Sherrill, Anna I. Krylov, Edward F. C. Byrd, and Martin Head-Gordon. Energies and analytic gradients for a coupled-cluster doubles model using variational Brueckner orbitals: Application to symmetry breaking in O [sub 4][sup+]. *J. Chem. Phys.*, 109(11):4171, 1998.

[185] SR Gwaltney and M. Head-Gordon. A second-order correction to singles and doubles coupled-cluster methods based on a perturbative expansion of a similarity-transformed Hamiltonian. *Chem. Phys. Lett.*, 323(1):21–28, 2000.

[186] F. L. Hirshfeld. Bonded-atom fragments for describing molecular charge densities. *Theo. Chim. Acta*, 44(2):129–138, 1977.

[187] R.G. Parr, P.W. Ayers, and R.F. Nalewajski. What is an atom in a molecule? *Journal of Physical Chemistry A*, 109(17):3957–3959, 2005.

[188] E. R. Davidson and A. A. Jarzecki. Multi-Reference Perturbation Theory. In H. Kirao, editor, *Recent Advances in Multireference Methods*, pages 31–63. World Scientific, 1990.

[189] M. R. Hoffmann. Quasidegenerate perturbation theory using effective hamiltonians. In D. R. Yarkony, editor, *Modern Electronic Structure Theory*, volume 2, pages 1166–1190. World Scientific, Singapore, 1995.

[190] W. D. Laidig, P. Saxe, and R. J. Bartlett. The description of N and F potential energy surfaces using multireference coupled cluster theory. *J. Chem. Phys.*, 86:887, 1987.

[191] T. Yanai and G. K.-L. Chan. Canonical transformation theory for multireference problems. *J. Chem. Phys.*, 124:194106, 2006.

[192] R. Gaudoin and K. Burke. Lack of hohenberg-kohn theorem for excited states. *Phys. Rev. Lett.*, 93(17):173001, Oct 2004.

[193] Andreas Görling. Proper treatment of symmetries and excited states in a computationally tractable kohn-sham method. *Phys. Rev. Lett.*, 85(20):4229–4232, Nov 2000.

[194] NI Gidopoulos, PG Papaconstantinou, and EKU Gross. Spurious Interactions, and Their Correction, in the Ensemble-Kohn-Sham Scheme for Excited States. *Physical Review Letters*, 88(3):33003, 2002.

[195] Mel Levy and Ágnes Nagy. Variational density-functional theory for an individual excited state. *Phys. Rev. Lett.*, 83(21):4361–4364, Nov 1999.

[196] Emilio Artacho, M. Rohlfing, M. Côté, P. D. Haynes, R. J. Needs, and C. Molteni. Structural relaxations in electronically excited poly(*para*-phenylene). *Phys. Rev. Lett.*, 93(11):116401, Sep 2004.

[197] D. Ceresoli, E. Tosatti, S. Scandolo, G. Santoro, and S. Serra. Trapping of excitons at chemical defects in polyethylene. *The Journal of Chemical Physics*, 121(13):6478–6484, 2004.

[198] Oleg Pankratov and Matthias Scheffler. Localized excitons and breaking of chemical bonds at iii-v (110) surfaces. *Phys. Rev. Lett.*, 75(4):701–704, Jul 1995.

[199] Murilo L. Tiago, Sohrab Ismail-Beigi, and Steven G. Louie. Photoisomerization of azobenzene from first-principles constrained density-functional calculations. *The Journal of Chemical Physics*, 122(9):094311, 2005.

[200] T. Liu, W.-G. Han, F. Himo, G.M. Ullmann, D. Bashford, A. Toutchkine, K.M. Hahn, and L. Noodleman. Density functional vertical self-consistent reaction field theory for solvatochromism studies of solvent-sensitive dyes. *Journal of Physical Chemistry A*, 108(16):3545–3555, 2004.

[201] Mel Levy. Electron densities in search of hamiltonians. *Phys. Rev. A*, 26(3):1200–1208, Sep 1982.

[202] John P. Perdew and Mel Levy. Extrema of the density functional for the energy: Excited states from the ground-state theory. *Phys. Rev. B*, 31(10):6264–6272, May 1985.

[203] P. H. Dederichs, S. Blügel, R. Zeller, and H. Akai. Ground states of constrained systems: Application to cerium impurities. *Phys. Rev. Lett.*, 53(26):2512–2515, Dec 1984.

[204] JF Janak. Proof that? E/? n_ {i}= ε in density-functional theory. *Physical Review B*, 18(12):7165–7168, 1978.

[205] R. Bauernschmitt and R. Ahlrichs. *Chem. Phys. Lett.*, 256:454–464, 1996.

[206] Mark E. Casida, Christine Jamorski, Kim C. Casida, and Dennis R. Salahub. Molecular excitation energies to high-lying bound states from time-dependent density-functional response theory: Characterization and correction of the time-dependent local density approximation ionization threshold. *The Journal of Chemical Physics*, 108(11):4439–4449, 1998.

[207] David J. Tozer and Nicholas C. Handy. Improving virtual kohn–sham orbitals and eigenvalues: Application to excitation energies and static polarizabilities. *The Journal of Chemical Physics*, 109(23):10180–10189, 1998.

[208] A. Wasserman and K. Burke. Rydberg Transition Frequencies from the Local Density Approximation. *Phys. Rev. Lett.*, 95(16):163006–+, October 2005.

[209] R. van Leeuwen and E. J. Baerends. *Phys. Rev. A*, 49:2421–2431, 1994.

[210] A. Erdelyi. Asymptotic forms for laguerre polynomials. *J. Indian Math. Soc.*, 24:235–250, 1960.

[211] K. Kaufmann, W. Baumeister, and M. Jungen. Universal Gaussian basis sets for an optimum representation of Rydberg and continuum wavefunctions. *J. Phys. B: At. Mol. Opt. Phys*, 22:2223–2240, 1989.

[212] J.P. Perdew and K. Schmidt. Density Functional Theory and Its Application to Materials, V. *CP577 (American Institute of Physics, Melville, NY, 2001).*

[213] Axel D. Becke. Current density in exchange-correlation functionals: Application to atomic states. *The Journal of Chemical Physics*, 117(15):6935–6938, 2002.

[214] M. Levy. *Proc. Natl. Acad. Sci. U.S.A.*, 76:6062, 1979.

[215] M. Levy. *Phys. Rev. A*, 26:1200, 1982.

[216] E. H. Lieb. *Int. J. Quantum Chem.*, 24:224, 1983.

[217] M. Levy and J. P. Perdew. In R. M. Dreizler and J. da Providencia, editors, *Density Functional Methods in Physics*, pages 11–30. Plenum, New York, 1985.

[218] Q. Wu and W. Yang. A direct optimization method for calculating density functionals and exchange–correlation potentials from electron densities. *The Journal of Chemical Physics*, 118:2498, 2003.

[219] Qingsheng Zhao, Robert C. Morrison, and Robert G. Parr. From electron densities to kohn-sham kinetic energies, orbital energies, exchange-correlation potentials, and exchange-correlation energies. *Phys. Rev. A*, 50(3):2138–2142, Sep 1994.

[220] P. H.-L. Sit, Matteo Cococcioni, and Nicola Marzari. Realistic quantitative descriptions of electron transfer reactions: Diabatic free-energy surfaces from first-principles molecular dynamics. *Physical Review Letters*, 97(2):028303, 2006.

[221] Jorg Behler, Bernard Delley, Sonke Lorenz, Karsten Reuter, and Matthias Scheffler. Dissociation of o[sub 2] at al(111): The role of spin selection rules. *Physical Review Letters*, 94(3):036104, 2005.

[222] T. Van Voorhis and M. Head-Gordon. *Mol. Phys.*, 100:1713–1721, 2002.

[223] Neepa T. Maitra, Fan Zhang, Robert J. Cave, and Kieron Burke. Double excitations within time-dependent density functional theory linear response. *The Journal of Chemical Physics*, 120(13):5932–5937, 2004.

[224] H. Munthe-Kaas. High order Runge-Kutta methods on manifolds. *Applied Numerical Mathematics*, 29(1):115–127, 1999.

Chiao-Lun Cheng
11 Tg Rhu Rd # 18-01
Singapore 436896

http://www.thechiao.com
+65 6345-0355
chiao@alum.mit.edu

Objective

- Computational Physicist looking to solve challenging complex problems with strong analytical skills and systematic, mathematical mindset

Education

- **Massachusetts Institute of Technology** **Cambridge, MA**
  Ph.D., Physical Chemistry, ***GPA: 5.000/5.000***, 2008
  GRE Verbal: 630/800, Math: 800/800, Writing: 4.5/6

- **University of California, Berkeley** **Berkeley, CA**
  B.S. Chemistry, High Honors, ***GPA: 3.844/4.000***, 2003
  B.A. Molecular and Cell Biology, High Distinction in General Scholarship, 2003
  Physics Minor, 2003

- **University of California, Irvine** **Irvine, CA**
  Chemistry and Biology Double Major, ***GPA: 3.886/4.000***, 1999 - 2001

Work Experience

- **Associate Consultant** McKinsey and Company, **Oct 2008 -**
  New York Business Technology Office **New York, NY**

- **Research Assistant** Massachusetts Institute of Technology **Nov 2003 - Aug 2008**
  Supervisor: Professor Troy Van Voorhis **Cambridge, MA**
  - computational simulations of electron movement in molecules
  - troubleshooting complex computational systems

- **Research Assistant** University of California, Berkeley **May 2002 - May 2003**
  Supervisor: Professor Judith Klinman **Berkeley, CA**
  - theoretical and experimental work investigating quantum tunnelling in a soybean enzyme

- **Research Assistant** University of California, Berkeley **Sep 2001 - May 2002**
  Supervisor: Professor Paul Bartlett **Berkeley, CA**
  - organic synthesis of a digestive enzyme inhibitor

Leadership Activities

- **2008 Battlecode Competition (6 / 196)** **Jan 2008**
  Massachusetts Institute of Technology **Cambridge, MA**
  - annual **artificial intelligence** programming competition
  - consideration of multi-dimensional **implementational limitations** and **rival strategies** while steering development under **tight time and resource constraints** in a 4-person team that ultimately placed top 6 out of 196 teams

- **2007 Battlecode Competition (Top 16 / 157)** **Jan 2007**
  Massachusetts Institute of Technology **Cambridge, MA**

- **2007 MIT Taiwanese Career Fair (Organizer)** **Nov 2006 - Feb 2007**
  Massachusetts Institute of Technology **Cambridge, MA**
  - designed and implemented online resume collection system
  - **logistics**, **budgeting**, and term **negotiation** with companies as part of a core 3-person team
  - inaugural career fair of its series at MIT, attended by about 200 people

Publications

- Jeremy S. Evans, Chiao-Lun Cheng, and Troy Van Voorhis,
  "Spin-charge separation in molecular wire conductance simulations"
  Phys. Rev. B (submitted)
- Chiao-Lun Cheng, Qin Wu, and Troy Van Voorhis,
  "Rydberg energies using excited state density functional theory"
  J. Chem. Phys. (accepted)
- Qin Wu, Chiao-Lun Cheng and Troy Van Voorhis,
  "Configuration interaction based on
  constrained density functional theory: A multireference method"
  J. Chem. Phys. 127, 164119 (2007)
- Chiao-Lun Cheng, Jeremy S. Evans, and Troy Van Voorhis,
  "Simulating molecular conductance using real-time density functional theory"
  Phys. Rev. B 74, 155112 (2006)

Languages

Natural Languages: English (native), Chinese/Mandarin (native), Taiwanese (fluent)

Computer Languages: Python, C++, Fortran 77, BASH, LaTeX, Common Lisp